# Predicting performance of glassy polymers : evolution of the thermodynamic state during processing and service life

# Predicting performance of glassy polymers

*Evolution of the thermodynamic state
during processing and service life*

# Predicting performance of glassy polymers

*Evolution of the thermodynamic state*
*during processing and service life*

PROEFSCHRIFT

ter verkrijging van de graad van doctor aan de
Technische Universiteit Eindhoven, op gezag van de
Rector Magnificus, prof.dr.ir. C.J. van Duijn, voor een
commissie aangewezen door het College voor
Promoties in het openbaar te verdedigen
op donderdag 27 november 2008 om 16.00 uur

door

**Tom Antonius Philomena Engels**

geboren te Helden

Dit proefschrift is goedgekeurd door de promotor:

prof.dr.ir. H.E.H. Meijer

Copromotoren:
dr.ir. L.E. Govaert
en
dr.ir. G.W.M. Peters

voor opi en pap

# Contents

# Summary

Modern design environments integrate shaping and making and the processes involved are supported by numerical tools that aid distinct steps in the total design process. We find numerical codes that allow simulation of filling, and subsequent cooling, in injection molding, and finite element packages that evaluate the mechanical response of the final product under the desired loading conditions. These examples illustrate the existence of two different parts of the design world to be distinguished: (i) the processing of the product and (ii) the service life of the product. Up till now, no real interaction between the two worlds exists. Processing analyses are concerned with the melt state and the service-life region focuses on the solid state, each requiring its own numerical tools and set of material parameters. In polymers it is, however, the processing step which largely determines the behavior in the solid state and, therefore, the two worlds need to be coupled.

Proper knowledge of the thermodynamic state of a polymer material, as e.g. reflected in the value of the yield stress, enables one to accurately predict both short- and long-term performance of polymer test pieces. Taking into account the evolution of the thermodynamic state during service life well below the glass transition temperature, called progressive aging, by applying an effective time approach, proved to be important to predict even the endurance limit in long-term loading. Although the results are rather useful, a drawback exists in the fact that the initial thermodynamic state of any product has to be determined, using mechanical testing. This might be a trivial exercise in the case of a standardized test piece with homogeneous properties; in the case of a -more- complex product, possessing heterogeneous properties, it is not. Moreover, for true product optimization one would like to predict the final properties of a product in a virtual environment, without even the need of making a prototype.

In this thesis, a method is presented that predicts the development of yield stress distributions in injection molded products of glassy polymers directly from processing conditions. A first modeling approach is based on the evolution kinetics of the effec-

tive time and gives good predictions of properties after processing. This approach, however, neglects the kinetic character of the glass transition, $T_g$. Therefore a second more precise and detailed approach, based on structural relaxation, is applied in a model that acknowledges the kinetics of the glass transition and the non-equilibrium state of the polymer below $T_g$. Although good predictions for the thermodynamic state after processing result, this model fails to quantitatively capture progressive aging. Therefore the first approach, that preserves the ability to capture the evolution of properties well below $T_g$, is preferred and validated both on experimental test pieces and on actual products.

Predictions on performance are made under the assumption of ductile failure, and no explicit criterion for embrittlement was incorporated. Under the influence of progressive aging a transition from a ductile to a brittle failure mode can be experienced. To predict the failure mode, a critical hydrostatic stress criterion is introduced that serves as a threshold value for the onset of cavitation which is the initiation of craze formation. Based on the evolution of the thermodynamic state this molecular weight dependent threshold can be surpassed and a transition in failure mode results.

The modeling approach presented in this thesis combines the two design worlds. It enables the prediction of the performance of products made of polymer glasses, starting from the processing conditions and ending with the way in which the product will fail. This opens the way to true product optimization in a complete virtual environment without the need of performing even a single mechanical test.

This thesis has resulted in the following publications:

- L.E. Govaert, T.A.P. Engels, E.T.J. Klompen, G.W.M. Peters and H.E.H. Meijer, Processing-induced properties in glassy polymers: development of the yield stress in polycarbonate, International Polymer Processing, XX(2), 170-177, (2005)

- T.A.P. Engels, L.E. Govaert, G.W.M. Peters and H.E.H. Meijer, Processing-induced properties in glassy polymers: application of structural relaxation to yield stress development, Journal of Polymer Science: Part B: Polymer Physics, 44, 121-1225 (2006)

- T.A.P. Engels, L.E. Govaert and H.E.H. Meijer, Predicting properties of molded polymer glasses: the influence of flow and temperature history, International Polymer Processing, *submitted*, (2008)

- T.A.P. Engels, L.C.A van Breemen, L.E. Govaert and H.E.H. Meijer, Predicting age-induced embrittlement of glassy polymers, Polymer, *submitted*, (2008)

- T.A.P. Engels, B.A.G. Schrauwen, L.E. Govaert and H.E.H. Meijer, Improvement of the long-term performance of impact-modified polycarbonate by selected heat treatments, Macromolecular Materials and Engineering, *submitted*, (2008)

The author contributed to a number of publications outside the scope of this thesis:

- T.A.P. Engels, B.A.G. Schrauwen, L.C.A. van Breemen and L.E. Govaert, Predicting the yield stress of polymer glasses directly from processing conditions: application to miscible systems, International Polymer Processing, *submitted*, (2008)

- L.E. Govaert, T.A.P. Engels, M. Wendlandt, T.A. Tervoort and U.W. Suter, Does the strain hardening modulus of glassy polymers scale with the flow stress?, Journal of Polymer Science, Part B: Polymer Physics, *accepted*, (2008)

- L.C.A. van Breemen, T.A.P. Engels, C.G.N. Pelletier, L.E. Govaert and J.M.J. den Toonder, Numerical simulation of flat-tip micro-indentation of glassy polymers: influence of loading speed and thermodynamic state, Philosophical Magazine, 88, *accepted*, (2008)

- S.H.M. Söntjens, R.A.E. Renken, G.M.L. van Gemert, T.A.P. Engels, A.W. Bosman, H.M. Janssen, L.E. Govaert and F.P.T. Baaijens, Thermoplastic elastomers based on strong and well-defined hydrogen-bonding interactions, Macromolecules, 41(15), 5703-5708, (2008)

- T.H. Smit, T.A.P. Engels, P.I. Wuisman and L.E. Govaert, Time-dependent mechanical strength of 70/30 poly(L,DL-lactide): shedding light on the premature failure of degradable spinal cages, Spine, 33(1), 14-18, (2008)

- E.T.J. Klompen, T.A.P. Engels, L.E. Govaert and H.E.H. Meijer, Modelling of the post-yield response of glassy polymers: influence of thermomechanical history, Macromolecules, 38(16), 6997-7008, (2005)

- E.T.J. Klompen, T.A.P. Engels, L.C.A. van Breemen, P.J.G. Schreurs, L.E. Govaert and H.E.H. Meijer, Quantitative prediction of long-term failure of Polycarbonate, Macromolecules, 38(16), 7009-7017, (2005)

Furthermore, the following publications are in preparation, and soon to be submitted:

- D.J.A. Senden, T.A.P. Engels and L.E. Govaert, The role of physical ageing in the embrittlement of polycarbonate during steam-sterilization, in preparation for Journal of Materials Science.

- H.A. Visser, T.C. Bor, M. Wolters, T.A.P. Engels and L.E. Govaert, Life-time prediction of load-bearing polymer glasses, in preparation for Macromolecules.

- L.E. Govaert, T.A.P. Engels, S.H.M. Söntjens and T.H. Smit, Time-dependent failure of polylactides in static loading conditions: phenomenology and modeling, in preparation for Biomaterials

- S.H.M. Söntjens, T.A.P. Engels, T.H. Smit and L.E. Govaert, Time-dependent failure of polylactides in static loading conditions: influence of molecular degradation, in preparation for Biomaterials

# Introduction[1]

## 1.1  Failure in glassy polymers

Catastrophic failure of polymer artifacts, either upon impact (e.g. of protective products such as airbags and helmets) or after prolonged exposure to load (for instance supporting structures, high-pressure pipes), limits their ultimate useful lifetime. Hence, understanding of that process and, ideally, being able to accurately predict when and under which circumstances failure occurs is of critical importance, not only for the selection of the materials employed in such objects, but also for selecting the proper processing parameters during their fabrication and for choosing the product's optimal geometrical design for safe use. This issue is complex in the case of semi-crystalline polymers, because they are essentially heterogeneous systems where inside an amorphous matrix anisotropic crystallites are present with a size and orientation that depend on the molecular weight distribution of the polymer and the conditions under which the material is processed. As a consequence, these structural features, and the associated mechanical properties, generally exhibit strong variations throughout even a single processed object. Also for the much more simple single-phase amorphous polymers the final properties are inhomogeneous, e.g. due to non-uniform cooling during processing, which leads to differences in thermodynamic state of the material throughout a product, affecting the mechanical properties.

This thesis addresses the complex issue of predicting the long- and short-term performance of products of amorphous polymers. The relevance of the problem stems from the self-evident recognition that an essential requirement for the safe application of load-bearing components is the possibility to predict the time-to-failure under de-

---

[1]Reproduced in part from: L.E. Govaert, T.A.P. Engels, S.H.M. Söntjens and T.H. Smit, Time-dependent failure in load-bearing polymers. (2008)

signed load specifications. In the absence of quantitative methods for (mechanical) lifetime prediction, producers can only meet required safety standards by reverting to lengthy, full-scale testing and certification procedures. Problems of this nature can be resolved with new predictive tools that will ultimately enable developers and process engineers to locate the weakest link in their product, to facilitate true optimization in design, and, ideally, allow them to offer a time-of-use-before-failure guarantee.

The framework to be developed must not only predict the above-referred failure of materials and products in long-term use, but equally important, predict short-term failure, such as occurring upon impact loading. Particularly in the latter case, storage and/or service-induced structural changes, and associated property evolution, may constitute unwanted dangers. An illustrative example is the case of products that are designed to fail, at an unknown time, in a specific failure mode (e.g. airbag covers in automobiles). Of great concern is, of course, that the product also displays the designed failure mode after being in use for many years.

## 1.2 Phenomenology of failure

To predict the performance of glassy polymers, first we need to further define the properties under investigation: the short- and long-term mechanical properties. Figure 1.1 (left) demonstrates the short-term performance as measured in a tensile test under constant strain rate. Initially the material displays a linear region, where the stress increases proportionally with strain. At higher stresses the response becomes non-linear and subsequently reaches a maximum; the so-called yield stress. This maximum marks the onset of plastic deformation, and soon after the material displays necking, a strain-localization phenomenon [1]. In this process a localized plastic deformation zone is formed that subsequently propagates along the entire length of the test bar whereas the applied force remains almost constant. Upon further straining the necked region approaches the ends of the test bar where the geometry increases to the clamping area, the force needed to yield these regions increases, as does the stress in the already necked regions, and the material breaks at a stress level that depends strongly on molecular weight [2; 3]. From a mechanical point of view, the moment of neck initiation can be regarded as the point where the material fails, since there it loses its mechanical integrity.

The long-term performance is illustrated in Figure 1.1 (right), where in a creep experiment the evolution of strain under a constant stress is shown. Although the load is approximately 15% below the yield stress, a time-dependent mechanical response is observed. The deformation of the sample increases gradually in time, with the rate of deformation becoming constant after a short time, while at longer loading times the deformation rate increases leading to a subsequent failure of the material. The mode of failure observed is similar to that observed in the short-term tensile test; necking. For this reason this phenomenon is sometimes referred to as delayed yielding [4; 5].
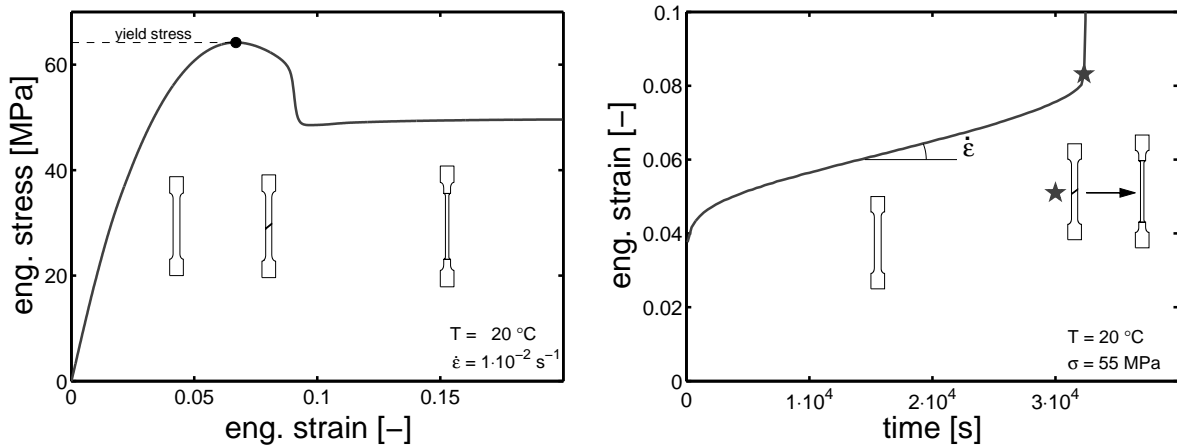
**Figure 1.1:** Left: Deformation behavior of polycarbonate in uniaxial extension at a constant strain rate of $10^{-2}\text{s}^{-1}$. Right: Creep test under a constant load of 55 MPa.
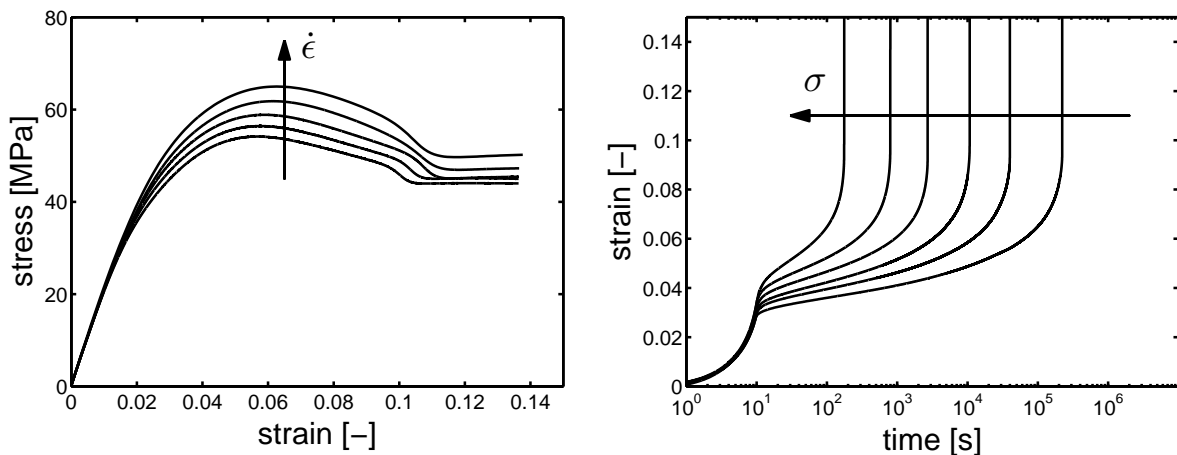


**Figure 1.2:** Left: Stress versus strain for increasing strain rates. Right: Strain versus time for increasing stresses.

The time scale at which a polymer glass fails proves to depend on the loading conditions applied. This is illustrated in Figure 1.2, which gives the tensile response of a polycarbonate test bar for different loading rates (left), and the creep response of the same geometry for different stress levels (right). Figure 1.2 (right) brings us to the remarkable insight that it is not the question *whether* the material will fail under static load, but rather *when* it will fail under the specified load. The higher the strain rate applied, the higher the yield stress observed and, the higher the stress level, the faster the material deforms and fails. The rate dependence of the yield stress and the stress-dependence of the time-to-failure are shown in Figure 1.3, and are found to give semi-logarithmic relations where the yield stress is linearly dependent on the logarithm of the loading rate applied with a slope $\alpha$ (Figure 1.3, left), and the stress applied is linearly dependent on the logarithm of the time-to-failure with the same
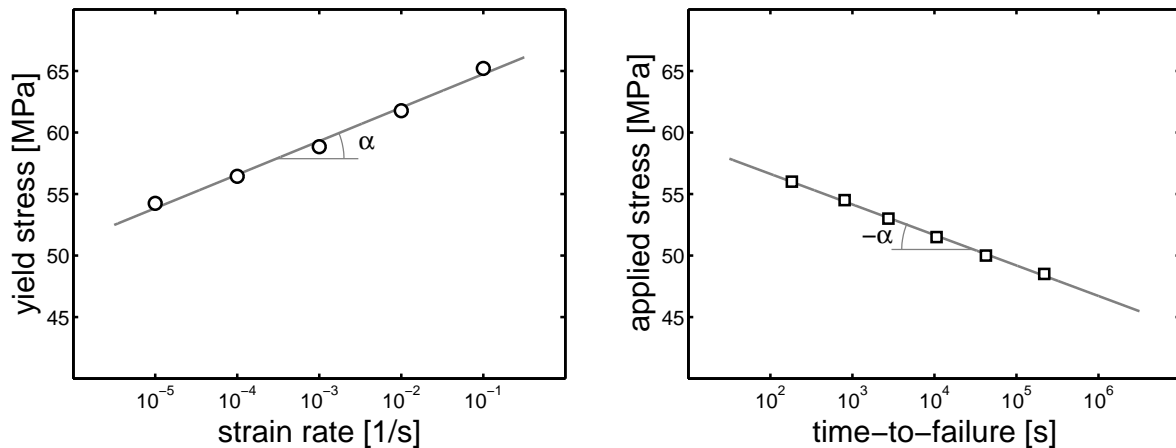
**Figure 1.3:** Left: Rate dependence of the yield stress. Right: Stress dependence of the time-to-failure.

absolute slope $\alpha$ (Figure 1.3, right). It thus seems that the kinetics of failure under applied strain rates and applied stresses are strongly related.

## 1.3 Molecular origin

Let us now examine the physical background of the time-dependent failure processes observed. Amorphous polymers consist of long, covalently bonded molecules that are randomly distributed throughout the material. Each molecule has the ability to change its spatial conformation by rotation over covalent bonds that form the backbone of the chain, and in its equilibrium state a random coil is the most probable conformation. The rate at which a chain can change its conformation depends on temperature and stress. At high temperatures conformational changes are fast and chains can move freely with applied deformation (rubberlike behavior). At low temperatures (below the glass transition temperature), chain mobility decreases drastically and the material virtually "vitrifies" [6] and becomes a glass, although changes in chain conformation are still feasible. Due to the low mobility of the chains, these conformational amendments are generally not observable within practical experimental time scales. This situation changes drastically upon application of stress. Similar to temperature, an applied stress enhances main-chain mobility, and, as a result, the effects of changes in chain conformations become noticeable. Typically the material's relaxation times decrease by orders of ten in magnitude by applying multiples of 10 MPa [7].

Now we investigate what happens during a standard tensile test. In the initial stage of loading, where the stress is still low, chain mobility is negligible, and the modulus is determined by the intermolecular interactions between individual chains. With increasing stress, chain mobility increases, and gradually changes in chain conformation start to contribute to the deformation (strain) of the material. At the stress
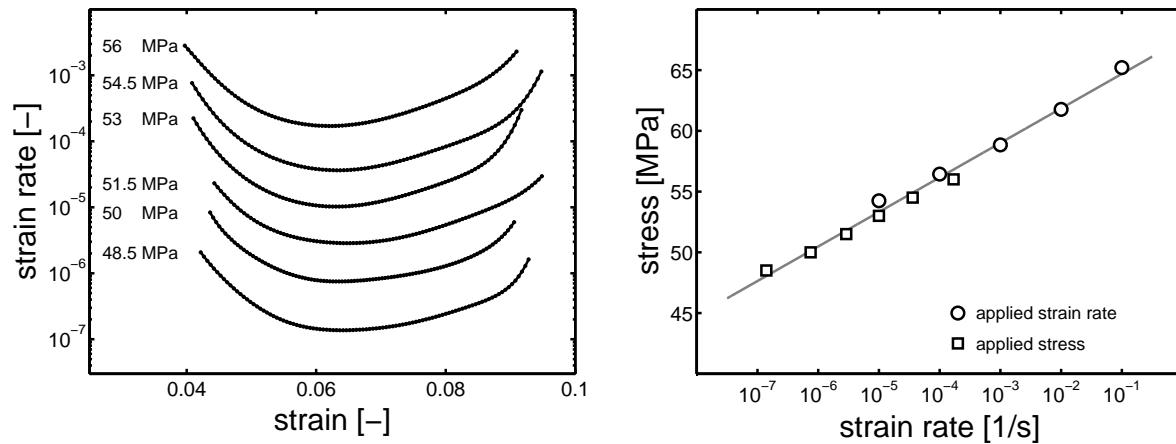
**Figure 1.4:** Left: Evolution of strain rate during creep at various loads (derived from the data of Figure 1.3 Right). Right: Stress as a function of strain rate. Tensile experiments ($\bigcirc$), and creep experiments ($\square$).

level where the plastic strain rate resulting from chain mobility exactly matches the experimentally applied strain rate, the material flows and this stress is called the yield stress. In other words, applied stress induces a state of enhanced molecular mobility that stimulates a dynamic rearrangement of molecular segments, resulting in a steady rate of plastic flow. The magnitude of this plastic flow rate not only depends on the stress, but also on the temperature applied.

For further illustration, we consider the deformation of polycarbonate under a static stress; the creep curves in Figure 1.2 (right). From this figure we determine the evolution of strain rate as a function of strain, a so-called Sherby-Dorn plot [8] (Figure 1.4, left). In this plot we can observe that, at each load, the strain rate initially decreases (primary creep) until it reaches a steady state of flow, where the strain rate remains more or less constant (secondary creep). It was first demonstrated by Bauwens-Crowet et al. [9] that the steady state obtained in static loading is identical to that obtained at the yield stress in a constant strain rate experiment. This is demonstrated in Figure 1.4 (right), that presents the steady state values of stress and strain rate obtained from tensile tests at a constant strain rate and creep tests under static loading. Both yield exactly the same curve.

In summary: we now established that an applied stress induces a state of enhanced molecular mobility in polymer glasses that results in a steady rate of plastic flow, and eventually failure, that is equivalent to the failure mode observed under loading with a constant strain rate.

## 1.4 Intrinsic deformation behavior

To understand the reason for strain localization, we have to study the stress-strain response in an experimental setup in which a sample deforms homogeneously up to
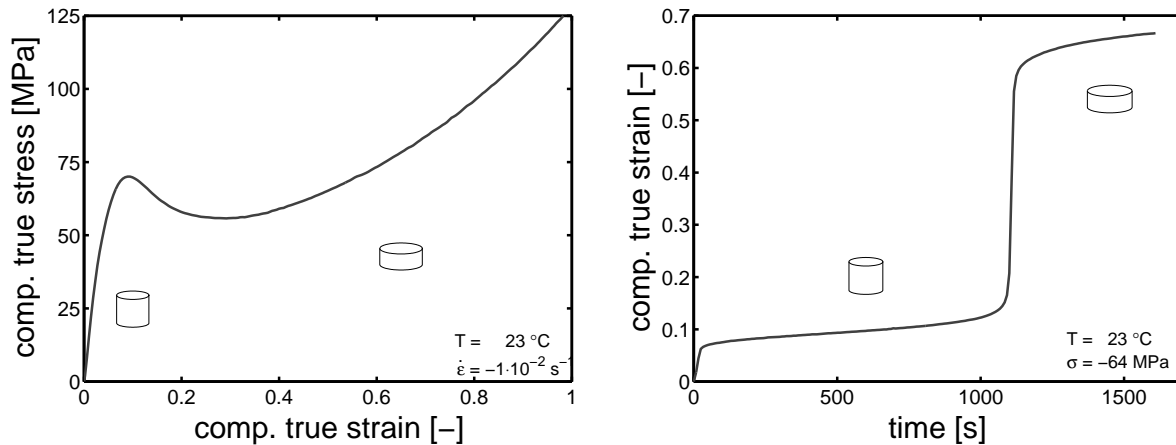
**Figure 1.5:** Left: Intrinsic deformation behavior of PC in uniaxial compression. Right: Intrinsic deformation under a constant true compressive stress.

large plastic deformations. Examples of such experiments are uniaxial compression tests [10; 11] or video-controlled tensile tests [12], and the stress-strain curves, thus obtained, are generally referred to as the material's intrinsic stress-strain response. An illustrative example is presented in Figure 1.5 (left), which shows the intrinsic response of polycarbonate in a uniaxial compression test at a constant rate of strain. In contrast to the behavior in uniaxial extension, see Figures 1.1 (left) and 1.2 (left), the sample does not neck but deforms homogeneously over the entire strain range covered.

After the yield point, the intrinsic stress-strain response of polymer glasses displays two characteristic phenomena: strain softening, the initial decrease of true stress with strain, and strain hardening, the subsequent upswing of the true stress-strain curve (Figure 1.5, left). Where strain softening is caused by the removal, upon straining, of local valleys in the energy landscape of the intermolecular interactions, strain hardening is generally interpreted as the result of a stress contribution of the orienting molecular network [10; 11; 13]. When applying a constant true compressive stress, a similar picture is observed (Figure 1.5, right), and comparable to Figures 1.1 (right) and 1.2 (right), the static load induces a steady rate of plastic flow. Plastic deformation accumulates steadily, until, at a critical level of plastic strain, strain softening sets in (here at t ~ 1000s) and the deformation rapidly increases until it is stabilized by strain hardening [14].

Regarding the intrinsic mechanical response of glassy polymers, there are two time dependencies that need to be considered [15]. The first one we already encountered: it is the time dependence of the mechanical properties itself. The influence of strain rate on the intrinsic behavior of polycarbonate is presented in Figure 1.6 (left) and with increasing strain rate the yield stress increases, similarly to the observations in tensile testing, see Figure 1.2 (left). In the post-yield region, the curves shift upwards at higher strain rates by the same amount as the yield stress.

The second time-dependency that is of importance is the influence of the age of the
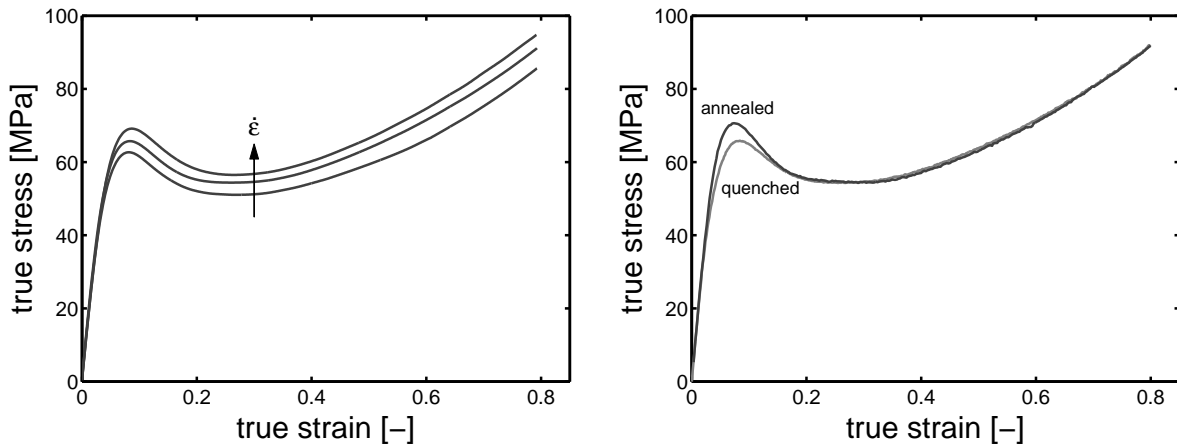
**Figure 1.6:** Intrinsic deformation behavior of PC in uniaxial compression. Left: Influence of strain rate. Right: Influence of physical aging.

material. Polymer glasses are generally not in thermodynamic equilibrium, and, as a result, display a persistent drive towards equilibrium (physical aging), leading to a gradual change in mechanical properties over time [16; 17]. This process can be accelerated by storing the material at an elevated temperature below its glass transition temperature; a heat-treatment called annealing. In Figure 1.6 (right), the intrinsic response of an annealed sample of polycarbonate is compared to that of a rapidly cooled sample (quenched). Physical aging results in an increase of both modulus and yield stress, but upon plastic deformation the differences between the curves disappear and eventually they fully coincide at a strain of approximately 0.2. Apparently all influence of thermal history is erased at that strain and both samples are transformed to a similar, mechanically 'rejuvenated' state [15; 18]. From Figure 1.6 (right) it follows that an increase in yield stress, due to a thermal treatment, directly implies an increase in strain softening, which results in a more severe localization of strain, sometimes leading to complete embrittlement [19]. The influence of molecular weight on the intrinsic response is usually small and negligible [15], which makes thermal history the key factor in influencing the intrinsic properties of a specific polymer glass. A change in thermal history is also reflected in the long-term failure behavior of polymer glasses [14]. This is demonstrated for polycarbonate in Figure 1.7. Figure 1.7 (left) presents the yield stress vs strain rate in uniaxial extension for quenched and annealed samples. As a result of annealing, the yield stress increases, but the kinetics (slope of the curve) remain unchanged. As can be witnessed in Figure 1.7 (right), the increase in yield stress is accompanied by an improvement in the life-time under constant stress. Depending on the effectiveness of the treatment, the improvement may be by orders of magnitude [14]. The second point of interest is that the slope of applied stress versus the logarithm of time to failure is the same for both thermodynamic states. Again, the absolute value of this slope is identical to that observed for the yield stress versus the logarithm of strain rate [9; 14] (Figure 1.7, left).

With respect to the mode of failure, it is in particular the post-yield characteristics of the polymer, i.e. strain softening and strain hardening, that play a determining role
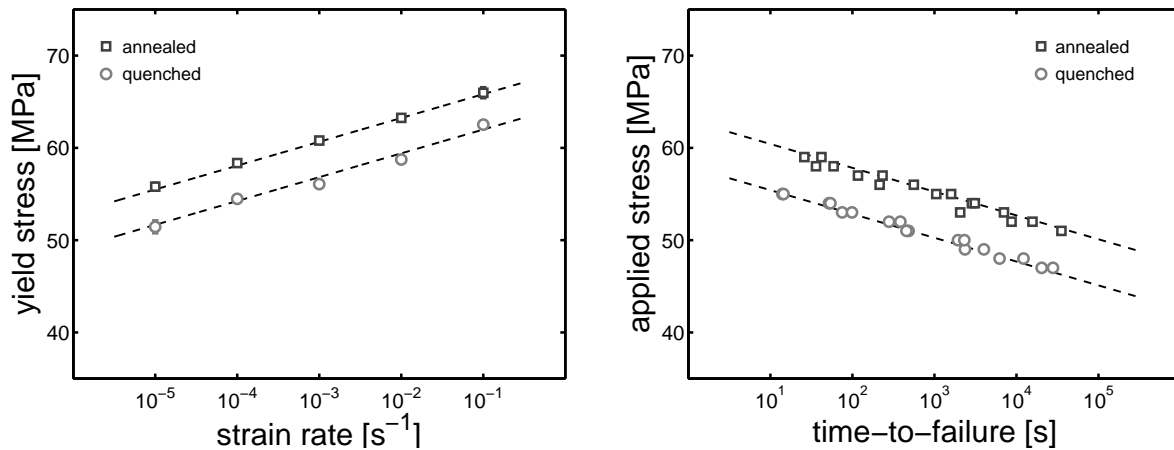
**Figure 1.7:** Left: Yield stress versus strain rate in uniaxial extension for annealed and quenched PC. Right: Time-to-failure versus applied stress for annealed and quenched PC.

[18; 19]. In the vicinity of stress concentrations, strain softening inevitably leads to the formation of localized plastic deformation zones. The initial size and evolution of these zones is determined by a subtle interplay between the amount of strain softening and the amount of strain hardening. If the strain hardening is sufficiently strong, the deformation zones are stabilized and the deformation expands in a controlled fashion to the bulk of the material. Typical examples of such ductile behavior are shear band formation and necking. In the case of insufficient strain hardening, on the other hand, the material will be inclined to deform plastically by crazing, extremely localized zones of plastic deformation that act as a precursor for cracks and thus induce a brittle failure mode [18; 19].

To illustrate this we compare the mechanical responses of polycarbonate (PC) and polystyrene (PS). Most striking here is the difference in macroscopic failure, PC shows a ductile failure mode via necking and PS fails brittle by crazing (Figure 1.8, left). This can be rationalized by the differences in the intrinsic stress-strain curves of PC and PS presented in Figure 1.8 (right). In uniaxial compression, localization of strain is absent, and both polymers can be deformed to high (compressive) strains. Polystyrene exhibits, compared to polycarbonate, a pronounced strain softening and only a weak contribution of strain hardening. In uniaxial extension, the strain localizations in PS cannot be stabilized and evolve almost without limit, ultimately leading to the initiation of crazes and macroscopic failure. Polycarbonate, on the other hand, displays only a moderate amount of strain softening and a much stronger contribution of the strain hardening. Localized plastic deformation zones, induced by strain softening, are now stabilized and spread out to other regions in the material. As a result a larger volume participates in the deformation and shear yielding and stable necking are observed. Despite, also polycarbonate will initiate crazes if a more severe localization is introduced by changing the geometry of the test, e.g. by adding a notch [3; 20], and that is why all polymers in the end must be made heterogeneous, e.g. by adding rubbery particles, to deal with the localizations of strain.
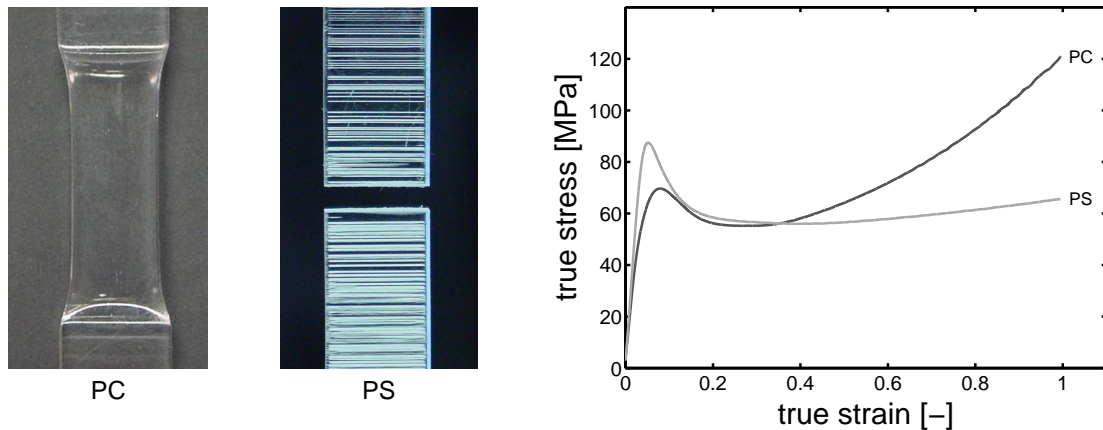
**Figure 1.8:** Left: Mode of failure of polycarbonate, PC, (ductile) and polystyrene, PS, (brittle). Right: Comparison of the intrinsic deformation behavior of PC and PS.

As explained above, the amount of strain softening can be altered by thermal treatments, like annealing. Even small changes in yield stress can have major consequences for the macroscopic deformation behavior. For instance, a subtle increase in strain softening induced by annealing, leads to severe localization of strain and brittle fracture in low-molecular weight polycarbonate [14; 19]. On the other hand, by removing strain softening through mechanical pre-conditioning [21], also polystyrene becomes ductile and can be deformed in uniaxial extension up to strains of 30%. These experiments clearly indicate the dominant role of strain softening in localization and failure of glassy polymers.

## 1.5 Competition between lifetime and embrittlement

As demonstrated in Figure 1.7, it is the value of the yield stress that represents a measure for long-term performance of a polymeric material, but also for the tendency of a polymer to localize its strain. Figure 1.9 shows the evolution of yield stress over time for different annealing temperatures, taken from [15]. Upon annealing the yield stress increases significantly, while the rate of increase is higher for higher annealing temperatures. As discussed before, simultaneously the life-time under static loading will increase. However, the materials tendency to localize strain also increases and, in the case of a notched Izod test bar, a transition from ductile to brittle behavior is induced, see Figure 1.9 (right) (reproduced from [22]). The time at which the ductile-to-brittle transition is encountered depends on the annealing temperature, and higher annealing temperatures lead to shorter times to embrittlement. This ductile-to-brittle transition is, in contrast to the yield and post-yield properties, molecular weight dependent [23; 24]. Clearly there is a trade-off between performance gained on the long-term versus the performance lost on short-term impact loading. The ability to predict where the gain in life-time is cancelled out by the loss in ductility is,
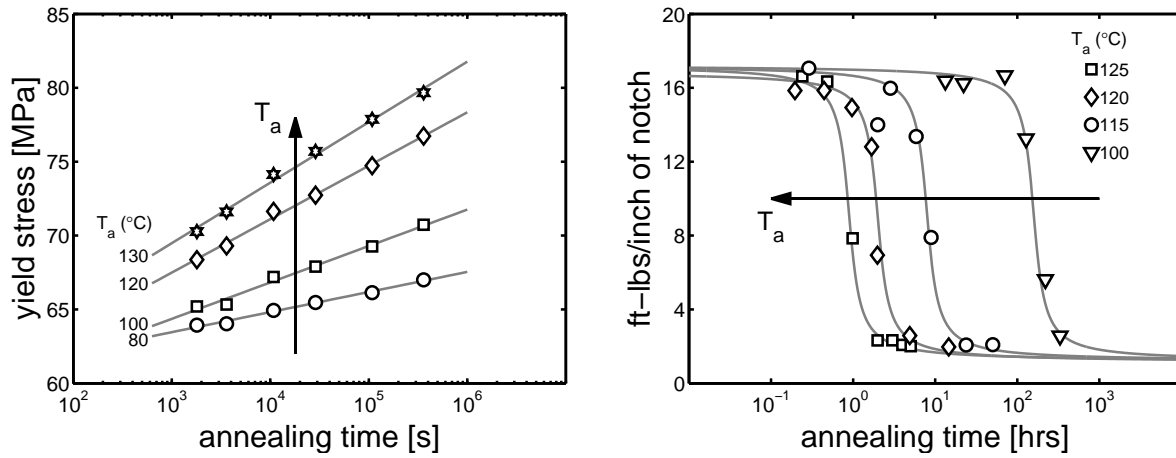
**Figure 1.9:** Left: Yield stress as a function of annealing time for different annealing temperatures. Right: Izod impact as a function of annealing time for different annealing temperatures.

self-evidently, of great importance in polymer engineering and science.

## 1.6 Scope of this thesis

This thesis builds on the constitutive framework for glassy polymers that has been developed in the Eindhoven group over the past decades, which in its latest form can be found in [15]. This constitutive model distinguishes between the contribution of segmental motion, represented by a compressible Maxwell type of spring-dashpot combination and the entropic elasticity of the entangled macromolecular network. The specific characteristics of the deformation of a polymer glass are obtained by defining the stress-, pressure- and state-dependent viscosity, $\eta$, in the Maxwell element as:

$$\eta(\bar{\tau}, \mathsf{p}, \mathsf{S}) = \eta_{0,\mathsf{r}} \underbrace{\frac{\bar{\tau}/\tau_0}{\sinh(\bar{\tau}/\tau_0)}}_{(\mathrm{I})} \underbrace{\exp\left(\frac{\mu\mathsf{p}}{\tau_0}\right)}_{(\mathrm{II})} \underbrace{\exp\left(\mathsf{S}(\mathsf{t}, \bar{\gamma}_\mathsf{p})\right)}_{(\mathrm{III})} \tag{1.1}$$

Here, part (I) relates to the stress- and temperature-dependence of the rate of plastic flow for the reference state, while part (II) represents the pressure dependence required for the correct description of the mechanical response in complex stress fields. The combination of (I) and (II) yields the rate-dependent plastic flow response according to a pressure-modified Eyring flow expression [25; 26]. Finally, part (III) represents the dependence of the viscosity on the thermodynamic state expressed by the state parameter, S, that uniquely determines the actual state of the material, reflected e.g. in the actual yield stress. In the course of time, and upon deforma-
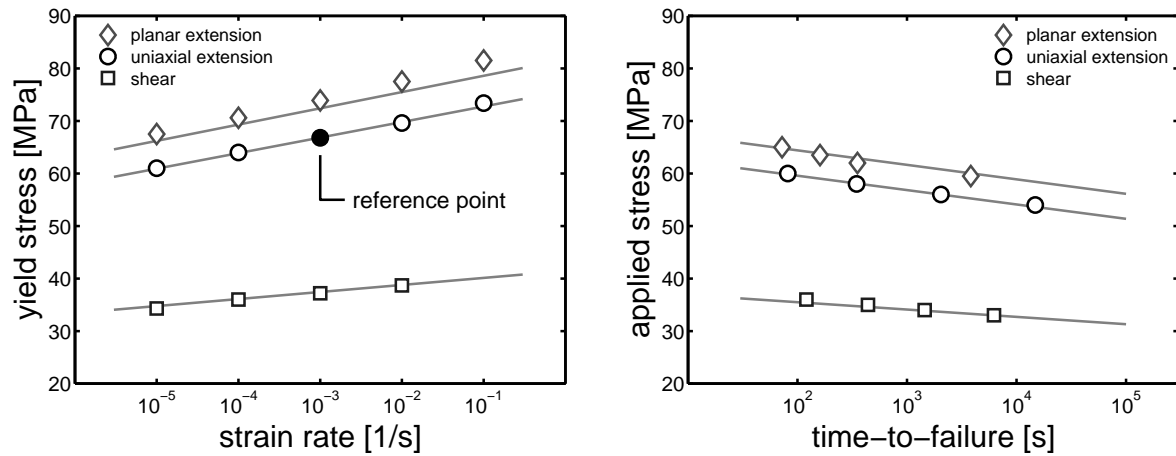
**Figure 1.10:** Experimental and numerical results for different loading geometries. Left: Yield stress versus applied strain rate. Right: Time-to-failure versus applied stress. Symbols are experiments; lines are model predictions.

tion, two processes occur that alter the state of the material: i) $S_a(t)$, physical aging leading to an increase in yield stress, and ii) $R_\gamma(\bar{\gamma}_p)$, mechanical rejuvenation as it is expressed in the strain softening, that effectively decreases the stress with increasing equivalent plastic strain, $\bar{\gamma}_p$, from its maximum at yield to the strain-hardening values of the non-aged (completely rejuvenated, reference) material. It is assumed that these two processes are fully decoupled [15]:

$$S(t, \bar{\gamma}_p) = S_a(t) \cdot R_\gamma(\bar{\gamma}_p) \tag{1.2}$$

Since both rejuvenation and aging kinetics prove to be independent of the molecular weight of the polymer, the only unknown parameter in the model is the initial value of the state parameter, S, which can be directly determined from the yield stress measured in a single simple tensile test at a single strain rate [15]. An illustration of the model's capabilities is given in Figure 1.10, where the yield stress versus strain rate (left) and time-to-failure versus applied stress (right) are given for different loading geometries. The model describes the experimental results very well, both on the short-term as well as on the long-term, by only determining the exact thermodynamic state ($S_a$) at one reference point, here taken as the yield stress in uniaxial extension at a strain rate of $10^{-3}s^{-1}$.

Although the modeling approach proves to be very accurate at describing and predicting glassy polymer behavior, two main disadvantages still exist: 1) the initial thermodynamic state has to be determined by a mechanical test, seriously hindering the application of the model in a design environment, and 2) the model captures evolution of yield stress, but cannot predict when this evolution leads to brittle failure. For these two disadvantages we try to find solutions in this thesis. The organization of

the thesis is as follows:

In Chapter 2 we develop an approach based on the framework used to describe the evolution of properties in the glassy state, and expand this framework to incorporate the processing step. Although giving excellent predictions, it neglects the kinetics associated with the glass transition. Therefore, in Chapter 3, an approach is presented, based on the framework of structural relaxation, which predicts the thermodynamic state of the material by taking into account the thermal history that the material experiences during processing. The approach gives good predictions from processing, but is less accurate when applied to annealing below $T_g$. In Chapter 4 the tools developed in the previous two chapters are validated and certain assumptions verified. Chapter 5 deals with the question of embrittlement which accompanies the evolution of the yield-stress, and a possible constitutive criterion to indicate the onset of embrittlement is given. Then, in Chapter 6, we apply this knowledge to the decrease in long-term performance observed in rubber-toughened materials, and how to counteract this. Finally, in Chapter 7, general conclusions and recommendations are given.

# References

[1] P.I. Vincent. The necking and cold-drawing of rigid plastics. *Polymer*, 1:7–19, 1960.

[2] P.J. Flory. Tensile strength in relation to molecular weight of high polymers. *Journal of the American Chemical Society*, 67:2048–2050, 1945.

[3] P.I. Vincent. The tough-brittle transition in thermoplastics. *Polymer*, 1:425–444, 1960.

[4] D.J. Matz, W.G. Guldemond, and S.L. Cooper. Delayed yielding in glassy polymers. *Journal of Polymer Science: Polymer Physics Edition*, 10:1917–1930, 1972.

[5] I. Narisawa, M. Ishikawa, and H. Ogawa. Delayed yielding of polycarbonate under constant load. *Journal of Polymer Science: Polymer Physics Edition*, 16:1459–1470, 1978.

[6] G.B. McKenna. *Comprehensive Polymer Science, vol 2: Polymer Properties*, chapter Glass Formation and Glassy Behavior, pages 311–362. Pergamon Press, Oxford, 1989.

[7] T.A. Tervoort, E.T.J. Klompen, and L.E. Govaert. A multi-mode approach to finite, three-dimensional, nonlinear viscoelastic behaviour of polymer glasses. *Journal of Rheology*, 40:779–797, 1996.

[8] O.D. Sherby and J.E. Dorn. Anelastic creep of PMMA. *Journal of the Mechanics and Physics of Solids*, 6:145–162, 1954.

[9] C. Bauwens-Crowet, J-M. Ots, and J-C. Bauwens. The strain-rate and temperature dependence of yield of polycarbonate in tension, tensile creep and impact tests. *Journal of Materials Science Letters*, 9:1197–2101, 1974.

[10] E.M. Arruda and M.C. Boyce. Evolution of plastic anisotropy in amorphous polymers during finite straining. *International Journal of Plasticity*, 9:697–720, 1993.

[11] H.G.H. van Melick, L.E. Govaert, and H.E.H. Meijer. On the origin of strain hardening in glassy polymers. *Polymer*, 44:2493–2502, 2003.

[12] C. G'Sell, J.M. Hiver, A. Dahoun, and A. Souahi. Video-controlled tensile testing of polymers and metals beyond the necking point. *Journal of Material Science*, 27(18):5031–5039, 1992.

[13] T.A. Tervoort and L.E. Govaert. Strain-hardening behavior of polycarbonate in the glassy state. *Journal of Rheology*, 44(6):1263–1277, 2000.

[14] E.T.J. Klompen, T.A.P. Engels, L.C.A. van Breemen, P.J.G. Schreurs, L.E. Govaert, and H.E.H. Meijer. Quantitative prediction of long-term failure of polycarbonate. *Macromolecules*, 38(16):7009–7017, 2005.

[15] E.T.J. Klompen, T.A.P. Engels, L.E. Govaert, and H.E.H Meijer. Modelling of the post-yield response of glassy polymer: Influence of thermomechanical history. *Macromolecules*, 38(16):6997–7008, 2005.

[16] L.C.E. Struik. Orientation effects and cooling stresses in amorphous polymers. *Polymer Engineering and Science*, 18(10):799–811, 1978.

[17] J.M. Hutchinson. Physical aging of polymers. *Progress in Polymer Science*, 20:703–760, 1995.

[18] H.E.H. Meijer and L.E. Govaert. Mechanical performance of polymer systems: The relation between structure and properties. *Progress in Polymer Science*, 30:915–938, 2005.

[19] H.G.H. van Melick, L.E. Govaert, and H.E.H. Meijer. Localisation phenomena in glassy polymers: influence of thermal and mechanical history. *Polymer*, 44:3579–3591, 2003.

[20] R.A.W. Fraser and I.M. Ward. The impact fracture behaviour of notched specimens of polycarbonate. *Journal of Materials Science*, 12:459–468, 1977.

[21] L.E. Govaert, H.G.H. van Melick, and H.E.H. Meijer. Temporary toughening of polystyrene through mechanical pre-conditioning. *Polymer*, 42:1271–1274, 2001.

[22] D.G. Legrand. Crazing, yielding, and fracture of polymers. I. Ductile brittle transition in polycarbonate. *Journal of Applied Polymer Science*, 13:2129–2147, 1969.

[23] J.T. Ryan. Impact and yield properties of polycarbonate as a function of strain rate, molecular weight, thermal history and temperature. *Polymer Engineering and Science*, 18(4):264–267, 1978.

[24] G.L. Pitman, I.M. Ward, and R.A. Duckett. The effects of thermal pre-treatment and molecular weight on the impact behaviour of polycarbonate. *Journal of Materials Science*, 13:2092–2104, 1978.

[25] I.M. Ward. *Mechanical properties of solid polymers*. John Wiley & Sons, Chichester, New York, 1983.

[26] L.E. Govaert, P.H.M. Timmermans, and W.A.M. Brekelmans. The influence

of intrinsic strain softening on strain localisation in polycarbonate: Modelling and experimental validation. *Journal of Engineering Materials and Technology - Transactions of the ASME*, 122:177–185, 2000.

# An effective time approach to the evolution of yield stress[1]

## Abstract

A new method is employed to directly predict the development of yield stress distributions in injection molded products of glassy polymers. The approach is based on the results of a study on the temperature dependence of the evolution of yield stress during annealing of polycarbonate below $T_g$. In combination with the process-related thermal history, derived from numerical simulations of the injection molding process, an estimate of the yield stress distribution throughout a product can be obtained. Computed yield stresses of injection molded plates prove to be in excellent agreement with the experimental values, including their dependence on mold temperature and plate thickness.

---

## 2.1  Introduction

In load-bearing structural applications of polymers the occurrence of time-dependent failure (creep rupture) is a major concern. For a reliable design of load-bearing components, it is imperative to be able to estimate the life span under the design-load specifications.

Experimental observations show that the long-term failure response of glassy polymers is governed by the onset of plastic strain localization, similar to phenomena like crazing and necking observed during uniaxial tensile tests [1–6]. Over the past 15 years, considerable effort has been directed towards the numerical simulation of these strain localizations in glassy polymers and a number of 3D constitutive models were developed and validated, e.g. in the group of Mary Boyce at MIT [7–9], the group of Paul Buckley in Oxford [10–12], and in our Eindhoven group [13–15]. These developments enabled a quantitative analysis of localization and failure in glassy polymers [15–21], and revealed the crucial role of the intrinsic post-yield characteristics on macroscopic strain localization. Also the analysis and prediction of long-term static failure proved to be possible [22; 23].
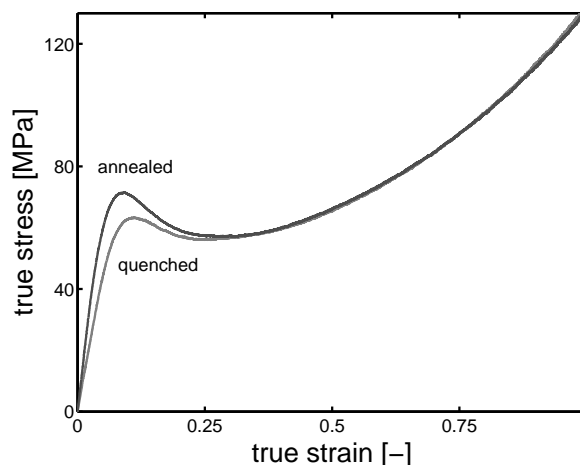


**Figure 2.1:** True stress-strain curves measured in uniaxial compression on PC in the quenched and annealed state (1 week, 120℃).

The intrinsic stress-strain response of polymers (i.e. the macroscopic response in homogeneous deformation) can be measured by using special experiments, e.g. compression tests [8; 21] or video-controlled tensile tests [24]. Figure 2.1 shows the intrinsic stress-strain response of polycarbonate (PC) in uniaxial compression. Typical features are strain softening, the decrease in true stress that is observed after passing the yield point, and strain hardening at large deformations. Strain hardening is generally interpreted as the result of a stress contribution of the orienting molecular network [8; 17; 25–28]. Strain softening is closely related to the occurrence of physical aging. This is demonstrated in Figure 2.1 that compares the intrinsic response of

an annealed and a quenched PC sample. Annealing results in an increase of both modulus and yield stress, but upon plastic deformation the differences between both curves disappear and they fully coincide at a strain of approximately 0.3. Apparently all influence of thermal history is erased at that strain and both samples are transformed to a similar, mechanically rejuvenated state. From Figure 2.1 it is clear that an increase in yield stress, due to a thermal treatment, will directly imply an increase in strain softening. The influence of molecular weight on the intrinsic response is usually small and negligible [12; 15], which makes thermal history the key factor in influencing the intrinsic properties of a specific polymer glass. The thermal history is also reflected in the long-term failure behavior of polymer glasses. This was demonstrated for PC, where an annealing treatment, leading to an increase in yield stress, improved the lifetime under constant stress by orders of magnitude [22; 23].

In our constitutive model [14; 15; 19–22], all variations in thermal history are conveniently captured in the variation of a single state parameter "S", which actually uniquely describes the amount of strain softening during yielding. In short-term loading, physical aging does not play a significant role and the intrinsic behavior of a polymer glass does not change in time. For long-term loading conditions this does not hold and the change in intrinsic behavior is captured by a time-, temperature- and stress-dependent evolution of the state parameter S. This evolution was characterized by annealing PC samples at 80-130℃ for a specified period of time, cooling the material slowly and determining the yield stress at room temperature. The enhanced model was subsequently employed to simulate the long-term failure response of PC in static loading, where it was shown that, without the application of additional failure criteria, the time scale on which failure occurs could be predicted accurately [23]. Moreover, the model successfully predicted the occurrence of the endurance limit that is observed in the experiments. Since for PC both the intrinsic behavior and aging proved to be independent of molecular weight, the measurement of the tensile yield stress at a single strain rate is sufficient to enable a quantitative prediction of the long-term failure behavior of samples with an arbitrary thermal history [15; 22; 23]. This fact enables the numerical evaluation, and even optimization, of the design life of structural components. In practice, the initial thermal history of a polymer glass is determined by the cooling step during processing. High cooling rates lead to a low yield stress and slow cooling results in a high yield stress. Thus the fabrication process makes the intrinsic properties vary through the product as a result of variations in cooling rate over both thickness and length of even simple, rectangular samples.

In the present investigation, it is attempted to develop a method that can be used to predict the development of mechanical properties during processing. Starting point is the temperature dependence of the evolution of the state parameter S during annealing treatments on polycarbonate below $T_g$ [15; 22]. In combination with the process-related thermal history, which can be derived from numerical simulations of the injection molding process (using commercially available simulation software), an estimate of the yield stress distribution throughout the product could be obtained.

## 2.2 Background

### Constitutive approach

The basis of any 3D constitutive model for solid polymers is the split of the total stress in two contributions, first proposed by Haward and Thackray [25]:

$$\sigma = \sigma_s + \sigma_r \tag{2.1}$$

here $\sigma_r$ denotes the strain hardening contribution that is attributed to molecular orientation of the entanglement network, modeled using a Neo-Hookean elastic expression [14; 27]. The contribution $\sigma_s$ accounts for the rate-dependent plastic flow response, attributed to intermolecular interactions on a segmental scale [13; 23], and represented by a non-linear Maxwell model [29] as suggested by Baaijens [30]. Table 2.1 summarizes the equations of the constitutive model.

**Table 2.1:** Summary of the constitutive model employed [14; 15]

$$\sigma = \sigma_s + \sigma_r \qquad \eta(\bar{\tau}, T, p, S) = \eta_{0,r}(T)\frac{\bar{\tau}/\tau_0}{\sinh(\bar{\tau}/\tau_0)}\exp\left(\frac{\mu p}{\tau_0}\right)\exp(S(t, \bar{\gamma}_p))$$

$$\sigma_r = G_r \tilde{\boldsymbol{B}}^d \qquad \eta_{0,r} = \eta_{0,r,\text{ref}}\exp\left(\frac{\Delta U_y}{R}\left(\frac{1}{T} - \frac{1}{T_{\text{ref}}}\right)\right) \quad ; \quad \tau_0 = \frac{RT}{V_y^*}$$

$$\sigma_s = K(J-1) + G\tilde{\boldsymbol{B}}_e^d \qquad S(t_{\text{eff}}(t, T, \bar{\tau}), \bar{\gamma}_p) = S_a(t_{\text{eff}}(t, T, \bar{\tau}))\cdot R_\gamma(\bar{\gamma}_p)$$

$$\dot{J} = J\text{tr}(\boldsymbol{D}) \qquad S_a(t_{\text{eff}}(t, T, \bar{\tau})) = c_0 + c_1\cdot\log(t_{\text{eff}}(t, T, \bar{\tau}) + t_a)$$

$$\overset{\circ}{\tilde{\boldsymbol{B}}}_e = (\boldsymbol{D}^d - \boldsymbol{D}_p)\cdot\tilde{\boldsymbol{B}}_e + \tilde{\boldsymbol{B}}_e\cdot(\boldsymbol{D}^d - \boldsymbol{D}_p) \qquad R_\gamma(\bar{\gamma}_p) = \frac{\left(1+(r_0\cdot\exp(\bar{\gamma}_p))^{r_1}\right)^{\frac{r_2-1}{r_1}}}{\left(1+r_0^{r_1}\right)^{\frac{r_2-1}{r_1}}}$$

$$\boldsymbol{D}_p = \frac{\sigma_s^d}{2\eta(\bar{\tau}, T, p, S)} \qquad t_{\text{eff}}(t, T, \bar{\tau}) = \int_0^t a_T^{-1}(T(t'))a_\sigma^{-1}(\bar{\tau}(t'))dt'$$

$$\bar{\tau} = \sqrt{\frac{1}{2}\text{tr}(\sigma_s^d\cdot\sigma_s^d)} \qquad a_T(T) = \exp\left(\frac{\Delta U_a}{R}\left(\frac{1}{T} - \frac{1}{T_{\text{ref}}}\right)\right)$$

$$\dot{\bar{\gamma}}_p = \sqrt{2\text{tr}(\boldsymbol{D}_p\cdot\boldsymbol{D}_p)} \qquad a_\sigma(\bar{\tau}) = \frac{\bar{\tau}/\tau_a}{\sinh(\bar{\tau}/\tau_a)} \quad ; \quad \tau_0 = \frac{RT}{V_a^*}$$

Under isothermal conditions the nonlinearity of the model is completely governed by a stress-, pressure- and state-dependent viscosity $\eta$, defined as [15]:

$$\eta(\bar{\tau}, p, S) = \eta_{0,r} \underbrace{\frac{\bar{\tau}/\tau_0}{\sinh(\bar{\tau}/\tau_0)}}_{(I)} \underbrace{\exp\left(\frac{\mu p}{\tau_0}\right)}_{(II)} \underbrace{\exp\left(S(t, \bar{\gamma}_p)\right)}_{(III)} \tag{2.2}$$

The parameter $\eta_{0,r}$ denotes the zero viscosity for the completely rejuvenated state. The part marked (I), with $\bar{\tau}$ the equivalent stress, represents the stress dependent part of the viscosity governed by the parameter $\tau_0$. Part (II) is the pressure dependent part, governed by the pressure dependence $\mu$ and the hydrostatic pressure p. The combination of part (I) and (II) gives a rate dependent plastic flow response according to the pressure modified Eyring flow expression [14]. Finally, part (III) represents the dependence of the viscosity on the state of the material expressed by the parameter S.

In time and upon deformation two processes occur, a) physical aging, leading to an increase in yield stress, and b) strain softening, leading to a decrease in yield stress. In our model approach it is assumed that these two are fully decoupled, or:

$$S(t, \bar{\gamma}_p) = S_a(t) \cdot R_\gamma(\bar{\gamma}_p) \tag{2.3}$$

The parameter $S_a$ can be regarded as a state parameter that uniquely determines the current state of the material. It is the evolution of this parameter that enables us to capture changes in mechanical properties with physical aging. The kinetics of the evolution of this parameter are given below, see Equations (2.5-2.13). The function $R_\gamma$ describes the strain softening process, the erasure of thermal history via mechanical rejuvenation that develops with plastic deformation. It is expressed as:

$$R_\gamma(\bar{\gamma}_p) = \frac{\left(1 + (r_0 \cdot \exp(\bar{\gamma}_p))^{r_1}\right)^{\frac{r_2-1}{r_1}}}{\left(1 + r_0^{r_1}\right)^{\frac{r_2-1}{r_1}}} \tag{2.4}$$

where $\bar{\gamma}_p$ denotes the equivalent plastic strain, and $r_0, r_1$ and $r_2$ are fitting parameters.

The essence of the influences of physical aging and strain softening, modeled with the state parameter S (Equation (2.3)), is illustrated in Figure 2.2. As schematically shown in Figure 2.2 (left), Equation (2.2) gives a linear relation between the yield stress and the logarithm of strain rate, typical for Eyring flow. As a result of the thermal history during processing, the value of the parameter $S_a$ will be initially unequal to zero, which actually shifts the yield stress along the log (strain rate) axis. At a constant strain rate, this results in an increase in yield stress compared to the reju-
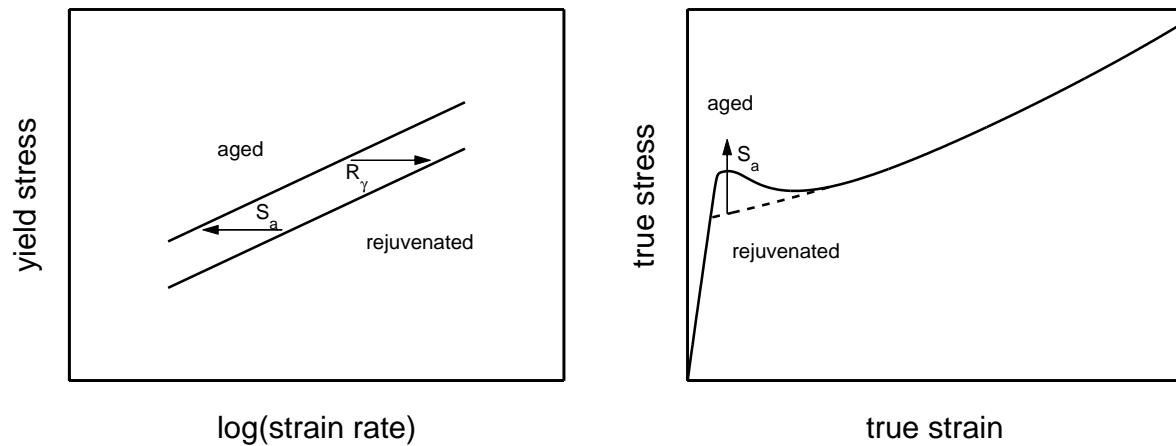
**Figure 2.2:** Left: Schematic representation of the influence of physical aging and strain softening on the strain rate dependence of the yield stress. Right: Schematic representation of the intrinsic stress-strain curve indicating the influence of physical aging and strain softening.

venated state. Upon deformation, the increasing equivalent plastic strain $\bar{\gamma}_p$ triggers strain softening (Equation (2.4)) and the yield stress shifts back to that of the rejuvenated state. As a result, the yield stress drops with increasing strain and the intrinsic stress-strain curve evolves to that of the rejuvenated state (see Figure 2.2 (right)).

**Table 2.2:** Material parameters obtained for polycarbonate [15]

| polycarbonate | | |
| --- | --- | --- |
| $K$ | 3750 | [MPa] |
| $G$ | 308 | [MPa] |
| $\eta_{0,r}$ | $2.1 \cdot 10^{11}$ | [Pa· s] |
| $\tau_0$ | 0.7 | [MPa] |
| $\mu$ | 0.08 | [-] |
| $S_a$ | – | [-] |
| $r_0$ | 0.965 | [-] |
| $r_1$ | 50 | [-] |
| $r_2$ | −5 | [-] |
| $G_r$ | 26 | [MPa] |

A full characterization, using this approach, was performed on PC in previous work [15]. There it was shown that, with identical thermal history, the influence of molecular weight on the intrinsic properties was negligible. This implies that the parameters

determined (listed in Table 2.2) are independent of the molecular weight distribution. The key parameter, needed to adjust for differences in thermal history, is the initial value of the state parameter S: $S_a$. This is demonstrated in Figure 2.3 where two curves of samples with different thermal histories are accurately described, just by changing the initial value of $S_a$.
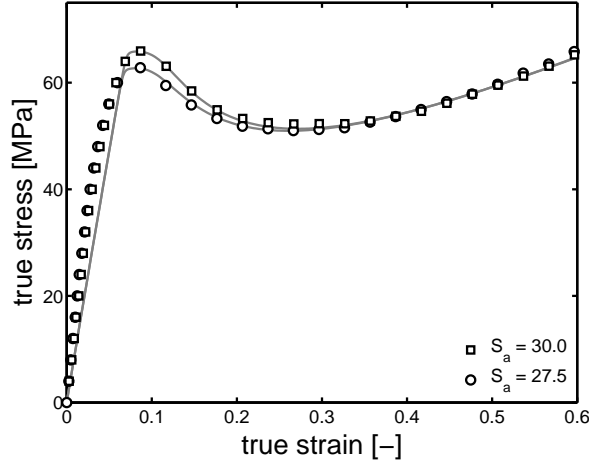


**Figure 2.3:** True stress versus true strain in uniaxial compression at a strain rate of $10^{-4}$ s$^{-1}$. Model prediction (solid lines) compared to experimental results (symbols), for two polycarbonate samples with different initial thermal histories.

The value of $S_a$, required to complete the characterization of a sample with an arbitrary thermal history, can in principle be determined directly from the yield stress measured in an uniaxial tensile test according to [15]:

$$\sigma_y(\dot{\epsilon}_0) = \frac{3\tau_0}{\sqrt{3}+\mu}\left(\ln\left(2\sqrt{3}\cdot\dot{\epsilon}_0\cdot\eta_{0,r}/\tau_0\right) + S_a\right) + \frac{\sqrt{3}}{\sqrt{3}+\mu}\cdot G_r\cdot\left(\lambda_y^2 - \lambda_y^{-1}\right) \qquad (2.5)$$

or vice versa:

$$S_a = \frac{\sqrt{3}+\mu}{3\tau_0}\cdot\sigma_y(\dot{\epsilon}_0) - \ln\left(2\sqrt{3}\cdot\dot{\epsilon}_0\cdot\eta_{0,r}/\tau_0\right) - \frac{1}{\sqrt{3}\cdot\tau_0}\cdot G_r\cdot\left(\lambda_y^2 - \lambda_y^{-1}\right) \qquad (2.6)$$

where $\sigma_y(\dot{\epsilon}_0)$ is the yield stress measured at a strain rate $\dot{\epsilon}_0$, $G_r$ is the strain-hardening modulus and $\lambda_y$ the draw ratio at the yield point.

## Aging kinetics [15; 22]

The evolution of yield stress was studied by annealing PC samples for a specified period of time, cooling the material slowly and determining the yield stress at room temperature. Figure 2.4 (left) shows the increase in (true) yield stress, and the corresponding value of the state parameter $S_a$ according to Equation (2.6), for four different annealing temperatures. Typically, the increase in yield stress is more pronounced for higher temperatures, as was also observed by Golden et al. [31], and Bauwens-Crowet and Bauwens [32]. The results obtained at various temperatures can be combined into a single master curve using (annealing) time-temperature superposition. In Figure 2.4 (right), the resulting master curve is presented for a reference temperature of 80℃. The shift factors $a_T(T)$, used to construct the master curve, are accurately described by an Arrhenius relation:

$$a_T(T) = \exp\left(\frac{\Delta U_a}{R} \cdot \left(\frac{1}{T} - \frac{1}{T_{ref}}\right)\right) \qquad (2.7)$$

where $\Delta U_a$ denotes the activation energy, R is the universal gas constant, T the annealing temperature and $T_{ref}$ the reference temperature. A good description of the shift data was obtained for an activation energy $\Delta U_a$ of 205 kJ/mol.
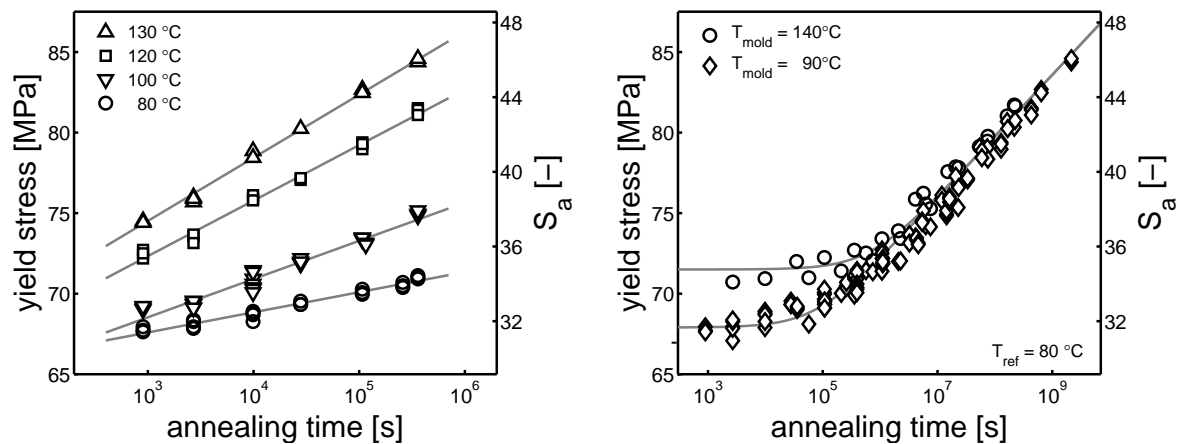


**Figure 2.4:** Left: Evolution of yield stress (room temperature, strain rate $10^{-2}$ s$^{-1}$), and the corresponding value of the state parameter $S_a$, as a function of annealing time for different annealing temperatures. Samples were injection molded with a mold temperature of 90℃. Solid lines are to guide the eye, symbols indicate experimental data. Right: Master curves ($T_{ref}$ =80℃) for the evolution of yield stress/$S_a$ for injection molded PC samples having two different initial thermal histories: i) mold temperature 90℃ and ii) mold temperature 140℃. The drawn lines are model predictions using Equation (2.7) (see text).

Figure 2.4 (right) also shows the master curve for PC samples with a different initial thermal history, more specifically the samples were injection molded with a higher mold temperature (140°C rather than 90°C). Two important ob servations can be made: 1) there appears to be an "ineffective" period of time, during which the increase in yield stress is negligible, and 2) at long annealing times the evolution curves of both samples coincide, the initial differences have disappeared.

We proposed that the parameter $S_a$ displays a logarithmic evolution:

$$S_a(t) = c_0 + c_1 \log\left(\frac{t_{eff} + t_a}{t_0}\right) \tag{2.8}$$

where $t_0 = 1s$, and the effective aging time $t_{eff}$ is defined as:

$$t_{eff} = \int_0^t a_T^{-1}(T) dt' \tag{2.9}$$

with $a_T(T)$ the shift function presented in Equation (2.7), this time with a reference temperature $T_{ref} = 22°C$. The fitting parameters $c_0$ and $c_1$ in Equation (2.8) are constants with $c_0 = -4.41$ and $c_1 = 3.3$. The parameter $t_a$ is introduced in the model as an "ineffective" time period. In Equation (2.8) it actually serves as the "initial age" of the sample, more specifically, the time that a sample with no thermal history ($S_a = 0$) has to age at room temperature to get the same thermodynamic state. In the evolution equation (Equation (2.8)), the changes in $S_a$ will be negligible as long as the effective aging time is smaller than the initial age $t_a$.
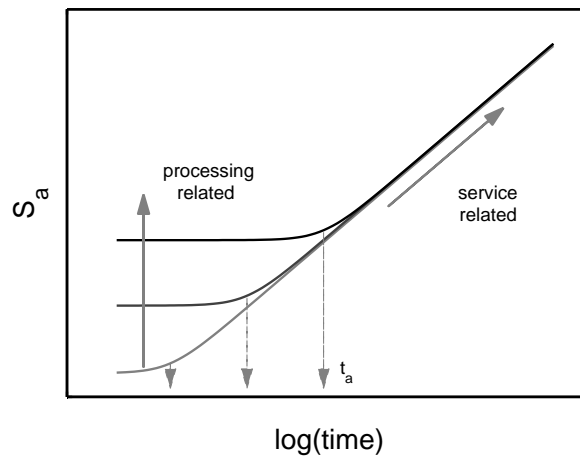


**Figure 2.5:** Schematic representation of the evolution of $S_a$ for different initial states.

The essence of the approach is schematically represented in Figure 2.5. The initial value of $S_a$, determined by the thermal history during processing, is linked to a unique value of the initial age $t_a$:

$$\log\left(\frac{t_a}{t_0}\right) = \frac{(S_a(0) - c_0)}{c_1} \tag{2.10}$$

This specific value of $t_a$ determines the length of the ineffective aging period. As soon as the actual effective aging time becomes of the order of magnitude of $t_a$ the evolution of $S_a$ will proceed proportional to the logarithm of annealing time.

By using Equation (2.6), the evolution equation of $S_a$ can be translated to that of the yield stress, or:

$$\sigma_y(t) = \sigma_{y,0} + c \cdot \log\left(\frac{t_{eff} + t_a}{t_0}\right) \tag{2.11}$$

It should be noted, however, that the yield stress is strain-rate dependent. For a strain rate of $10^{-3} s^{-1}$ the values of the parameters are: $\sigma_{y,0} = 23.4$ MPa and $c = 3.82$ MPa.

## Process-induced yield stress development

Our attempt to predict the evolution of yield stress during processing is based on the assumption that the physical processes involved are identical to those governing the increase in yield stress during annealing. The process starts during the cooling process at the moment that the temperature passes through the glass transition temperature. From that moment on there will be a build-up of effective aging time with thermal history. In essence the end-level of $t_{eff}$ is equal to the parameter $t_a$, the initial age of the sample.

To predict the end-level of $t_{eff}$ after cooling, we apply the evolution of the effective time stated in Equation (2.9). As the build-up of the effective time can only occur in the glassy state, below the glass transition temperature $T_g$, the evolution equation is, to a first approximation, specified as:

$$
\begin{aligned}
T &> T_g &:& \quad \dot{t}_{eff,c} = 0 \\
T &\leq T_g &:& \quad t_{eff,c} = \int_0^{t_c} a_T^{-1}(T_c(t')) dt'
\end{aligned}
\tag{2.12}
$$

where $t_{eff,c}$ is the build-up of effective aging time during the cooling process, $T_c(t)$ the thermal history during cooling and $t_c$ the cooling time.

The resulting initial value of $S_a$, is subsequently defined, after Equation (2.8), by:

$$S_a(0) = c_0 + c_1 \cdot \log \left( \frac{t_{eff,c}}{t_0} + c_2 \right) \tag{2.13}$$

where $c_2 = 21.7$, is a constant added to ensure that $S_a = 0$ for $t_{eff,c} = 0$.

It should be noted that this first approximation of the evolution does not capture the complex dynamics around $T_g$ [33; 34]. The value of $T_g$ is actually introduced as an additional parameter rather than that it reflects kinetic vitrification. The influences of cooling rate or pressure on $T_g$ are therefore not yet covered. Moreover, the approach clearly lacks the concept of equilibrium, and hence is likely to overestimate the influence of aging close to $T_g$. Since the shift factor $a_T$ (Equation (2.7)) decreases with increasing temperature, the approach in Equation (2.12) will basically predict that the aging rate is the highest at $T_g$. In reality this is not the case: the material will still be in thermodynamic equilibrium at this temperature and therefore the aging rate will reduce to zero.

A more advanced kinetic approach, covering the apparent shortcomings mentioned above, will be discussed in Chapter 3. Here we will apply Equation (2.12) to make a first order evaluation of the development of the yield stress during processing.

## 2.3  Experimental

The material used was a commercial grade of polycarbonate, Lexan 141R, supplied by Sabic Innovative Plastics (Bergen op Zoom). Before processing, the material was dried under vacuum at 80℃ for a period of 24 hours.

Rectangular plates, with dimension $70 \times 70 \times 1$ mm$^3$ and $70 \times 70 \times 4$ mm$^3$ (see Figure 2.6), were injection molded on an Arburg 320S / all-rounder 500-150 injection molding machine. The mold was manufactured by Axxicon Moulds B.V. (Helmond, the Netherlands) and had a V-shaped runner of 4 mm thickness and an entrance of $70 \times 1$ mm$^2$ for the 1 mm thick plate and an entrance of $70 \times 2$ mm$^2$ for the 4 mm thick plate. The V-shaped runner caused the material to flow uniformly along the width of the cavity, which was proven by several short shot experiments. The injection temperature and flow rate were set to 280℃ and 90 cc/s for the 1 mm t hick plate and 50 cc/s for the 4 mm thick plate respectively. Since variation of the packing pressure (range 25 to 900 bar) proved to be of no influence on the measured properties of the plates, the packing pressure was set to 500 bar to minimize shrinkage and flash.
To investigate the influence of cooling rate, the mold cavity temperature was varied form 30℃ to 130℃ in steps of 10℃. After several shots the act ual mold temperature was measured. The cooling time was 60 s for the 1 mm thick samples and 150 s for the 4 mm thick samples.
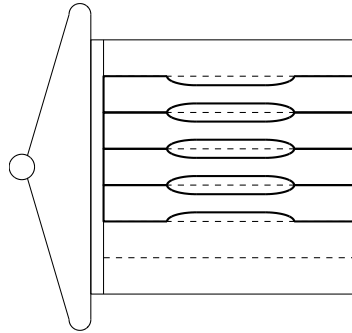
**Figure 2.6:** Schematic representation of the way the tensile specimens were prepared from the injection molded plates.

Rectangular bars of $70 \times 10 \times 1$ mm$^3$ and $70 \times 10 \times 4$ mm$^3$, with a gauge sections of $33 \times 5 \times 1$ mm$^3$ and $33 \times 5 \times 4$ mm$^3$, were cut from the plates of 1 mm thickness and 4 mm thickness respectively in flow direction as indicated in Figure 2.6. The engineering yield stress was subsequently determined in uniaxial extension on a Zwick Z010 universal tensile tester at a strain rate of $10^{-3}$ s$^{-1}$. The true yield stress values were estimated with the assumption that deformation up to the yield point was incompressible.

## 2.4 Numerical

Numerical simulations of the molding process were performed using MoldFlow MPI (release 5.0). The procedure was based on a standard 2.5D approach, i.e. a 2D mid-plane mesh to solve the pressure problem and a full 3D mesh for the velocity and temperature problem. Process variables were selected as described above. The rheological properties of Lexan 141R were taken from the standard MoldFlow library. The thermal history of each element was exported to MatLab, where the resulting $S_a$ values were calculated using Equations (2.12) and (2.13).

## 2.5 Results

### Constant cooling rates

We first investigate the development of mechanical properties when cooling from $T_g$ to room temperature at a constant cooling rate. For this specific case, the combination of Equation (2.7) and Equation (2.12) yields:

$$t_{\text{eff,c}}(t) = \int_0^t a_T^{-1}(T_g - \dot{T}_c \cdot t')dt' \tag{2.14}$$

where $\dot{T}_c$ is the cooling rate applied and $a_T(T)$ the shift factor, defined in Equation (2.7), for $T_{ref} = 22°C$. The calculated value of $t_{eff}$ is subsequently introduced in Equation (2.13) to calculate the value of $S_a$. With this value known, the yield stress at a specific strain rate can be determined using Equation (2.5).
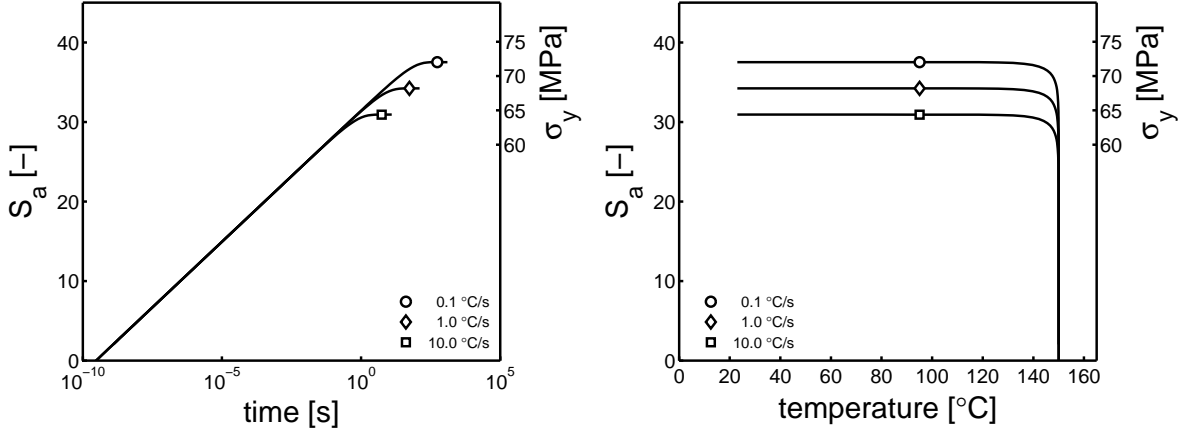


**Figure 2.7:** Left: Evolution of $S_a$ as a function of time for 3 different cooling rates. Right: Evolution of $S_a$ as a function of temperature for 3 different cooling rates. The right axis indicates the corresponding values of the yield stress at a rate of $10^{-3}$ s$^{-1}$.

The evolution curves of $S_a$ during cooling at rates of 0.1, 1 and 10°C/s are presented in Figure 2.7. The value of $T_g$ was chosen to be 150°C. Figure 2.7 (left) shows the increase of $S_a$ on a logarithmic time scale, where it can be observed that, at very short times, the development is linear with the logarithm of time, and appears to be independent of the cooling rate applied. Although this might appear physically unrealistic, there is a simple rationale. On small time scales ($< 0.1$ s) the reduction in temperature is still small and hence the rate of aging is still dominated by the temperature at which the evolution starts: $T_g$. This implies that the effective time $t_{eff}$ increases proportional with time, the temperature shift factor being equal to $a_T(T_g)$. At $T_g$ the aging rate is the highest, and it is not surprising that the simulation shows that a significant part of the yield stress development occurs in this $T_g$-dominated zone.

Figure 2.7 (right) shows the development of $S_a$ now plotted versus temperature, illustrating the fast increase of $S_a$ close to $T_g$. Furthermore, it is clear that the thermal history below 120°C does not significantly contribute to the structural evolution. The build-up of the yield stress appears to happen in the small temperature window between $T_g$ and 120°C. As a direct consequence, the actual value of $T_g$ can be expected to have a considerable influence on the final results. This is demonstrated in Figure 2.8, where the development of $S_a$ is plotted versus temperature for three different values of $T_g$, at a constant cooling rate of 10°C/s. A clear influence of $T_g$ on the final value of $S_a$ is found, with a difference of approximately 7 MPa in yield stress when decreasing $T_g$ from 160 to 140°C. Again it is observed that around 120°C the
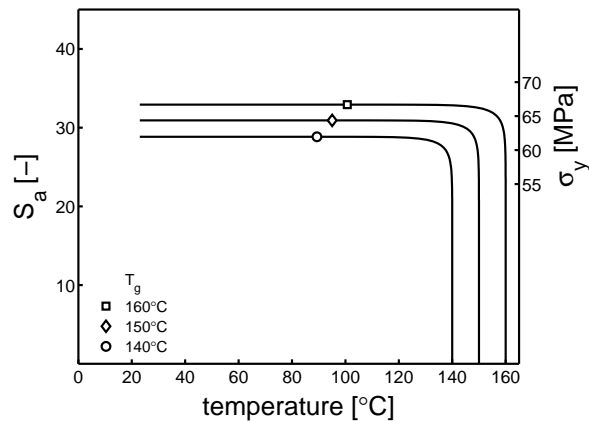
**Figure 2.8:** Evolution of $S_a$ as a function of temperature for 3 different values of $T_g$ at a cooling rate of 10℃/s. The right axis indicates the correspo nding values of the yield stress at a rate of $10^{-3}$ s$^{-1}$.

development of $S_a$ stagnates, irrespective of the value of $T_g$.

## Transient cooling rates in injection molding

From numerical simulations the thermal history during cooling could be obtained for each position in the plates. This is illustrated in Figure 2.9 where the thermal history over the thickness of the 1 mm plate is shown for a mold temperature of 100℃. The cooling rate is maximal at the surface, and minimal in the center of the plate. Subsequently we compute point wise the resulting local value of $S_a$ and the related value of the yield stress, see Figure 2.10. Near the surface we find a much lower yield stress compared to that in the center of the plate, related to the higher cooling rates occurring there. Within the runner this increase is the most pronounced, since there the material thickness is 3 mm, compared to 1 mm in the plate, stressing the influence of part thickness on the resulting properties.

The influence of the mold temperature on the distribution of the yield stress over the thickness of the 1 mm plate is presented in Figure 2.11. An increase in mold temperature leads to a slower rate of cooling and, consequently, an overall higher yield stress. Moreover, the reduction in yield stress near the surface is vanishing at higher mold temperatures, which is interesting and relevant for optimization procedures.

To enable comparison of the numerical predictions with the experimentally determined yield stresses, a thickness-weighted average of the computed yield stress distribution was determined. The average yield stresses, computed with 2 different values of $T_g$, are compared to the experimental data in Figure 2.12. This first result is quite promising. For both plate thicknesses the computed yield stresses are in excellent agreement with the experimental values and the trend of yield stress versus mold temperature is well covered.
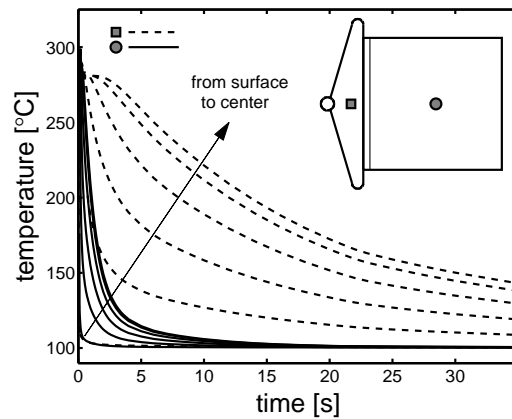
**Figure 2.9:** Variation of thermal history over the thickness of the plate on the two positions indicated. In the direction of the arrow the curves represent the history closer to the center of the plate.
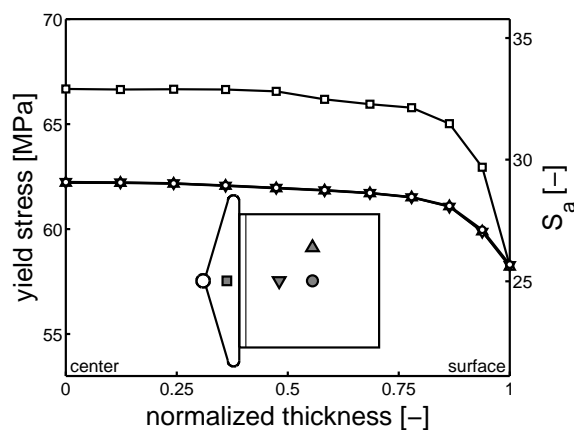


**Figure 2.10:** Distribution of $S_a$, and the corresponding yield stress, over the thickness of the plate at the positions indicated. The mold temperature in this simulation was 100°C.

A point of criticism to the present approach is that the value of $T_g$ is introduced as a parameter that is regarded to be constant. In reality $T_g$ will be dependent on cooling rate, which might reflect in the predicted distribution of yield stress over the sample thickness. An improved approach to the evolution kinetics, inspired by structural relaxation theories [33], will be discussed in Chapter 3.

The influence of flow-induced orientation was thus far neglected. Even for the 1 mm plates the yield stress measured *perpendicular* to the flow direction proved to be approximately the same to that *in* flow direction. This could be expected, since, in the case of a glassy polymer, the flow-induced anisotropy can be fully attributed to the (rather small) stress contribution of the oriented molecular network [35]. For semi-crystalline polymers the anisotropy is much stronger, since it is governed by orientation of the crystalline material [36; 37].
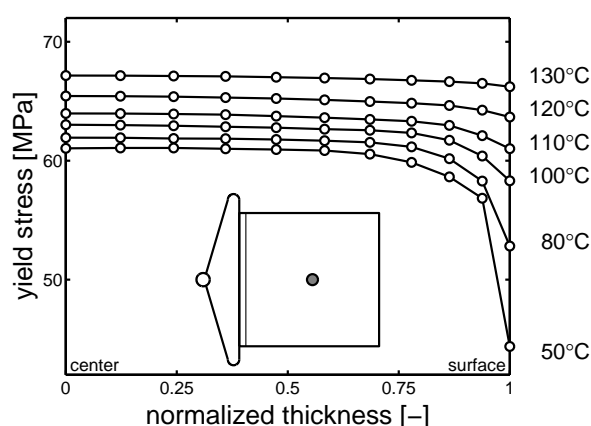
**Figure 2.11:** Distribution of $S_a$ over the thickness of the plate at the position indicated for the various values of the mold temperature.
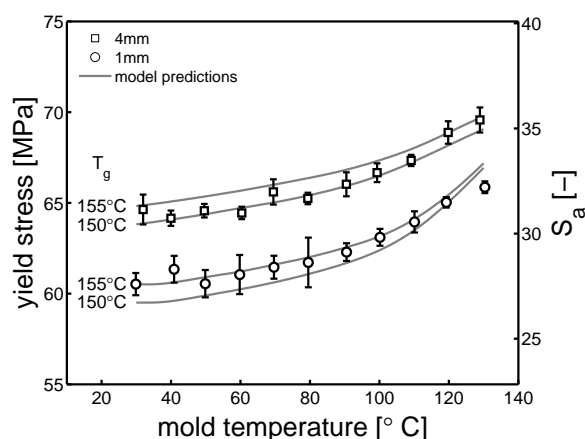


**Figure 2.12:** Yield stress, for a strain rate $10^{-3}$ s$^{-1}$, as a function of mold temperature. Solid lines: model predictions using the $T_g$ indicated. Markers: experimental data.

## 2.6  Conclusions

We developed a new simulation tool that enables the analysis of the development of mechanical properties during processing of glassy polymers. Although the application here was limited to the prediction of the yield stress, the corresponding predicted value of the state parameter directly enables advanced numerical analysis which can be employed to predict the life-span of a product under design specifications [22; 23]. Ultimately, this tool will allow us to quantitatively predict long-term properties of polymeric products, including failure, without the need of performing even a single mechanical test. In combination with numerical simulations of the injection molding process (using e.g. MoldFlow), this opens new possibilities for optimization of load-bearing polymer components by designing both the product shape (wall-thickness) and processing conditions required.

# References

[1] H. Niklas and H.H. Kausch von Schmeling. Molekularstruktur und mechanische Eigenschaften von Polyvinylchloride III. Mitteilung: Ursachen zeitabhängiger Festigkeitseigenschaften von PVC-Rorhen. *Kunstoffe*, 53:886–891, 1963.

[2] D.H. Ender and R.D. Andrew. Cold drawing of polystyrene under dead load. *Journal of Applied Physics*, 36:3057–3062, 1965.

[3] R.M. Ogorkiewicz and A.A.M. Sayigh. The strength of rigid PVC. *British Plastics*, 7:126–128, 1967.

[4] K.V. Gotham. Long-term strength of thermoplastics: the ductile-brittle transition in static fatigue. *Plastics & Polymers*, 40:59–64, 1972.

[5] D.J. Matz, W.G. Guldemond, and S.L. Cooper. Delayed yielding in glassy polymers. *Journal of Polymer Science, Polymer Physics Ed.*, 10:1917–1930, 1972.

[6] I. Narisawa, M. Ishikawa, and H. Ogawa. Delayed yielding in polycarbonate under constant load. *Journal of Polymer Science, Polymer Physics Ed.*, 16:1459–1470, 1978.

[7] M.C. Boyce, D.M. Parks, and A.S. Argon. Large inelastic deformation of glassy polymers, Part I: Rate dependent constitutive model. *Mechanics of Materials*, 7(1):15–33, 1988.

[8] E.M. Arruda and M.C. Boyce. Evolution of plastic anisotropy in amorphous polymers during finite straining. *International Journal of Plasticity*, 9(6):697–720, 1993.

[9] O.A. Hasan, M.C. Boyce, X.S. Li, and S. Berko. An investigation of the yield and post-yield behavior and corresponding structure of poly(methyl methacrylate). *Journal of Polymer Science, Part B: Poymer Physics*, 31(2):185–197, 1993.

[10] C.P. Buckley and D.C. Jones. Glass-rubber constitutive model for amorphous polymers near the glass transition. *Polymer*, 36(17):3301–3312, 1995.

[11] C.P. Buckley, P.J. Dooling, J. Harding, and C. Ruiz. Deformation of thermosetting resins at impact rates of strain. part 2: constitutive model with rejuvenation. *Journal of Mechanical Physics of Solids*, 52(10):2355–2377, 2004.

[12] J.J. Wu and C.P. Buckley. Plastic deformation of glassy polystyrene: A unified model of yield and the role of chain length. *Journal of Polymer Science, Part B: Polymer Physics*, 42(11):2027–2040, 2004.

[13] T.A. Tervoort, E.T.J. Klompen, and L.E. Govaert. A multi-mode approach to finite, three-dimensional, non-linear viscoelastic behavior of polymer glasses. *Journal of Rheology*, 40:779–797, 1996.

[14] L.E. Govaert, P.H.M. Timmermans, and W.A.M. Brekelmans. The influence of intrinsic strain softening on strain localization in polycarbonate: Modelling and experimental validation. *Journal of Engineering Materials and Technology*, 122:177–185, 2000.

[15] E.T.J. Klompen, T.A.P. Engels, L.E. Govaert, and H.E.H Meijer. Modelling of the post-yield response of glassy polymer: Influence of thermomechanical history. *Macromolecules*, 38(16):6997–7008, 2005.

[16] M.C. Boyce and E.M. Aruda. An experimental and analytical investigation of the large strain compressive and tensile response of glassy polymers. *Polymer Engineering and Science*, 30(20):1288–1298, 1990.

[17] M.C. Boyce, E.M. Aruda, and R. Jayachandran. The large strain compression, tension, and simple shear of polycarbonate. *Polymer Engineering and Science*, 34(9):716–725, 1994.

[18] P.D. Wu and E. van der Giessen. On neck propagation in amorphous glassy polymers under plane strain tension. *International Journal of Plasticity*, 11:211–235, 1995.

[19] H.G.H van Melick, O.F.J.T. Bressers, J.M.J. den Toonder, L.E. Govaert, and H.E.H. Meijer. A micro-indentation method for probing the craze-initiation stress in glassy polymers. *Polymer*, 44:2481–2491, 2003.

[20] H.G.H. van Melick, L.E. Govaert, and H.E.H. Meijer. Prediction of brittle-to-ductile transitions in polystyrene. *Polymer*, 44:457–465, 2003.

[21] H.E.H. Meijer and L.E. Govaert. Multi-scale analysis of mechanical properties of amorphous polymer systems. *Macromolecular Chemistry and Physics*, 204:274–288, 2003.

[22] L.E. Govaert, E.T.J. Klompen, and H.E.H. Meijer. A novel approach to creep rupture in glassy polymers. In *proceedings of the 12th international conference of deformation yield and fracture of polymers*, pages 21–24. Institute of materials, 2003.

[23] E.T.J. Klompen, T.A.P. Engels, L.C.A. van Breemen, P.J.G. Schreurs, L.E. Govaert, and H.E.H. Meijer. Quantitative prediction of long-term failure of polycarbonate. *Macromolecules*, 38(16):7009–7017, 2005.

[24] C. G'Sell, J.M. Hiver, A. Dahoun, and A. Souahi. Video-controlled tensile testing of polymers and metals beyond the necking point. *Journal of Material Science*, 27(18):5031–5039, 1992.

[25] R.N. Haward and G.Thackray. Use of a mathematical model to describe isothermal stress-strain curves in glassy themoplastics. *Proceedings of the Royal Society of London A*, 302(1471):453–472, 1967.

[26] R.N. Haward. The application of a Gauss-Eyring model to predict the behavior of thermoplastics in tensile experiments. *Journal of Polymer Science, Part B: Polymer Physics*, 33(10):1481–1494, 1995.

[27] T.A. Tervoort and L.E. Govaert. Strain-hardening behavior of polycarbonate in the glassy state. *Journal of Rheology*, 44(6):1263–1277, 2000.

[28] H.G.H. van Melick, L.E. Govaert, and H.E.H. Meijer. On the origin of strain hardening in glassy polymers. *Polymer*, 44:2493–2505, 2003.

[29] T.A. Tervoort, R.J.M. Smit, W.A.M. Brekelmans, and L.E. Govaert. A constitutive equation for the elasto-viscoplastic deformation of glassy polymers. *Mechanics of Time-Dependent Materials*, 1(3):269–291, 1998.

[30] F.P.T. Baaijens. Calculations of residual stresses in injection molded products. *Rheologica Acta*, 30:284–299, 1991.

[31] J.H. Golden, B.L. Hammant, and E.A Hazell. Effect of thermal pretreatment on

the strenght of polycarbonate. *Journal of Applied Polymer Science*, 11(8):1571–1579, 1967.

[32] C. Bauwens-Crowet and J.C. Bauwens. Annealing of polycarbonate below the glass transition: Quantitative interpretation of the effect on yield stress and differential scanning calorimetry measurements. *Polymer*, 23(11):1599–1604, 1982.

[33] G.B. McKenna. *Comprehensive Polymer Science, vol 2: Polymer Properties*, chapter Glass Formation and Glassy Behavior, pages 311–362. Pergamon Press, Oxford, 1989.

[34] J.M. Hutchinson. Physical aging of polymers. *Progress in Polymer Science*, 20(4):703–760, 1995.

[35] L.E. Govaert and T.A. Tervoort. Temperature dependence of the strain hardening behaviour of polycarbonate. *Journal of Polymer Science, Part B: Polymer Physics*, 42(11):2041–2049, 2004.

[36] B.A.G. Schrauwen, L.C.A. van Breemen, A.B. Spoelstra, G.W.M. Peters, L.E. Govaert, and H.E.H. Meijer. Deformation and failure of oriented semi-crystalline polymers. *Macromolecules*, 37(23):8618–8633, 2004.

[37] J.A.W. van Dommelen, B.A.G. Schrauwen, L.C.A. van Breemen, and L.E. Govaert. Micromechanical modelling of the tensile behavior of oriented polyethylene. *Journal of Polymer Science, Part B: Polymer Physics*, 42(16):2983–2994, 2004.

# A structural relaxation approach to the evolution of yield stress[1]

## Abstract

A method is presented to predict the yield stress distribution throughout an injection-molded product of an amorphous polymer as it results from processing conditions. The method employs the concept of structural relaxation combined with a fictive temperature following the Tool-Narayanaswamy-Moynihan formalism. The thermal history, as it is experienced by the material during processing, is obtained by means of numerical simulation of the injection molding process. The resulting predictions of yield stress distributions show to be in excellent agreement with experimental findings, both for different mold temperatures, as for different part thicknesses.

## 3.1 Introduction

In the current engineering practice there is a great variety of numerical tools available to design polymer products. Examples include commercial codes that aid the optimization process in tool design. In the field of injection molding, these codes (e.g. Moldex3D, Moldflow MPI) not only allow the analysis of mold filling, but, in the case of glassy polymers, also give access to numerical evaluation of residual stresses and dimensional stability (shrinkage, warpage) [1–3]. However, information concerning mechanical properties, such as the yield stress distribution in a product or time-to-failure when placed under a static load, is not provided by these codes. Despite mechanical properties are of high interest for the use of polymers in structural, load bearing applications since they determine the life-time of the final product and the corresponding loading range. With proper knowledge of these properties, true product optimization becomes possible.

Long-term failure of glassy polymers under static loading is dominated by plastic instabilities leading to plastic strain localization [4–9]. These plastic instabilities are the same as those found for short-term failure, observed in tensile testing under constant strain rate [10]. In the last 15 years a lot of effort has been invested by a number of groups at different universities into the development and validation of 3D constitutive models that can describe this localization behavior of glassy polymers, e.g. in the group of Mary Boyce at MIT [11–13], the group of Paul Buckley in Oxford [14–16] and in our Eindhoven group [17–19]. It was shown in subsequent quantitative studies [10; 19–24] that it is the large strain intrinsic behavior (yield, strain softening and subsequent strain hardening) of the polymer that determines the macroscopic localization behavior, and thus failure. The model developed in our group proved to be capable of also predicting the long term static failure [25; 26], including a static fatigue limit when aging kinetics were taken into account.

Here we build on the constitutive model developed in our group. In its latest form [19] it can account for aging kinetics far below the glass transition temperature, i.e. the increase of yield stress with time, and predict long-term failure of glassy polymers. The rate at which aging takes place depends on both the temperature and the stress [19; 27]. Moreover, it has been shown that upon plastic deformation all prior effects of aging can be erased, and a rejuvenated material is obtained [18; 28]. Both thermal and mechanical history are captured by the single state parameter "S". This parameter thus describes aging and effectively determines the value of the yield stress as a function of the time, temperature and stress. The state parameter is defined with respect to the fully rejuvenated material as a reference state ($S = 0$). The effects of aging and rejuvenation are combined through a simple multiplicative relation, i.e. $S = S_a \cdot R_\gamma$, where $S_a$ represents the aging kinetics, and $R_\gamma$ represents the rejuvenation kinetics.

In Chapter 2 [29] we showed that it is possible to predict the yield stresses, i.e. $S_a$, of injection molded products to a very good degree of agreement with experimental results. These predictions are based on a phenomenological approach in which we

assume that the kinetics of aging, measured by annealing treatments well below the glass transition temperature, $T_g$, and written in an analytical form, can be applied to the transient temperature history that follows from the injection molding process analysis [19]. By integration of the analytical formulation of the aging kinetics with respect to temperature, the local values of $S_a$ can be obtained. Since the annealing treatments were performed well below $T_g$ no equilibrium kinetics were taken into account (the increase in yield stress can not be endless; it will eventually arrive at its equilibrium value). The development of the yield stress was initiated when passing $T_g$, i.e. a fixed temperature point in this case. This is, however, far from reality. The glass transition temperature is not a single temperature point, but rather a temperature region in which the equilibrium melt falls from equilibrium [30]. Strongly coupled to these equilibrium kinetics is the phenomenon of physical aging.

Aging (and relaxation) of glassy polymers has attracted a lot of attention in literature, and a number of reviews are available [31–33]. Although aging and relaxation are used to describe time-dependent phenomena of a great variety of different properties, for example, volume, enthalpy, yield stress and viscoelastic properties, they are in nature the same. All are a result of the kinetically governed non-equilibrium state of the polymer below the glass transition temperature, which leads to time dependent behavior [30]. With respect to the modeling of aging phenomena, two main topics can be distinguished. The fist one is the development of mechanical properties during use, that is, properties as they result from processing are not modeled, but rather taken as an initial state of the material, and the evolution of properties over long periods of time are followed. Illustrative examples are the development of linear viscoelastic properties [34] and yield stress [27] as a function of elapsed time after quenching. The second topic is related to the modeling of the properties as they develop during different (often complex) thermal histories, that is, the evolution of properties through the $T_g$ region are followed and modeled. Examples of this approach can be found for volume and enthalpy relaxation, where a number of models are available that quite adequately describe the non-equilibrium kinetics [35–40]. To our knowledge, such an approach has never been attempted with respect to the development of yield stress. Bauwens-Crowet and Bauwens [27] used a one-parameter relaxation model approach to describe the increase in yield stress upon annealing, which was somewhat similar to the one-parameter modeling approach of Hutchinson and Kovacs [41] to describe the increase in enthalpy overshoot, but this approach is limited in its usability and can certainly not describe the development of yield stress as a result of processing conditions. Since it is the yield stress, and the related strain softening, that determines the failure, it is important to be able to accurately describe the aging kinetics of polymers and to use these kinetics to predict the yield stress distribution from processing conditions.

In this study we present a method to predict the yield stress as a function of thermal history as a result of processing conditions which incorporates the equilibrium kinetics associated with the glass transition. To do so we will adopt the TNM (Tool-Narayanaswamy-Moynihan [35; 36; 42]) formalism to describe the aging kinetics of the yield stress, or more correctly: the yield stress retardation.

## 3.2  Modeling

Structural relaxation models have been used successfully in the past to describe volume and enthalpy relaxation of amorphous polymers. The essence of these models is that they recognize the non-equilibrium state of an amorphous glass below the glass transition temperature and use the distance from equilibrium as a driving force for the relaxation kinetics. The two main approaches are the TNM (Tool-Narayanaswamy-Moynihan) model [36] and the KAHR (Kovacs-Aklonis-Hutchinson-Ramos) model [38]. Both are multiparameter models and are, in principle, equivalent. The TNM model uses the fictive temperature, $T_f$, as defined by Tool [42], to fully define the thermodynamic state of the material, whereas the KAHR model uses the distance of the property under investigation from its equilibrium value as a state parameter. Here, we will adopt the TNM model approach to describe the aging and equilibrium kinetics of amorphous polymers. Rather than directly describing the yield stress retardation we will apply the TNM model to the zero viscosity which is rate and loading geometry independent, unlike the yield stress itself, e.g. the yield stress measured in compression is not equal to the one measured in tension. Adaptation was done such that the model is applicable in a 3D constitutive model. Note that this so-called zero viscosity, the viscosity at zero shear rate, is associated to *segmental chain mobility* (related to yield), and should not be confused with the zero-shear viscosity used by rheologists to describe the *melt* viscosity at zero shear rate.

### TNM model

The TNM model uses a fictive temperature, $T_f$, to fully define the state of the material, and the difference between this fictive temperature and the current temperature is the force driving the non-equilibrium glass towards equilibrium. For a given property, P, (e.g. volume or enthalpy) at a given non-equilibrium temperature, T, the fictive temperature, $T_{f,P}$, can be seen as the equilibrium temperature at which this property has the same value as at the given non-equilibrium temperature, see Figure 3.1. The property P is given by:

$$
\begin{aligned}
P(T, \xi) &= P_e(T_0) + \alpha_{Pl} \cdot [T - T_0] + \alpha_{Ps} \cdot [T_f(T, \xi) - T] \\
&= P_e(T) + \alpha_{Ps} \cdot [T_f(T, \xi) - T]
\end{aligned}
\tag{3.1}
$$

where $\alpha_{Ps} = \alpha_{Pl} - \alpha_{Pg}$, and $\xi$ is the reduced time, defined later.

In Equation (3.1), $T_0$ is a temperature well above the glass transition temperature, $T_g$, $\alpha_{Pl}$ is the slope of property P in the liquid state, $\alpha_{Pg}$ is the slope of property P in the glassy state and $P_e$ signifies that P is in the equilibrium of the liquid state. The slopes of the liquid and glassy state are here assumed to be constant but can very well be
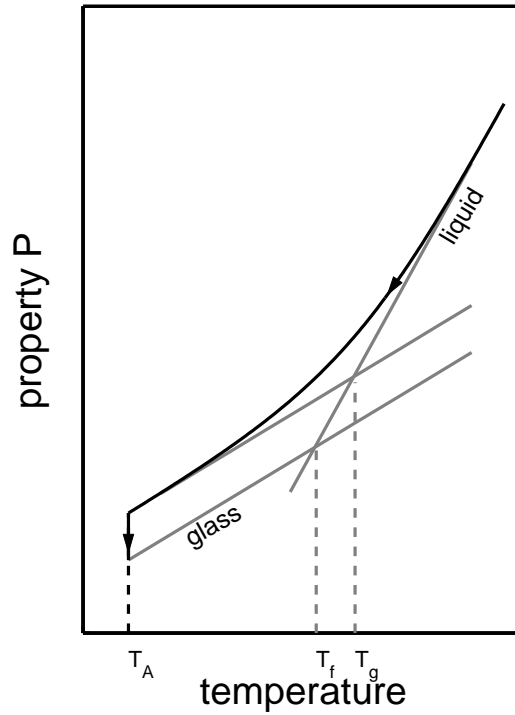
**Figure 3.1:** Non-equilibrium kinetics of property P and definition of fictive temperature, $T_f$, as a result of (transient) temperature and annealing temperature, $T_A$.

a function of temperature. In that case Equation (3.1) is written as:

$$P(T, \xi) = P(T, \infty) + \int_T^{T_f} \alpha_{Ps}(T')dT' \tag{3.2}$$

In the case of constant slopes, Equation (3.1), it is easily concluded that the relation basically describes two straight lines, i.e. the liquid state and the glass state, where the lines themselves depend on temperature, T. The fictive temperature, $T_f$, determines on which of the two curves we are at a specific temperature. The equilibrium state is here also called liquid state, although in the case of polymers, the nomenclature "the melt state" would also be appropriate (The TNM model finds its origins in the field of anorganic glasses, and therefore the term liquid is mostly used. We will use the terms liquid and melt here interchangeably).

The relaxation of property P now follows from the relaxation of the fictive temperature. This relaxation is equivalent in nature to stress relaxation and, therefore, can be described analogously. Assuming thermorheological simple behavior and using the linearity of the reduced time, the relaxation of the fictive temperature is given by:

$$T_f(T, \xi) = T - \int_0^\xi M_P(\xi - \xi') \frac{dT}{d\xi'} d\xi' \tag{3.3}$$

where $M_P$ is the relaxation function and $\xi$ the reduced time.

The relaxation function is defined by a stretched exponential to account for a distribution of relaxation times. This is not a true distribution in the form of a discrete spectrum as is used in the case of the KAHR model [38], but rather a mathematical convenient way which is mostly attributed to Kolhrausch [43], Williams and Watts [44]. The relaxation function and reduced time are given by, respectively:

$$M_P(\xi) = \exp\left(-\left(\frac{\xi}{\tau_{Pr}}\right)^\beta\right) \quad ; \quad \xi(t) = \tau_{Pr} \int_0^t \frac{dt'}{\tau_P(T, T_f)} \tag{3.4}$$

where $\tau_{Pr}$ is the relaxation time at a reference temperature, $\beta$ is a parameter which describes the nonexponentiality or width of the distribution of relaxation times and $\tau_P$ is the current relaxation time.

The widely and successfully used definition of the relaxation time, $\tau_P$, of the TNM model is applied here. This definition, however, lacks theoretical justification and reflects in essence a phenomenological approach. It should, however, be possible to use other definitions of the relaxation time which do have physical relevance, such as the Adam-Gibbs relation [45; 46].

The relaxation time, $\tau_P$, is defined by:

$$\tau_P(T, T_f) = A \exp\left(\frac{x\Delta H}{RT} + \frac{(1-x)\Delta H}{RT_f}\right) \tag{3.5}$$

where A is a pre-exponential factor, x defines the degree of nonlinearity, $\Delta H$ is the activation enthalpy and R the ideal gas constant.

## Application to the zero viscosity of segmental chain mobility

To describe the evolution of the yield stress we apply the structural relaxation kinetics to the zero viscosity as illustrated in Figure 3.2 (note that the *logarithm* of the viscosity is plotted versus the inverse of the temperature). For an uniaxial tensile test the relation between yield stress, $\sigma_y$, and zero viscosity, $\eta_0$, is given by:
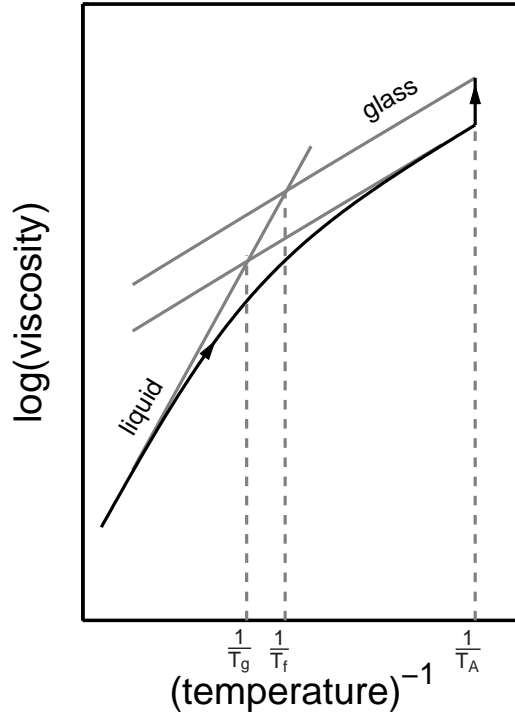
**Figure 3.2:** Non-equilibrium kinetics of the viscosity.

$$\sigma_y = \sigma_s + \sigma_r \tag{3.6}$$

$$\sigma_s = 3\eta\dot{\epsilon}_0 \quad ; \quad \sigma_r = G_r(\lambda_y^2 - \lambda_y^{-1}) \tag{3.7}$$

where $\sigma_s$ is the stress contribution arising from secondary interactions, $\sigma_r$ is the stress contribution of the entanglement network, $\eta$ is the stress- and pressure-dependent viscosity, $\dot{\epsilon}_0$ the strain rate applied, $G_r$ the strain-hardening modulus and $\lambda_y$ the draw ratio at yield. A more elaborate derivation is given in the Appendix.

The viscosity, $\eta$, is defined by:

$$
\begin{aligned}
\eta(T, p, \bar{\tau}, S) &= A_{rej}\tau_0\exp\left(\frac{\Delta U}{RT}\right)\exp\left(\frac{\mu p}{\tau_0}\right)\exp(S)\frac{\bar{\tau}/\tau_0}{\sinh(\bar{\tau}/\tau_0)} \\
&= \eta_0(T, p, S)\frac{\bar{\tau}/\tau_0}{\sinh(\bar{\tau}/\tau_0)}
\end{aligned}
\tag{3.8}
$$

where

$$S(t, T, \bar{\gamma}_p) = S_a(t, T) \cdot R_\gamma(\bar{\gamma}_p) \tag{3.9}$$

In Equation (3.8) p is the hydrostatic pressure, $\bar{\tau}$ the equivalent stress, S the state parameter, $A_{rej}$ a pre-exponential factor related to the rejuvenated state, $\tau_0$ the characteristic stress or modulus, $\Delta U$ the activation energy, and $\mu$ the pressure dependence. Equation (3.9) is already explained in the Introduction and basically describes the aging dependence of the viscosity through the function $S_a(t, T)$ and the rejuvenation dependence through $R_\gamma(\bar{\gamma}_p)$, where $\bar{\gamma}_p$ is the equivalent plastic strain. The definitions of the equivalent stress and equivalent plastic strain are given in the Appendix (Equations (3.25) and (3.26)).

The idea of using structural relaxation to describe the effect of physical aging on the yield stress is not new. Buckley [14] already proposed in his paper on the constitutive modeling of amorphous polymers to use the fictive temperature to describe the structural state of the material. In a later publication [15] he also added the notion that there should be an evolution contributed to the fictive temperature. The use of the fictive temperature by Buckley in this sense is the same as the use of the state parameter $S_a$ [19] to describe the thermo-mechanical history of the material as done here.

The use of structural relaxation models to describe the zero viscosity of a material is somewhat trivial, since the basis of these models is the relaxation kinetics as governed by the viscosity of the material. It is therefore surprising that not more use has been made of these models to describe aging phenomena of mechanical properties, such as the increase of yield stress with time, or to use them to predict the mechanical properties after a 'complex' thermal history, such as the thermal history resulting from processing.

Our constitutive model in its current form uses the rejuvenated state as a reference state. This is the state in which all effects of prior thermal history have been erased [13; 28]. Although the rejuvenated state is a well defined state from a mechanical viewpoint, from the viewpoint of structural relaxation and equilibrium kinetics this state is poorly defined and is the non-equilibrium state, furthest from equilibrium, which can only be attained by mechanical deformation. In practice, the value of $A_{rej}$ (see Equation (3.8)), which defines the rejuvenated state, is effectively an input parameter for the model and therefore known. To be able to fit the relaxation kinetics as derived in this study to the current constitutive framework, we will omit working from the rejuvenated state, and therefore will use $A_0(S_a) = A_{rej}\exp(S_a)$ for the pre-exponential parameter. To determine the value of the state parameter from the zero viscosity as it follows from the kinetics developed here will be a trivial exercise, which yields the following definition of the zero viscosity:

$$\eta_0(T, p, S_a) = A_0(S_a)\frac{RT}{V^*}\exp\left(\frac{\Delta U + \mu p V^*}{RT}\right) \tag{3.10}$$

where $\tau_0 = \frac{RT}{V^*}$ has been substituted to account for the temperature dependence of the characteristic stress, and $V^*$ is the specific activation volume. Note that S has been replaced by $S_a$, since we are only interested in the initial yield stress and thus $R_\gamma(\bar{\gamma}_p)$ is not yet developing, assuming that plastic deformation only starts to develop after the point of yield.

To use the structural relaxation framework for the zero viscosity we need the temperature dependence of the zero viscosity both above and below the glass transition temperature. The temperature dependence of the non-equilibrium viscosity below $T_g$ is known to follow an Arrhenius form. Well above $T_g$ (in the range of $T_g + 10°C < T_g < T_g + 100°C$) the temperature dependence of the equilibrium polymer melt in general follows VTF (Vogel-Tammann-Fulcher) or WLF (Williams-Landel-Ferry) behavior [30; 47]. Since we are interested in the mechanical properties as they develop below $T_g$ as a result of non-equilibrium kinetics, the correct description of the temperature dependence of the viscosity well above $T_g$ is not relevant here. In the transition region, however, it was shown [48; 49] that the temperature dependence of the equilibrium glass shifts towards an Arrhenius dependence. This Arrhenius behavior of the equilibrium glass was verified only in a temperature window of a couple of tens of degrees below $T_g$, since below, relaxation times become large and equilibrium can not be obtained on an experimentally acceptable timescale. In Chapter 2 [29] we showed that all structure development takes place in a temperature window of approximately $T_g > T > T_g - 20/30°C$. The use of an Arrhenius type of temperature dependence of the equilibrium viscosity below $T_g$ therefore appears to be acceptable.

Using the Arrhenius type of temperature dependence of the zero viscosity both in the liquid state, $\Delta U_l$, as in the glassy state, $\Delta U_g$, and assuming that $\Delta U \gg \mu p V^*$, Equation (3.1) in combination with Equation (3.10) can be rewritten to:

$$\ln(\eta_0(T, \xi)) = \ln\left(\frac{A_0(S_a)R}{V^*}\right) + \ln(T) + \left(\frac{\Delta U_l}{R}\right)\frac{1}{T}$$
$$+ \left(\frac{\Delta U_l - \Delta U_g}{R}\right)\left(\frac{1}{T_f(\xi)} - \frac{1}{T}\right) \tag{3.11}$$

where the first three terms on the right hand side correspond to $P_e(T)$ and the last term to $\alpha_{Ps} \cdot [T_f - T]$.

Together, Equations (3.3), (3.4), (3.5) and (3.11) form the basis of the framework which is needed to apply the concept of structural relaxation to the zero viscosity. Now the appropriate input parameters for the model need to be determined.

## 3.3  Experimental

Tensile bars were directly injection molded, or alternatively machined from injection-molded plates. Both type of bars were made from the same grade of polycarbonate, Lexan 141R, supplied by Sabic Innovative Plastics (Bergen op Zoom). Before injection molding, the polycarbonate was dried under vacuum at 80℃ for a period of 24 hours. All injection molding was performed on an Arburg 320S all-rounder 500-150.

The molded tensile bars were shaped according to the ISO 527 norm. The mold, manufactured by Axxicon Mould Technology (Helmond, the Netherlands), was kept on a temperature of 90℃. These specimen were used for anneal ing experiments close to $T_g$. The samples were pre-dried at 80℃ for 24 hours, and subsequ ently annealed in an Heraeus hot air circulation oven at 135℃, 140 ℃ and 145℃ for times up till 9 days. Before testing samples were allowed to cool to room temperature.



parallel    perpendicular
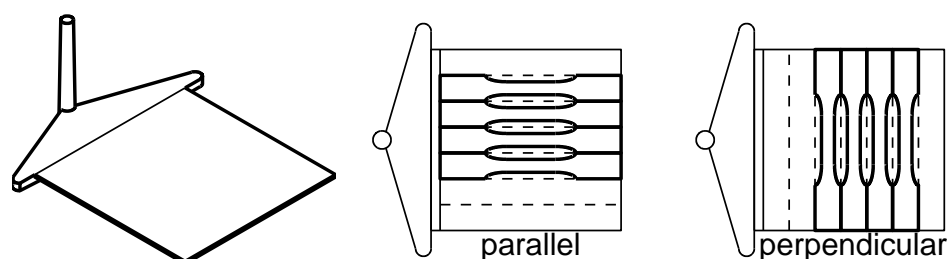
**Figure 3.3:** Injection molded plate and tensile specimen machined thereof.

Next to the tensile bars, rectangular plates with dimensions $70 \times 7 \times 1$ mm$^3$ and $70 \times 70 \times 4$ mm$^3$ were injection molded , see Figure 3.3. The mold (again from Axxicon Mould Technology) had a V-shaped runner of 4 mm thickness and an entrance of $70 \times 1$ mm$^2$ for the 1 mm thick plates and an entrance of $70 \times 2$ mm$^2$ for the 4 mm thick plates. The shape of the runner in combination with the entrance size caused the material to fill the cavity uniformly along the width of the cavity, which was proven by several short shot experiments. Melt temperature was set to 280℃ and injection rates were 90 cc/s and 50 cc/s for the 1 mm and 4 mm plates respectively. A packing pressure of 500 bar was used to minimize shrinkage. Variation of the packing pressure from 25 bar to 900 bar proved to have no effect on the measured properties of the plates. To investigate the influence of the temperature history, the mold cavity temperature was varied from 30℃ to 130℃ in steps of 10℃. Co oling times were 60 s and 150 s for the 1 mm and 4 mm thick plates respectively. From the 1 mm thick injection-molded plates, rectangular bars of $70 \times 10$ mm$^2$ were cut parallel and perpendicular to the flow direction. From the 4 mm thick plates, bars were only taken parallel to the flow direction. Gauge sections of $33 \times 5$ mm$^2$ were then machined into these bars, see Figure 3.3 (right).

Uniaxial yield stresses for both specimen geometries were determined on a Zwick Z010 universal tensile tester. All measurements were performed at a linear strain

rate of $10^{-3}$ s$^{-1}$. The measured engineering yield stress was converted to true yield stress under the assumption of incompressibility up to the point of yield.

# 3.4  Numerical

## Numerical implementation

The evolution of the zero viscosity for the injection-molded tensile bars was calculated assuming constant cooling rates and homogeneous temperature conditions. This was done because the exact processing conditions for these bars were unknown. Furthermore the annealing process can be considered as an isothermal process in which no temperature distributions exist in the samples. Calculations were performed by evaluation of Equations (3.3), (3.4), (3.5) and (3.11). For a detailed description of the numerical implementation of the TNM model the reader is referred to [39]. Temperature histories for the rectangular plates were obtained by means of numerical simulation of the injection molding process using the commercial injection molding simulation package Moldflow MPI (release 5.0). A 2.5D approach was used since the width versus thickness ratio of the plates is very high, i.e. pressures are calculated 2D and the temperature and velocity field fully 3D. Process variables were taken the same as mentioned in the experimental section. Material properties of Lexan 141R were taken from the standard Moldflow library. The Moldflow simulations provided temperature histories for a number of layers over the thickness of the sample. The calculated thermal histories were exported and post-processed (Matlab) to determine the evolution of the zero viscosity using Equations (3.3), (3.4), (3.5) and (3.11). The temperature histories of the surface layers could not be used since cooling was so fast that at the first increment temperatures were already below $T_g$, see Figure 3.8.

## Numerical strategy

The numerical results are obtained using a set of relaxation time parameters that were obtained by applying an optimization routine, nonlinear least-squares, to the yield stress results of the annealing treatments (Figure 3.6) and the injection-molded samples of 1mm thickness (Figure 3.9). The parameter set is given in Table 3.2. All model descriptions and predictions are made with this single parameter set. The results for the 4mm thick injection molding samples are true predictions.

## 3.5  Results

### Determination of the non-equilibrium temperature dependence

To derive the temperature dependency of the zero viscosity in the glassy state, use is made of literature results of yield stress versus strain rate measured at different temperatures for two different material states, Bauwens-Crowet and Bauwens [27], see Figure 3.4 and similar data measured by Klompen [50]. Furthermore, data by Bauwens-Crowet et al. [51] of yield stress versus temperature over a large temperature range (from -120℃ to +120℃), measured at a single stra in rate, are used.
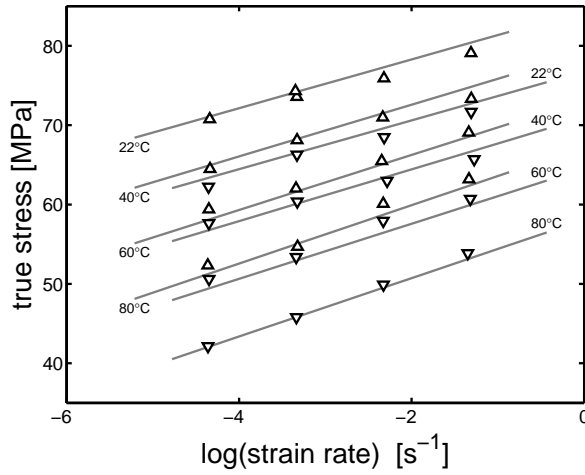


**Figure 3.4:** Yield stress versus strain rate at different temperatures (as indicated) and for two different initial material states; as-received ($\triangledown$) and annealed ($\triangle$); lines are a guide to the eye, taken from [27].

Using the 3D constitutive framework and the boundary conditions that apply to uni-axial extension under constant strain rate, the following relation can be derived to determine the zero viscosity from uniaxial yield stresses:

$$\eta_0 = \frac{RT}{V^*} \frac{1}{\sqrt{3}} \frac{1}{\dot{\epsilon}_0} \sinh \left( \frac{\sigma_y - \sigma_r(\lambda_y)}{\sqrt{3}} \frac{V^*}{RT} \right) \tag{3.12}$$

where $\dot{\epsilon}_0$ is the strain rate applied, $\sigma_y$ the yield stress and $\sigma_r(\lambda_y)$ the hardening contribution at the point of yield. For a complete derivation of this experimental relation the reader is referred to the Appendix.

To be able to apply this relation, a number of parameters is required. Most parameters are taken to be the same as used Chapter 2 [29], see Table 3.1, but the determination of the activation energy and activation volume is done here again, since the literature values gave unsatisfactory results.

**Table 3.1:** Material parameters obtained for polycarbonate [19]

| | polycarbonate | |
|---|---|---|
| K | 3750 | [MPa] |
| G | 308 | [MPa] |
| $A_{rej}$ | $3.0 \cdot 10^{11}$ | [s] (@295K) |
| $\mu$ | 0.08 | [-] |
| $S_a$ | – | [-] |
| $r_0$ | 0.965 | [-] |
| $r_1$ | 50 | [-] |
| $r_2$ | -5 | [-] |
| $G_r$ | 26 | [MPa] |

By using the temperature dependence of the zero viscosity as follows from Equation (3.10) an activation energy, $\Delta U$ of 326 kJ/mol is found. The activation volume is determined from the yield stresses, and is found to be $3.50 \cdot 10^{-3}$ m$^3$/mol. These values are in good agreement with literature values [27; 50; 52], although the activation energy is slightly higher.
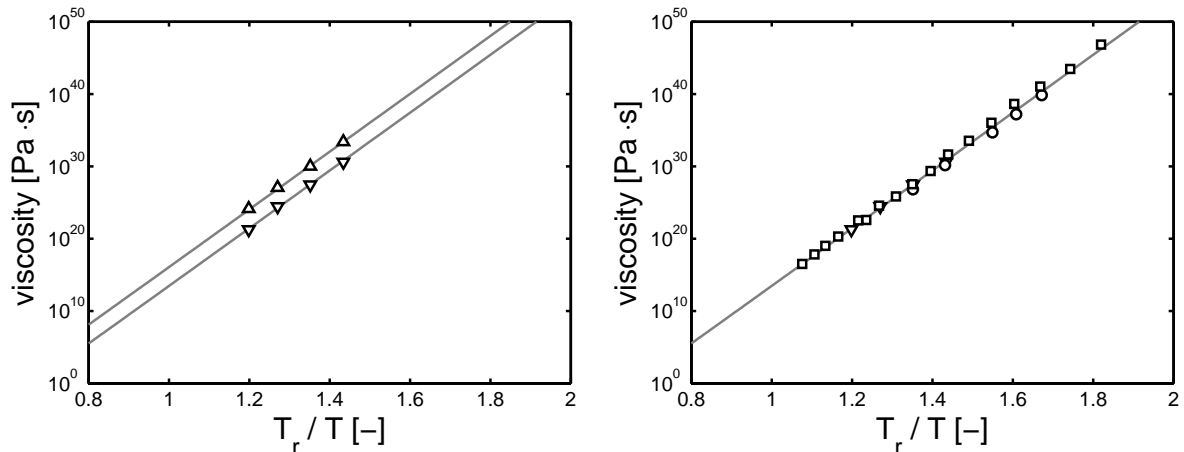


**Figure 3.5:** Left: Zero viscosities determined from the yield data of Figure (3.4); two different initial material states: quenched ($\triangledown$) and annealed ($\triangle$). Lines are Arrhenius fits with an activation energy of 326 kJ/mol. Right: Zero viscosities determined form yield data of Bauwens [27; 51] ($\square$, $\triangledown$) and Klompen [50] ($\bigcirc$), showing good correspondence of the temperature dependency between different studies for quenched material.

Applying Equation (3.12) to the yield stresses of Figure 3.4 gives the zero viscosities as shown in Figure 3.5 (left). Note that since the zero viscosity is strain-rate independent, the four different strain rates per temperature reduce to one zero viscosity. $T_r$ is an arbitrary reference temperature and is taken to be 150°C; a literature value for the glass transition temperature of polycarbonate. The temperature dependency for the different initial material states can be seen to be the same. In Figure 3.5 (right) the literature yield data of Bauwens-Crowet et al. [51] and Klompen [53] are added. It can be seen that all the yield data result in zero viscosities which are in good agreement with each other over a wide temperature range.

## Determination of the equilibrium temperature dependence

To determine the temperature dependence of the zero viscosity in the liquid state, use is being made of equilibrium yield data as measured by performing annealing experiments close to $T_g$, see Figure 3.6. Equilibrium data implies the plateau values of the yield stress which are obtained after annealing up to equilibrium. Similar plateaus are found in literature for the enthalpy overshoot for polycarbonate [54] and polystyrene [55; 56] when they are annealed for long periods at temperatures not too far below $T_g$.
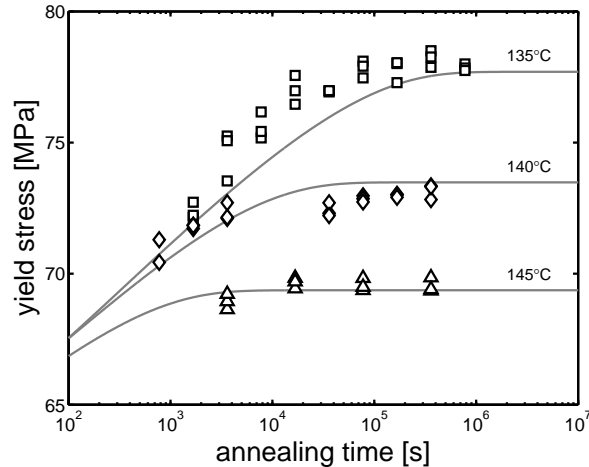


**Figure 3.6:** Yield stress versus annealing time for three different annealing temperatures; 135°C ( □ ), 140°C ( ◊ ) and 145°C ( △ ); solid lines are model predictions.

Since the yield stresses are measured at room temperature they must be shifted back to the elevated temperatures at which equilibrium was obtained. This can be done by rewriting Equation (3.10) with respect to two temperatures, giving the ratio between the viscosities at those temperatures:

$$\frac{\eta_0(T_1)}{\eta_0(T_2)} = \frac{T_1}{T_2} \exp\left(\left(\frac{\Delta U_g + \mu p V^*}{R}\right)\left(\frac{1}{T_1} - \frac{1}{T_2}\right)\right) \tag{3.13}$$

since $\Delta U_g \gg \mu p V^*$ this reduces to:

$$\frac{\eta_0(T_1)}{\eta_0(T_2)} = \frac{T_1}{T_2} \exp\left(\frac{\Delta U_g}{R}\left(\frac{1}{T_1} - \frac{1}{T_2}\right)\right) \tag{3.14}$$

where $\Delta U_g$ is the activation energy of the glassy state.
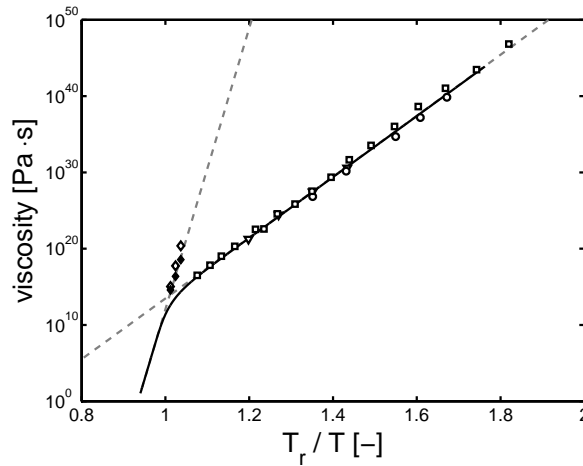


**Figure 3.7:** Equilibrium zero viscosities derived from the equilibrium yield stresses of Figure 3.6 (♦) and equilibrium zero viscosities taken from [27] (◊); dashed lines are Arrhenius fits, and the solid line is a model prediction.

In Figure 3.7 the values for the equilibrium viscosities as determined from our own annealing experiments are shown (closed symbols), as well as values for the equilibrium viscosities which were determined from literature equilibrium yield stresses measured by Bauwens-Crowet and Bauwens [27] (open symbols). An activation energy of 1.50 MJ/mol is found for our equilibrium viscosities, whereas the activation energy of the literature values seems somewhat higher. Since the exact experimental conditions and data of the literature equilibrium values are unknown, we do not want to speculate as to where the difference in activation energies comes from. Possible molecular weight effects, for instance, should be examined in the future. For all model predictions the equilibrium activation energy of 1.50 MJ/mol was used.

Now that the temperature dependencies of both the equilibrium glass and the non-equilibrium glass are established, we have a framework which allows us to apply structural relaxation to the zero viscosity. From the evolution of the zero viscosity, we should be able to predict the development of the yield stress as a result of processing conditions. The parameters which describe the relaxation times which dominate the zero viscosity are found by means of an optimization routine applied to both annealing and processing results and are given in Table 3.2:

**Table 3.2:** TNM model parameters

| Zero viscosity parameters | | |
|---|---|---|
| $\Delta U_l$ | 1.50 | [MJ/mol] |
| $\Delta U_g$ | 326 | [kJ/mol] |
| $V^*$ | $3.5 \cdot 10^{-3}$ | [m³/mol] |
| TNM parameters | | |
| $\ln(A)$ | $-247.6$ | [s] |
| x | 0.25 | [-] |
| $\Delta H$ | 865.4 | [kJ/mol] |
| $\beta$ | 0.54 | [-] |

## Annealing experiments up to equilibrium

Tensile bars were annealed up to equilibrium, see Figure 3.6. To predict these annealing results, constant cooling and heating rates have been assumed. It was shown, however, that the final equilibrium curves (the total curves depicted in Figure 3.6) are not influenced by the processing conditions. Different cooling rates will result in different non-equilibrium yield stresses, but when annealing is performed at temperatures close to $T_g$ up to equilibrium, where the relaxation times are much shorter, the final response is hardly influenced by the prior thermal history. As can be seen, the model descriptions fit the experimental results well.

## Prediction from the injection molding process

Figure 3.8 shows the predicted distribution of the yield stress over the thickness of the sample for various mold temperatures. The values at the surface layers could not be calculated due to the limited temperature information at these positions. Already in the first time-increment of the simulations the surface layers adopt a temperature below $T_g$, making an evolution through the transition region impossible. It can be seen that with increasing mold temperature a more uniform stress distribution is obtained.
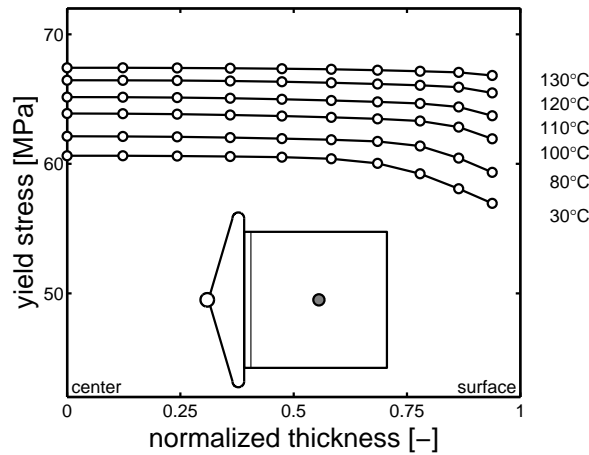
**Figure 3.8:** Distribution of the yield stress over the normalized thickness of the injection molded samples for various mold temperatures.

These results are in qualitative agreement with the results of yield stress distribution in Chapter 2 [29].
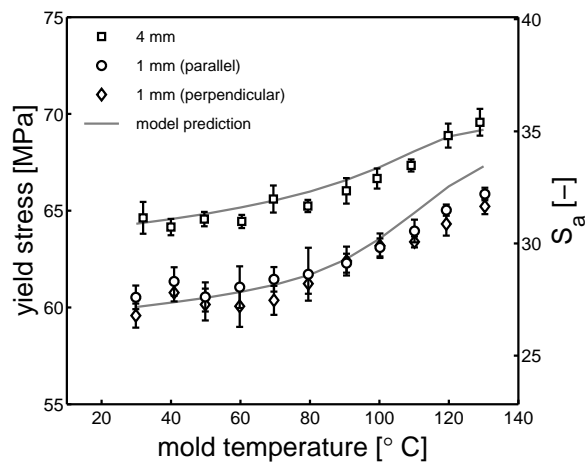


**Figure 3.9:** Experimental yield stresses for samples 4 mm thick (□) and 1 mm thick (○), versus model predictions (lines).

From the yield stress distributions over the thickness of the samples an area-weighted yield stress can be calculated. The resulting average yield stresses versus mold temperatures, ranging from 30℃ to 130℃ are given in Fi gure 3.9. For the 1mm thick samples, yield stresses both parallel and perpendicular to the flow direction are shown, whereas for the 4 mm thick samples only yield stresses parallel to the flow direction are shown. From the results of the 1 mm thick samples it can be seen that there is a minor influence of orientation ($< 0.5$ MPa on average), given the difference between the results of the yield stresses parallel and perpendicular to flow. However, it has to be noted that the processing conditions for the 1 mm thick samples are the

most extreme as to expected differences in yield stresses due to molecular orientation. Therefore the influence of orientation is omitted in this study and isotropic conditions are assumed.

As noted earlier, the parameter set used in this study was obtained by a fitting routine on both the annealing results of Figure 3.6 and the results for the 1 mm thick samples of Figure 3.9. The discrepancies between model descriptions and experimental results for the 1 mm thick samples are a direct result of using two data sets. The annealing results pose somewhat different demands on the parameters than the processing results. The model results for the 4 mm thick samples of Figure 3.9 are, however, true predictions.

It is interesting to see that slope of the predicted yield stress versus mold temperature shows a decrease at 130°C for both sample thicknesses. This d ecrease in slope can also be seen in the experimental results. The decrease can be attributed to the fact that at high mold temperatures the yield stress is still evolving when the product is ejected from the mold. The rapid cooling on air, which then follows, prohibits further evolution of the yield stress.

## Application to annealing

In Figure 3.10 (right) the literature zero viscosities of Figures 3.5 and 3.7 are reproduced. The solid lines in this figure are model predictions and the dotted line is the equilibrium state. The model predictions are, since the thermal histories of the samples are unknown, calculated by using constant cooling rates. Effectively the initial cooling rate, from point A to point B, was used as a fitting parameter. To predict the right values for the quenched zero viscosities in the glassy state a cooling rate of 1.0°C/s was used, which is a quite realistic cooling rate.
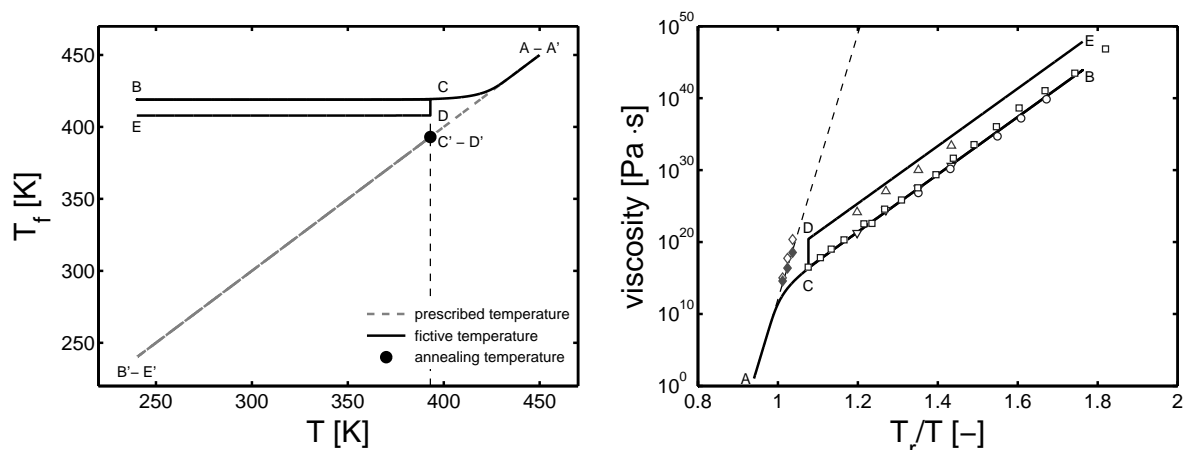


**Figure 3.10:** Left: Fictive temperature versus prescribed temperature; cooling and heating rates are constant. Right: Corresponding evolution of the viscosity as a function of the prescribed temperature history

In Figure 3.10 (left) the evolution of the fictive temperature, $T_f$ versus the applied temperature corresponding to the evolution of the zero viscosity of Figure 3.10 (right) can be seen. The prescribed temperature history starts at an initial temperature, $T_0$, well above $T_g$ (A'). In the equilibrium state the fictive temperature is equal to the prescribed temperature (A = A'). First a constant cooling rate of 1.0°C/s is applied (B , B'). As soon as the relaxation times become too long, it can be seen that the fictive temperature deviates from the prescribed temperature and remains almost constant. Next an annealing period of several years is applied, but since the relaxation times are extremely long at such low temperatures there is no effect on the fictive temperature. Subsequently, an annealing step is applied, in which the temperature is increased with a constant heating rate of 1°C/s to an annealing temperature of 120°C (B'-C'). The annealing period was 46 hours, exactly t he same as the one Bauwens-Crowet and Bauwens used experimentally. During this annealing period the fictive temperature can be seen to evolve towards equilibrium (C-D). Finally a last cooling step is applied (D'-E'). The resulting predictions for the annealed zero viscosities can be seen to be slightly higher then the experimental values corresponding to an overestimation of the yield stress, see Figure 3.10 (right).

## Discussion

It is shown that the yield stresses as a result of processing conditions, i.e. mold temperature, can be predicted in good agreement with experimental results. The yield stress as a result of an annealing treatment can also be described quite satisfactory in a temperature window of 10-20°C below $T_g$. At temperatures further below $T_g$ model predictions showed to be in less agreement with experimental findings (see Figure 3.10 right-hand-side). This could however be expected, since the TNM model is reported to be valid only in a small temperature window of a couple of tens of degrees around $T_g$.

Further we want to note that the parameter set which was obtained in this study to describe the retardation of the zero viscosity, see Table 3.2, is different from the parameter set found by Hodge [57] to describe the enthalpy relaxation of polycarbonate by means of DSC measurements. This indicates that the time scale of zero viscosity retardation is different from the time-scale of enthalpy relaxation. Differences in relaxation time scales for different structural properties have been a topic of discussion in many different studies and it is generally accepted that time scales are different [31; 40]. We only wish to mention here that, although the time scales are different, the nonlinearity parameter, x, and the nonexponentiality parameter, $\beta$, show to be, within experimental uncertainty, the same as the ones found by Hodge [57]. This suggests a possible relation between the relaxation time spectrum of both processes. It was already shown by Adam et al. [58] and Bauwens-Crowet and Bauwens [27] that the increase in yield stress and the increase in enthalpy overshoot are qualitatively related. It should proof interesting to determine to what degree parameters from enthalpy relaxation studies can be used for the prediction of zero viscosity retardation.

## 3.6 Conclusions

The TNM structural relaxation model has been successfully applied to the retardation of the zero viscosity of polycarbonate to predict the evolution of the yield stress. It is shown that by means of simulation of the injection molding process and the thermal histories derived thereof, the yield stress resulting from processing can be predicted for a simple geometry. Furthermore, it is shown that annealing of polycarbonate up to equilibrium in a temperature region close to $T_g$ can be described as well. Annealing at lower temperatures, however, showed to be described less well.

The ability of predicting the yield stress of a product based only on the thermal history as a result of processing, obtained through simulation of this process, opens new routes to true optimization of polymer products. The knowledge of the yield stress of a product showed to be enough to numerically predict its long-term static fatigue lifetime [26]. Currently work is being performed to explore the capabilities of numerical prediction of dynamic loading conditions and impact conditions. If all aspects of polymer failure can be accounted for by means of numerical simulation of the processing step and the subsequent numerical evaluation of the loading conditions, a product can be designed for performance without ever doing a single experiment.

## References

[1] W.B. Young. Three dimensional analysis of shape deformation in injection molded optical lens. *International Polymer Processing*, 19(1):70–76, 2004.

[2] S. Ni. Reducing shrinkage and warpage for printer parts by injection molding simulation analysis. *Journal of Injection Molding Technology*, 6(3):177–186, 2002.

[3] H.E.H. Meijer. *Processing of polymers*, volume 18 of *Materials Science and Technology. A comprehensive treatment*, chapter Processing for properties, pages 3–75. Wiley-VCH, 1997.

[4] H. Niklas and H.H. Kausch von Schmeling. Molekularstruktur und mechanische Eigenschaften von Polyvinylchloride III. Mitteilung: Ursachen zeitabhängiger Festigkeitseigenschaften von PVC-Rorhen. *Kunstoffe*, 53:886–891, 1963.

[5] D.H. Ender and R.D. Andrew. Cold drawing of polystyrene under dead load. *Journal of Applied Physics*, 36:3057–3062, 1965.

[6] R.M. Ogorkiewicz and A.A.M. Sayigh. The strength of rigid PVC. *British Plastics*, 7:126–128, 1967.

[7] K.V. Gotham. Long-term strength of thermoplastics: the ductile-brittle transition in static fatigue. *Plastics & Polymers*, 40:59–64, 1972.

[8] D.J. Matz, W.G. Guldemond, and S.L. Cooper. Delayed yielding in glassy polymers. *Journal of Polymer Science, Polymer Physics Ed.*, 10:1917–1930, 1972.

[9] I. Narisawa, M. Ishikawa, and H. Ogawa. Delayed yielding in polycarbonate un-

der constant load. *Journal of Polymer Science, Polymer Physics Ed.*, 16:1459–1470, 1978.

[10] H.G.H. van Melick, L.E. Govaert, and H.E.H. Meijer. Localisation phenomena in glassy polymers: influence of thermal and mechanical history. *Polymer*, 44:3579–3591, 2003.

[11] M.C. Boyce, D.M. Parks, and A.S. Argon. Large inelastic deformation of glassy polymers, Part I: Rate dependent constitutive model. *Mechanics of Materials*, 7(1):15–33, 1988.

[12] E.M. Arruda and M.C. Boyce. Evolution of plastic anisotropy in amorphous polymers during finite straining. *International Journal of Plasticity*, 9(6):697–720, 1993.

[13] O.A. Hasan, M.C. Boyce, X.S. Li, and S. Berko. An investigation of the yield and post-yield behavior and corresponding structure of poly(methyl methacrylate). *Journal of Polymer Science, Part B: Poymer Physics*, 31(2):185–197, 1993.

[14] C.P. Buckley and D.C. Jones. Glass-rubber constitutive model for amorphous polymers near the glass transition. *Polymer*, 36(17):3301–3312, 1995.

[15] C.P. Buckley, P.J. Dooling, J. Harding, and C. Ruiz. Deformation of thermosetting resins at impact rates of strain. part 2: constitutive model with rejuvenation. *Journal of Mechanical Physics of Solids*, 52(10):2355–2377, 2004.

[16] J.J. Wu and C.P. Buckley. Plastic deformation of glassy polystyrene: A unified model of yield and the role of chain length. *Journal of Polymer Science, Part B: Polymer Physics*, 42(11):2027–2040, 2004.

[17] T.A. Tervoort, E.T.J. Klompen, and L.E. Govaert. A multi-mode approach to finite, three-dimensional, non-linear viscoelastic behavior of polymer glasses. *Journal of Rheology*, 40:779–797, 1996.

[18] L.E. Govaert, P.H.M. Timmermans, and W.A.M. Brekelmans. The influence of intrinsic strain softening on strain localization in polycarbonate: Modelling and experimental validation. *Journal of Engineering Materials and Technology*, 122:177–185, 2000.

[19] E.T.J. Klompen, T.A.P. Engels, L.E. Govaert, and H.E.H Meijer. Modelling of the post-yield response of glassy polymer: Influence of thermomechanical history. *Macromolecules*, 38(16):6997–7008, 2005.

[20] M.C. Boyce and E.M. Aruda. An experimental and analytical investigation of the large strain compressive and tensile response of glassy polymers. *Polymer Engineering and Science*, 30(20):1288–1298, 1990.

[21] M.C. Boyce, E.M. Aruda, and R. Jayachandran. The large strain compression, tension, and simple shear of polycarbonate. *Polymer Engineering and Science*, 34(9):716–725, 1994.

[22] P.D. Wu and E. van der Giessen. On neck propagation in amorphous glassy polymers under plane strain tension. *International Journal of Plasticity*, 11:211–235, 1995.

[23] H.G.H. van Melick, L.E. Govaert, and H.E.H. Meijer. Prediction of brittle-to-ductile transitions in polystyrene. *Polymer*, 44:457–465, 2003.

[24] H.E.H. Meijer and L.E. Govaert. Multi-scale analysis of mechanical properties of amorphous polymer systems. *Macromolecular Chemistry and Physics*, 204:274–288, 2003.

[25] L.E. Govaert, E.T.J. Klompen, and H.E.H. Meijer. A novel approach to creep rupture in glassy polymers. In *proceedings of the 12th international conference of deformation yield and fracture of polymers*, pages 21–24. Institute of materials, 2003.

[26] E.T.J. Klompen, T.A.P. Engels, L.C.A. van Breemen, P.J.G. Schreurs, L.E. Govaert, and H.E.H. Meijer. Quantitative prediction of long-term failure of polycarbonate. *Macromolecules*, 38(16):7009–7017, 2005.

[27] C. Bauwens-Crowet and J.C.Bauwens. Annealing of polycarbonate below the glass transition: Quantitative interpretation of the effect on yield stress and differential scanning calorimetry measurements. *Polymer*, 23:1599–1604, 1982.

[28] H.G.H. van Melick, L.E. Govaert, B. Raas, W.J. Nauta, and H.E.H. Meijer. Kinetics of ageing and re-embrittlement of mechanically rejuvenated polystyrene. *Polymer*, 44:1171–1179, 2003.

[29] L.E. Govaert, T.A.P. Engels, E.T.J. Klompen, G.W.M. Peters, and H.E.H. Meijer. Processing induced properties in glassy polymers: Development of the yield stress in polycarbonate. *International Polymer Processing*, XX(2):170–177, 2005.

[30] G.B. McKenna. *Comprehensive Polymer Science, vol 2: Polymer Properties*, chapter Glass Formation and Glassy Behavior, pages 311–362. Pergamon Press, Oxford, 1989.

[31] J.M. Hutchinson. Physical aging of polymers. *Progress in Polymer Science*, 20:703–760, 1995.

[32] I.M. Hodge. Enthalpy relaxation and recovery in amorphous materials. *Journal of Non-Crystalline Solids*, 169:211–266, 1993.

[33] C.A. Angell, K.L. Ngai, and G.B. McKenna. Relaxation in glassforming liquids and amorphous solids. *Journal of Applied Physics*, 88(6):3113–3157, 2000.

[34] L.C.E. Struik. *Physical aging of amorphous polymers and other materials*. Elsevier, Amsterdam, 1978.

[35] O.S. Narayanaswamy. Model of structural relaxation in glass. *Journal of the American Ceramic Society*, 54(10):491–498, 1971.

[36] C.T. Moynihan, P.B. Macedo, C.J. Montrose, P.K. Gupta, M.A. DeBolt, J.F. Dill, B.E. Dom, P.W. Drake, A.J. Easteal, P.B. Elterman, R.P. Moeller, H. Sasabe, and J.A. Wilder. Thermodynamic and transport properties of liquids near the glass transition temperature. Structural relaxation in vitreous materials. *Annals of the New York Academy of Sciences*, 279(Glass Transition Nat. Glassy State):15–35, 1976.

[37] M.A. DeBolt, A.J. Easteal, P.B. Macedo, and C.T. Moynihan. Analysis of structural relaxation in glass using rate heating data. *Journal of the American Ceramic Society*, 59(1-2):16–21, 1976.

[38] A.J. Kovacs, J.J. Aklonis, J.M. Hutchinson, and R. Ramos. Isobaric volume and

enthalpy recovery of glasses. (II). A transparent multiparameter theory. *Journal of Polymer Science: Polymer Physics Edition*, 17:1097–1162, 1979.

[39] I.M. Hodge and A.R. Berens. Effects of annealing and prior history on enthalpy relaxation in glassy polymers. 2. Mathematical modeling. *Macromolecules*, 15:762–770, 1982.

[40] G.W. Scherer. *Relaxation in glass and composites*. Krieger Publishing Company, 1986.

[41] J.M. Hutchinson and A.J. Kovacs. A simple phenomenological approach to the thermal behavior of glasses during uniform heating or cooling. *Journal of Polymer Science: Polymers Physics Edition*, 14:1575–1590, 1976.

[42] A.Q. Tool. Relation between inelastic deformability and thermal expansion of glass in its annealing range. *Journal of American Ceramic Society*, 29:240–253, 1946.

[43] F. Kohlrausch. *Annalen der Physik und Chemie*, 128:1–20,207–227,399–419, 1866.

[44] G. Williams and D.C. Watts. Non-symmetrical dielectric relaxation behavior arising from a simple empirical decay function. *Transactions of the Faraday Society*, 66:80–85, 1970.

[45] G. Adam and J.H. Gibbs. On the temperature dependence of cooperative relaxation properties in glass-forming liquids. *The Journal of Chemical Physics*, 43(1):139–146, 1965.

[46] I.M. Hodge. Effects of annealing and prior history on enthalpy relaxation in glassy polymers. 6. Adam-Gibbs formulation of nonlinearity. *Macromolecules*, 20:2897–2908, 1987.

[47] J.D. Ferry. *Viscoelastic Properties of Polymers*. John Wiley & Sons, 3rd edition, 1980.

[48] P.A. O'Connell and G.B. McKenna. Arrhenius-type temperature dependence of the segmental relaxation below $T_g$. *Journal of Chemical Physics*, 110(22):11054–11060, 1999.

[49] D. Cangialosi, M. Wubbenhorst, H. Schut, A. van Veen, and S.J. Picken. Dynamics of polycarbonate far below the glass transition temperature: A positron annihilaiton lifetime study. *Physical Review B*, 69:134206, 2004.

[50] E.T.J. Klompen. *Mechanical properties of solid polymers. Constitutive modelling of long and short term behaviour*. PhD thesis, Eindhoven University of Technology, 2005. Chapter 3.

[51] C. Bauwens-Crowet, J.C. Bauwens, and G. Homès. The temperature dependence of yield of polycarbonate in uniaxial compression and tensile tests. *Journal of Materials Science*, 7:176–183, 1979.

[52] C. Ho Huu and T. Vu-Khanh. Effects of physical aging on yielding kinetics of polycarbonate. *Theoretical and applied fracture mechanics*, 40:75–83, 2003.

[53] E.T.J. Klompen and L.E. Govaert. Nonlinear viscoelastic behaviour of thermorheologically complex materials - a modelling approach. *Mechanics of Time-Dependent Materials*, 3:49–69, 1999.

[54] C. Bauwens-Crowet and J.C. Bauwens. Annealing of polycarbonate below the glass transition temperature up to equilibrium: A quantitative interpretation of enthalpy relaxation. *Polymer*, 27:709–713, 1985.

[55] S.L. Simon, J.W. Sobieski, and D.J. Plazek. Volume and enthalpy recovery of polystyrene. *Polymer*, 42:2555–2567, 2001.

[56] J. Rault. Ageing of glass: role of the Vogel-Fulcher-Tammann law. *Journal of Physics: Condensed Matter*, 15:S1193–S1213, 2003.

[57] I.M. Hodge. Effects of annealing and prior history on enthalpy relaxation in glassy polymers. 4. Comparison of five polymers. *Macromolecules*, 16:898–902, 1982.

[58] G.A. Adam, A. Cross, and R.N. Haward. The effect of thermal pretreatment on the mechanical properties of polycarbonate. *Journal of Materials Science*, 10:1582–1590, 1975.

[59] H. Eyring. Viscosity, plasticity, and diffusion as examples of absolute reaction rates. *Journal of Chemical Physics*, 4:283–295, 1936.

# 3.A  Appendix

In the 3D constitutive model the total stress is the sum of two contributions; a driving stress, $\sigma_s$ and an hardening stress, $\sigma_r$:

$$\sigma = \sigma_s + \sigma_r \tag{3.15}$$

The driving stress accounts for the intermolecular interactions, and is decomposed into a deviatoric part ($^d$) and an hydrostatic part ($^h$):

$$\sigma_s = \sigma_s^d + \sigma_s^h \tag{3.16}$$

The deviatoric part is given by:

$$\sigma_s^d = G\widetilde{\boldsymbol{B}}_e^d = 2\eta\boldsymbol{D}_p \tag{3.17}$$

where G is the shear modulus, $\widetilde{\boldsymbol{B}}_e^d$ is the deviatoric part of the isochoric elastic left Cauchy-Green strain tensor, $\boldsymbol{D}_p$ is the plastic deformation rate tensor and $\eta$ is the viscosity.
The viscosity is described by the Eyring relationship [59] to describe flow, but also incorporates pressure dependence [18] and intrinsic strain softening and aging [19]:

$$
\begin{aligned}
\eta(T, p, \bar{\tau}, S) &= A_0(S)\tau_0 \exp\left(\frac{\Delta U}{RT}\right) \exp\left(\frac{\mu p}{\tau_0}\right) \frac{\bar{\tau}/\tau_0}{\sinh\bar{\tau}/\tau_0} \\
&= \eta_0(T, p, S)\frac{\bar{\tau}/\tau_0}{\sinh\bar{\tau}/\tau_0}
\end{aligned}
\tag{3.18}
$$

where p is the hydrostatic pressure, $\bar{\tau}$ the equivalent stress, $A_0(S)$ a pre-exponential factor related to the rejuvenated state in this paper depending upon the state parameter, S, $\tau_0$ the characteristic stress, $\Delta U$ the activation energy and $\mu$ the pressure dependence.

The state parameter ,S, is decomposed into the factor, $S_a(t, T)$, which describes ageing kinetics as a function of time and temperature, and $R_\gamma(\bar{\gamma})$ describes the softening kinetics [19]:

$$S(t, T, \bar{\gamma}_p) = S_a(t, T) \cdot R_\gamma(\bar{\gamma}_p) \tag{3.19}$$

The hydrostatic part is given by:

$$\sigma_s^h = K(J-1)\mathbf{I} \qquad (3.20)$$

where K is the bulk modulus, J the volume change factor and $\mathbf{I}$ the unity tensor.

The hardening stress accounts for the molecular network and is given by:

$$\sigma_r = G_r\widetilde{\mathbf{B}}^d \qquad (3.21)$$

where $G_r$ is the strain hardening modulus and $\widetilde{\mathbf{B}}^d$ is the deviatoric part of the isochoric left Cauchy-Green deformation tensor.

When incompressibility is assumed the total stress can be given by:

$$\sigma = -p\mathbf{I} + 2\eta\mathbf{D}_p + G_r\mathbf{B}^d \qquad (3.22)$$

For uniaxial deformation under a constant strain rate, the resulting Cauchy stress and hydrostatic pressure can be given by:

$$\sigma = 3\eta\dot{\epsilon}_p + G_r(\lambda^2 - \lambda^{-1}) = \sigma_s + \sigma_r \qquad (3.23)$$
$$p = -\eta\dot{\epsilon}_p - \tfrac{1}{3}G_r(\lambda^2 - \lambda^{-1}) = -\tfrac{1}{3}\sigma \qquad (3.24)$$

where $\dot{\epsilon}_p$ is the plastic strain rate and $\lambda$ the draw ratio.

Definition of equivalent measures:

$$\bar{\tau} = \sqrt{\tfrac{1}{2}\text{tr}\left(\sigma_s^d \cdot \sigma_s^d\right)} = \frac{1}{\sqrt{3}}\sigma_s \qquad (3.25)$$
$$\dot{\gamma}_p = \sqrt{2\text{tr}\left(\mathbf{D}_p \cdot \mathbf{D}_p\right)} = \sqrt{3}\dot{\epsilon}_p \qquad (3.26)$$

In combination with Equation (3.17) this gives:

$$\bar{\tau} = \eta\dot{\gamma}_p \qquad (3.27)$$
$$\sigma_s = 3\eta\dot{\epsilon}_p \qquad (3.28)$$

By evaluation of Equations (3.23) and (3.24) at the point of yield $(\sigma_y, \lambda_y)$, assuming that at the point of yield it holds that:

→ $\dot{\epsilon}_p = \dot{\epsilon}_0$ ; $\dot{\epsilon}_0$ being the applied strain rate

→ $R_\gamma(\bar{\gamma}_p = 0) = 1$, thus $S = S_a(t, T)$

→ $\bar{\tau} \gg \tau_0$ and therefore $\frac{\bar{\tau}/\tau_0}{\sinh(\bar{\tau}/\tau_0)} \approx \frac{1}{2}\exp(\bar{\tau}/\tau_0)$

and therefore the viscosity reduces to:

$$\eta = \frac{\tau_0}{\sqrt{3}\dot{\epsilon}_0}\left(\ln\left(2\sqrt{3}A_0(S_a)\dot{\epsilon}_0\right) + \frac{\Delta U}{RT} + \frac{\mu p}{\tau_0}\right) \tag{3.29}$$

the uniaxial yield stress can be given by:

$$\sigma_y = \sigma_s(\dot{\epsilon}_0) + \sigma_r(\lambda_y) \tag{3.30}$$

where

$$\sigma_s(\dot{\epsilon}_0) = \frac{3\tau_0}{\sqrt{3} + \mu}\ln\left(2\sqrt{3}A_0(S_a)\dot{\epsilon}_0\right) \tag{3.31}$$

$$\sigma_r(\lambda_y) = \frac{\sqrt{3}}{\sqrt{3} + \mu}G_r(\lambda_y^2 - \lambda_y^{-1}) \tag{3.32}$$

By combining Equations (3.28) and (3.30) and substitution of $\tau_0 = \frac{RT}{V^*}$, the zero viscosity can be directly determined from the yield stress by:

$$\eta_0 = \frac{RT}{V^*}\frac{1}{\sqrt{3}}\frac{1}{\dot{\epsilon}_0}\sinh\left(\frac{\sigma_y - \sigma_r(\lambda_y)}{\sqrt{3}}\frac{V^*}{RT}\right) \tag{3.33}$$

# Predicting properties of molded polymer glasses: the influence of flow and temperature history[1]

## Abstract

The influence of flow- and thermal history experienced during injection molding on the mechanical properties of amorphous polymers is investigated. Flow-induced orientation causes a small anisotropic effect on the yield stress, which can be regarded as negligible with respect to its absolute value. Its influence on the post-yield strain-hardening response is shown to be zero, in contrast to orientation which is applied during deformation below the glas transition.

Distributions of the yield stress as they result from inhomogeneous cooling during processing, predicted by a previously developed modeling approach, are validated and are in good agreement with experiment. Predictions of the mechanical performance for different mold temperatures during processing are also validated over a range of applied strain- and deformation rates and applied stresses and forces, for simple tensile bars and an actual product, and excellent agreement is found. It is shown that mold temperature has a tremendous influence on the life time of polymer products, which can differ by more than two orders of magnitude.

## 4.1 Introduction

Mechanical properties of injection-molded polymer products are influenced by processing conditions. For semi-crystalline polymers this influence is quite considerable and is expressed in the resulting anisotropic crystallinity and inhomogeneous morphology, which are both influenced by the temperature- and flow history experienced by the material during the filling, holding and cooling stages of the process. Flow has a pronounced effect on nucleation density and can also direct crystallization of the bulk by only orienting a small part of the material's high end tail of the molecular weight distribution. Anisotropic growth of shis-kebabs, or similar oriented structures occurs especially in the outer layers of the product [1; 2], but in the presence of hard or soft particles also in the core of a product [3]. Structure development and flow mutually influence each other enhancing the effect of flow since crystals form crosslinks in the entangled network increasing the relaxation time [4]. Samples taken from an injection molded product of a semi-crystalline polymer like polyethylene, display different failure behavior dependent on position and orientation, e.g. tough parallel to flow and brittle in perpendicular direction [5]. The yield stress in polypropylene samples varies as much as 25%, depending on the its orientation with respect to flow [5]. Many studies focuss on an experimental coupling of the macroscopic mechanical behavior and local distributions in microstructure [1; 6–9], others on predicting the properties of such heterogeneous products, either by using thermo-mechanical indices, related to the mean temperature and mean flow during processing [10; 11], or by accurate modeling of how the polymer responds subjected to an injection molding process [12; 13].

For amorphous polymers the effects of temperature and flow during injection molding are, in contrast, much less pronounced. Frozen-in molecular orientation causes some anisotropy [14; 15], localized in the skin layers since in the core fast relaxation occurs due to the limited molecular weight of the polymers used. However, upon further cooling relaxation time increases and even the slow flow due to post-filling in the holding stage, that compensates for shrinkage in the product, can induce orientation in the core as well [16]. Close to the gate the effect is most pronounced, since all material that flows under low strain rates during post-filling passes there. The most frequently used method to characterize frozen-in orientation is stress-optical [17; 18]. The main focus is on its effect on optical anisotropy in CD's and DVD's and in the warpage of products [19; 20]. Frozen-in orientation also influences mechanical properties like Young's modulus and yield stress, but since injection molded products are inhomogeneous in nature, these relations are usually investigated using homogeneous hot-drawn tapes or sheets where its influence can be quite considerable [21–24].

For molded amorphous polymers the most important parameter influencing properties is the temperature history experienced upon solidification from the melt. The kinematic nature of the glass transition, $T_g$ [25], and the inherent non-equilibrium state below $T_g$ are determining for the evolution of properties. Volume and enthalpy

relaxation can be accurately described [26–29], and recently also the yield stress distributions can be predicted [30; 31], with large consequence for the product's final time-to-failure [32]. From a structural viewpoint an accurate prediction of the yield stress is crucial for life-time predictions of structurally loaded polymer products.

In this paper we will investigate the influence of flow on orientation, and its subsequent influence on the value of the yield stress and the strain hardening modulus. Second, we will investigate how the temperature history, using different mold temperatures, results in different values of the yield stress and its distribution throughout the product and how this in the end influences the long-term failure of an injection molded product in the form of a thick-walled cup.

## 4.2 Experimental

### Materials

Materials used are injection molding grades of polycarbonate (PC): Lexan 121R, 141R and 101R, supplied as granules by Sabic Innovative Plastics (Bergen op Zoom, the Netherlands), an extrusion grade of polycarbonate, supplied as 10 mm diameter extruded rod (type unknown), and a 1 mm thick extruded sheet: Makrolon Sheet, Bayer. The molecular weights, and molecular weight distributions, of the Lexan grades are listed in Table 4.1: PC-LM (121R), PC-MM (141R) and PC-HM (101R). Table 4.1 also lists the number-average molecular weight corrected for the fraction of short chains which do not contribute to the connectivity in the material and act as a diluent, multiplied by the volume fraction of 'effective' polymer, $\phi\bar{M}_n^*$ [33; 34].

**Table 4.1:** Polycarbonate molecular weights

| grade | $\bar{M}_n$ [kg/mol] | $\bar{M}_w$ [kg/mol] | PDI | $\phi\bar{M}_n^*$ [kg/mol] |
|-------|------|------|------|------|
| PC-LM | 9.8 | 23.4 | 2.38 | 13.6 |
| PC-MM | 9.2 | 25.8 | 2.82 | 14.9 |
| PC-HM | 16.1 | 30.7 | 1.91 | 16.6 |

### Sample preparation

Tensile experiments are performed on samples machined from injection-molded rectangular plates, see Figure 4.1 (left). The plates with dimensions 70×70×2 mm³ are molded on an Arburg 320S all-rounder 500-150. The runner of the mold ensures uniform filling, as proven by several short shot experiments. Various processing conditions and PC grades are used, see Table 4.2; the melt temperature is kept constant

at 280°C. From the plates, bars with dimensions $70 \times 10 \times 2$ mm$^3$ are cut both parallel and perpendicular to the flow direction and fitted with gauge sections of $33 \times 5 \times 2$ mm$^3$, see Figure 4.1 (middle and right).
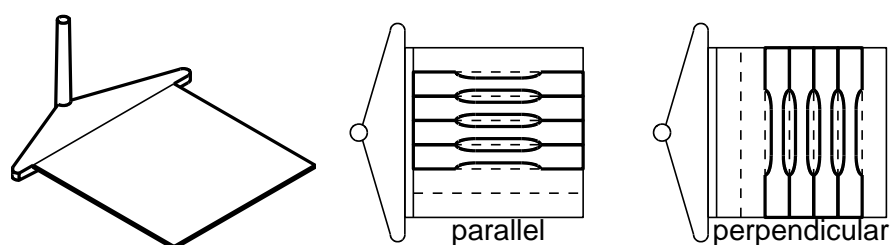


**Figure 4.1:** Injection molded samples and tensile bars made thereof.

**Table 4.2:** Processing conditions: mold temperature, $T_m$, injection velocity, $\dot{V}$, and holding/packing pressure, $P_p$.

| grade | $T_m$ [°C] | $\dot{V}$[cm$^3$s$^{-1}$] | $P_p$ [bar] |
|---|---|---|---|
| PC-MM | 45 | 10-30-50-70 | 50 |
| PC-MM | 45 | 10-70 | 50-500-1000 |
| PC-MM | 45 | 10 | 50 |
| PC-LM/MM/HM | 45-83-122 | 10 | 50 |

To investigate the influence of the temperature history on the distribution of yield stress over the thickness of a product, small bars with cross sections $2 \times 1$ mm$^2$ are taken from the centers of molded square plates, using the PC-MM grade, by a precision machining operation. Subsequently, increasingly thinner layers are removed from the surface of the $2 \times 1$ mm$^2$ cross section by a microtoming operation under cryogenic conditions, this to minimize a possible influence of machining on the thermodynamic state of the sample surface. To obtain different temperature histories, three mold temperatures are used: 30°C, 90°C and 130°C.

To verify the performance after injection molding, samples of the PC-MM grade are taken from injection molded rectangular plates with a thickness of 1mm, molded from the PC-MM grade. To obtain two different yield stresses, two mold temperatures are used: 30°C and 120°C. Cooling times are 60 seconds for both mo ld temperatures.

Compression testing samples are made from PC-MM and the extruded rod (PC-ER). Granules of PC-MM are dried under vacuum at 80°C for 24 hours an d compression molded into a 10 mm thick plate, from which $\varnothing 6 \times 6$ mm$^3$ cylindrical samples are machined. After drying under vacuum, the $\varnothing 10$ mm extruded rod is brought to a temperature well above $T_g$ to remove orientation present due to processing, and slowly cooled to room temperature. Subsequently $\varnothing 6 \times 6$ mm$^3$ and $\varnothing 10 \times 10$ mm$^3$ cylindrical samples are taken from the extruded rod. The $\varnothing 6 \times 6$ mm$^3$ samples are tested

without further treatment under different ambient temperatures ranging from 20℃ to 140℃. The ∅10×10 mm³ samples are compressed at a temperature of 170℃ to a true strain of 40% with a true strain rate of $10^{-2}s^{-1}$, followed by quick quenching in water to freeze in the applied orientation. These compressed samples are then machined into ∅6×6 mm³ samples which are tested at different ambient temperatures ranging from 20℃ to 135℃. Re-heating above $T_g$ shows that 15% of strain is frozen in after quenching.

Finally, as an example of a real product, a thick-walled cup shaped sample, see Figure 4.2, is used. The bottom ring of the cup has a diameter of 78 mm. The cup itself starts with an outer diameter of 65 mm and has a gradually decreasing diameter up till 60 mm at the top. We define Figure 4.2 (left) as the upright position (the way in which the samples was loaded in the load-frame). The thickness is around 3 mm in all cross-sections. The cup shaped sample is injection molded on an Arburg 320S allrounder 500-150, using the PC-MM grade. The melt temperature is set to 285℃; the injection rate to 50 ccm/s; and the packing pressure to 500 bars. Mold temperatures are set to 30℃ and 130℃. In both cases a cooling time of 120 se conds is used.
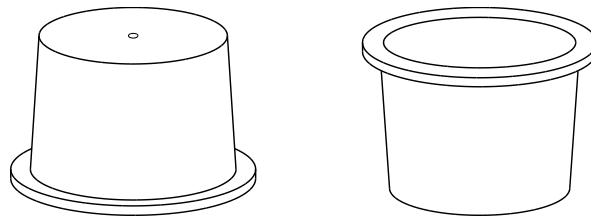


**Figure 4.2:** Injection molded cup.

## Methods

Tensile tests are performed on a Zwick Z010 universal tensile tester at a room temperature of 23℃. Experiments are performed by applying cons tant linear strain rates ($\dot{\epsilon} = \dot{x}/l_0$) or engineering stresses ($\sigma = F/A_0$). Unless indicated otherwise, a standard constant linear strain rate of $10^{-3}s^{-1}$ is used. All tensile yield stresses listed in the results section are engineering yield stresses, and taken as the mean value of 5 experiments; 68.3% confidence intervals are calculated.

Compression tests are performed on a servo-hydraulic MTS 831 Elastomer Testing System. True strain rate control is used, under the assumption of incompressibility, at a rate of $10^{-3}s^{-1}$. Correction is made for the finite stiffness of the compression setup. Friction between samples and compression platens is reduced by applying a thin film of teflon tape (3M 5480, PTFE skived film tape) onto the ends of the sample and lubricating the platens with a PTFE spray. During the compression tests no bulging or buckling of the samples is observed indicating that friction is sufficiently reduced. A hot air circulating temperature chamber controls the ambient temperature during

testing. Each sample is placed inside the temperature chamber for 15 minutes prior to testing to ensure that they are equilibrated to the test temperature.

Micro-indentation experiments are performed on a nano-indenter XP (MTS NanoInstruments, Oak Ridge, Tennessee) under displacement control. The indenter has a flat tip, effectively a flat-ended cone with a top angle of 70° and a circular contact area with diameter $10\mu$m. Correction for tip-sample misalignment is performed using a specially designed alignment tool. For details on the experimental technique see [35; 36]; and for the alignment tool see [36].

The cup shaped samples are tested on a Zwick 1475 tensile testing machine. The cups are placed in the machine with the tapered section to the top (see Figure 4.2 left). The bottom plate used has a flat circular recess to fit the outer diameter of the bottom ring of the cup. Samples are loaded with constant displacement rates, or constant forces. Experiments are performed at a room temperature of 23℃ and corrected for the finite stiffness of the setup.

## 4.3  Results

### Influence of flow on the yield stress

In Chapter 3 [31] a small influence on the yield stress was found due to orientation caused by flow experienced during injection molding. Here this influence of orientation is investigated over a broader range of processing conditions. Figure 4.3 (left) shows the results by plotting the yield stress of PC, both parallel and perpendicular to flow, as a function of injection velocity, all other processing conditions being equal. Somewhat surprisingly, the injection speed has almost no influence on the yield stress and at all speeds, the values measured parallel to flow are higher than the perpendicular ones, the differences between the two directions shown in Figure 4.3 (right). The so-called yield differences, $\Delta\sigma_y$, proves to be roughly independent of the injection velocity and its value is small, maximum 1 MPa.

The influence of molecular weight on the anisotropy is shown in Figure 4.4, where yield stresses and yield differences are given for three different mold temperatures: 45℃, 85℃, and 120℃. For all molecular weights the yield st ress is seen to substantially increase with mold temperature (ca. 5 MPa in the temperature window investigated), which is in complete accordance with the results of Chapter 2 on the prediction of yield stresses directly from processing conditions [30]. For all conditions the yield difference is small, again, and in the order of 0.5 MPa; for the PC-LM it appears to be somewhat smaller, albeit not significant.

In Figure 4.5 the influence of packing pressure on the anisotropy is shown. Three packing pressures are applied in combination with two injection velocities: 10 ccm/s (open markers) and 70 ccm/s (closed markers), all other processing conditions being constant. Packing pressure clearly has no influence on the absolute level of the yield
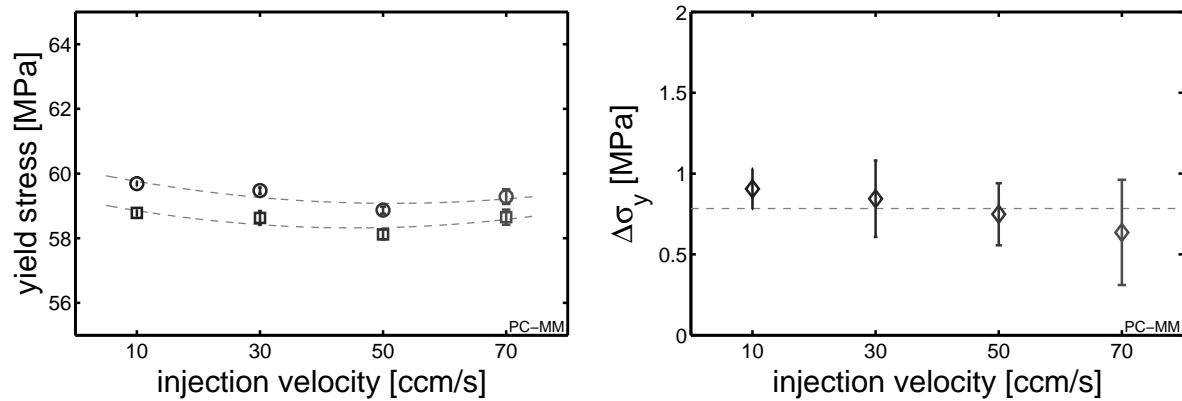
**Figure 4.3:** Influence of injection velocity on anisotropy. Left: yield stresses of PC parallel (○) and perpendicular (□) to flow. Right: The yield difference as a results of anisotropy.
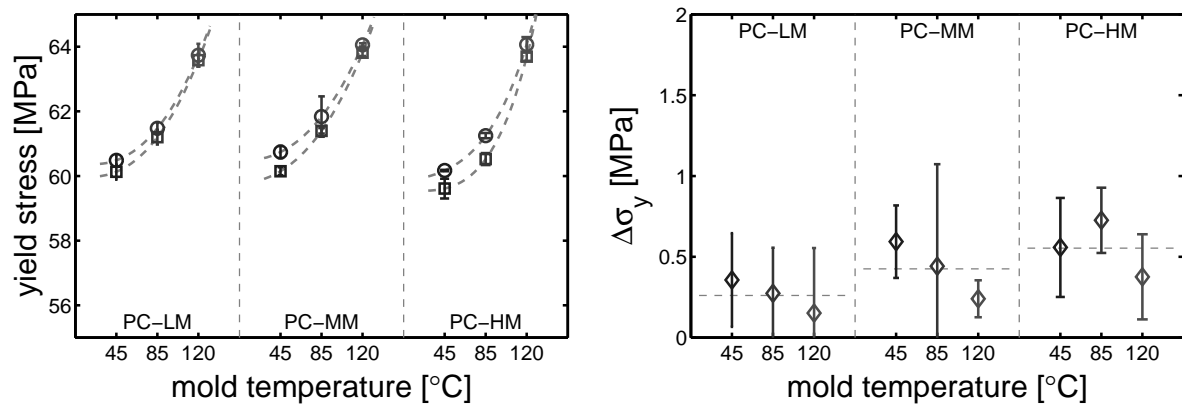


**Figure 4.4:** Influence of molecular weight on anisotropy. Left: Yield stresses parallel (○) and perpendicular (□) to flow. Right: The yield difference as a results of anisotropy.

stress and the yield difference, see Figure 4.5 (right), which is in the order of 1 MPa. The lower injection velocity (10 ccm/s) has a somewhat higher anisotropy, but the difference is not significant.

Anisotropy in the yield stress of injection-molded samples shows to be small and independent of processing conditions. The original assumption of isotropic material behavior [30; 31] therefore is valid. Of course this study does not cover the whole range of processing conditions in polymer processing in general, but it does span a large range with respect to injection molding. The anisotropy found is always in the order of 1 MPa, which correlates well with the value found in Chapter 3 [31], and therefore can be regarded as negligible with respect to the absolute value of the yield stress which is of the order of 60 MPa.
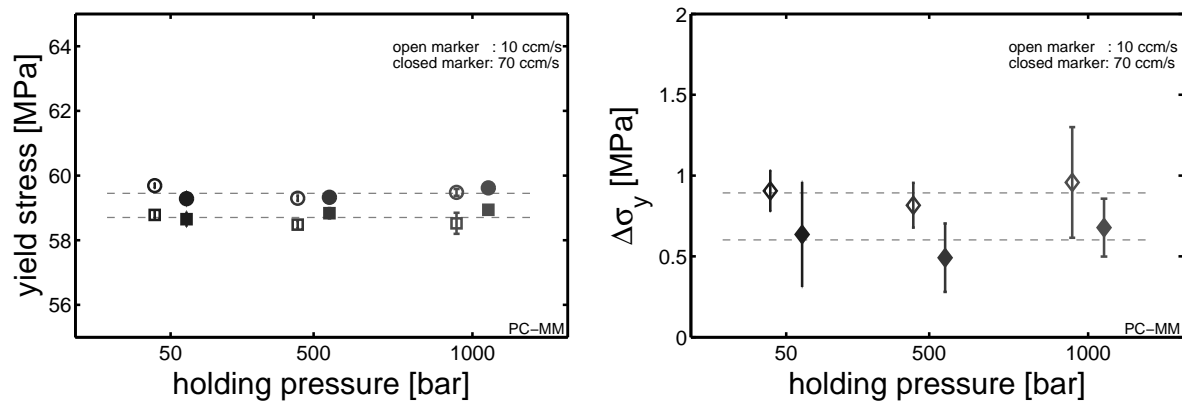
**Figure 4.5:** Influence of holding/packing pressure on anisotropy. Left: Yield stresses parallel (○) and perpendicular (□) to flow. Right: The yield difference as a results of anisotropy. Open symbols correspond to an injection velocity of 10 ccm/s; closed symbols to an injection velocity of 70 ccm/s.
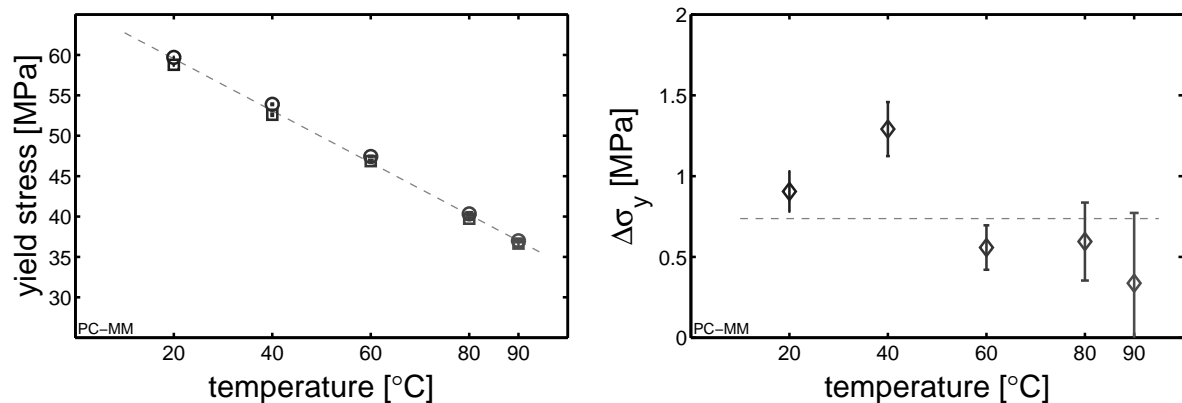


**Figure 4.6:** Influence of ambient temperature on anisotropy. Left: Yield stresses parallel (○) and perpendicular (□) to flow. Right: The yield difference as a results of anisotropy.

## Influence of flow-induced orientation on the intrinsic behavior

The flow-induced orientation unambiguously influences the yield stress, albeit that its influence is small. This is again demonstrated in Figure 4.6, where the influence of the ambient testing temperature on the anisotropy measured is presented. The yield stress strongly decreases with increasing test temperature, but the yield difference, Figure 4.6 (right), is more or less constant over the range of test temperatures used (mind that a 68% confidence interval is shown) and in the order of 0.5-1 MPa. Govaert and Tervoort [24] attributed such an anisotropic yield behavior to the contribution of a superimposed stress resulting from a prestrained hardening network, which is a result of frozen-in orientation. Following their modeling approach, based on the work of Haward and Thackray [37], under the assumption of incompressibility, the yield

difference, $\Delta\sigma_y$, can be given as:

$$
\begin{aligned}
\Delta\sigma_y \;=\;& \tfrac{3}{2}G_r\left(\lambda_\parallel^2 - \lambda_\perp^2\right) \\
&+\; \tfrac{1}{2}\left(6\frac{G_r^2}{\lambda_\parallel^2} - 3\frac{G_r^2}{\lambda_\parallel^4\lambda_\perp^4} - 3G_r^2\lambda_\perp^4 + 4\sigma_0^2\right) \\
&+\; \tfrac{1}{2}\left(6\frac{G_r^2}{\lambda_\perp^2} - 3\frac{G_r^2}{\lambda_\parallel^4\lambda_\perp^4} - 3G_r^2\lambda_\parallel^4 + 4\sigma_0^2\right)
\end{aligned}
\tag{4.1}
$$

with $\sigma_0$ the yield stress of the isotropic material, $G_r$ the strain hardening modulus (at the temperature of orientation: 3 MPa [24]), $\lambda_\parallel$ the amount of frozen-in orientation parallel to flow and $\lambda_\perp$ the amount of frozen-in orientation perpendicular to flow.

Values for $\lambda_\parallel$ and $\lambda_\perp$ are obtained by heating samples, taken parallel and perpendicular to flow, to a temperature above $T_g$, and measuring the width of the samples before, $w_0$, and after, $w$, from which the mean frozen-in orientation is determined. Mind that since the widths of the samples are analyzed, samples taken parallel to flow give the orientation perpendicular to flow and vice versa. The mean values found are $\lambda_\parallel = 1.086$ and $\lambda_\perp = 0.965$, giving a value of $\Delta\sigma_y \approx 1.1$ MPa, which is in good agreement with the values presented in Figures 4.3 to 4.6.

Another feature of the intrinsic behavior that can be influenced by flow-induced orientation is the strain-hardening response [38; 39]. No clear picture of the physics behind the strain hardening response of polymers below $T_g$ exists, although the search for its origin receives a lot of attention both from experimental and continuum modeling approaches [24; 38; 40–42], as from direct atomistic modeling [43–46]. Currently the most frequently used approach for describing the strain-hardening behavior is by using a rubber-elastic spring [47], with or without finite extensibility. Although this approach gives good results at constant temperatures and strain rates, it is known that the strain-hardening modulus is strain rate dependent [41], and that its temperature dependence (decreasing modulus with increasing temperature [39]) is in direct contradiction with the entropic nature of any rubber-elastic model [39; 47; 48]. Moreover, the molecular weight between entanglements, $M_e$, calculated from the strain-hardening modulus and assuming an entropic origin, is orders of magnitude larger below $T_g$ than above $T_g$, values below $T_g$ being unrealistically low [39; 40; 48]. Nevertheless, it gives good results over a broad range of experimental conditions [24; 37; 38; 41; 48–50], and is successfully used to describe the effect of pre-orientation which is applied below $T_g$ [51].

To investigate the influence of the pre-oriented network on post-yield deformation, compression experiments are used rather than tensile experiments, since they allow to investigate the large strain deformation behavior without any localization phenomena such as necking, since strain localization is prohibited due to the stabilizing effect of the steady increasing cross-sectional area. In Figure 4.7 isotropic samples (solid

lines) are compared with pre-oriented samples (dashed lines). Pre-orientation is obtained by pre-deforming isotropic samples above $T_g$ followed by rapid quenching to room temperature, effectively freezing-in 15% of orientation. The yield stresses are distinctively different, as expected due to the large difference in thermal history, i.e. slow cooling of the isotropic samples versus rapid quenching of the pre-deformed samples. The strain hardening response, however, is exactly the same. This is confirmed in Figure 4.7 (right) where the strain-hardening moduli are plotted versus temperature.
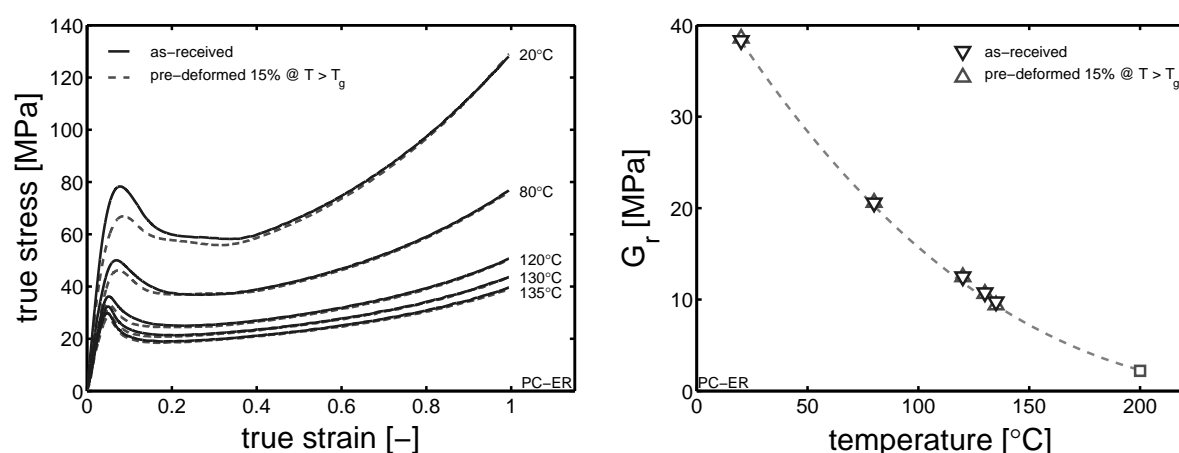


**Figure 4.7:** Influence of temperature and pre-orientation on strain hardening response. Left: Compressive true stress versus compressive true strain at various temperatures. Right: The strain-hardening modulus, $G_r$, versus temperature.

The fact that no influence of pre-orientation above $T_g$ is observed on the post-yield response at temperatures below $T_g$ can be rationalized by the results of Wendlandt et al. [42]. They found by solid-state NMR for PMMA that the finite deformation, both above and below $T_g$, can be described by an affine deformation scheme of entanglement points, albeit that the scale of affine deformation is significantly smaller below $T_g$ than above $T_g$. This implies that upon deformation above $T_g$, the chain segments between the entanglement points, orient in a non-affine manner and can basically be regarded as being isotropic. Therefore, during flow in the glassy state, the governing local deformation length-scale is much smaller than the one addressed above $T_g$, taking place on the scale of the isotropic chain segments between the entanglement points above $T_g$, and as a result any effect of pre-orientation is lost. This is demonstrated in Figure 4.8 where the results at 20°C for the isotropic and pre-oriented material are taken from Figure 4.7 (left), but now the result of a sample which received 15% pre-deformation below $T_g$ is added. Next to the absence of a distinct yield point, due to mechanical erasure of thermal history by mechanical rejuvenation during the 15% deformation [52], a clear increase in the hardening response can be seen with respect to the isotropic material and the material which was pre-deformed above $T_g$. Clearly a strong difference exists in pre-deformation above or below $T_g$
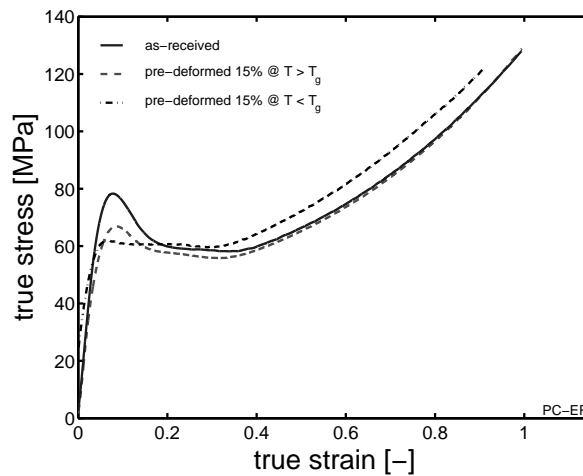
**Figure 4.8:** Influence of pre-deformation temperature on strain hardening response.

which can be related to the difference in scale of the deformation invoked. In conclusion, flow-induced orientation that is realized during injection molding, only has a minor influence on the polymer's intrinsic behavior. At least for amorphous polymers.

## Influence of thermal history on the yield-stress distribution

In Chapters 2 and 3 [30; 31] distributions of yield stresses throughout a polymer product were predicted based on the differences in temperature history experienced during molding. Fast cooling, e.g. at the mold surface, limits physical ageing leading to a low yield stress, while during slow cooling, e.g. in the core of the product, ageing is more pronounced as is the increase in yield stress. Verification was done using a mean yield stress calculated based on area averaging, and excellent agreement was found for different mold temperatures and mold thicknesses. Here we will attempt to also validate the distributions, first by using micro-indentation. Figure 4.9 (left) shows results of indentation with the use of a flat-tip and indeed a measurable distinction is found in force-displacement results for a quenched ($\sigma_y$ ~62 MPa)[1] and an annealed ($\sigma_y$ ~70 MPa)[1] material [35].

Applying indentation on samples molded with different mold temperatures, see Table 4.3, needs cross sectioning of samples using precision machining, followed by cryogenic microtoming of the surface in an attempt to avoid surface changes caused by sample preparation. Indents are made over the total width of the samples, see Figure 4.9 (right), and the resulting indentation forces (at an indentation depth of 2 $\mu$m) are given in Figure 4.10 (left). Although based on the calculated yield stress distributions, compare Figure 4.10 (right), differences in indentation forces are expected, they are not measured. (The decrease in indentation force at the edges is most likely

---

[1]note: listed yield stresses are engineering values measured at $\dot{\epsilon} = 1 \cdot 10^{-3} s^{-1}$
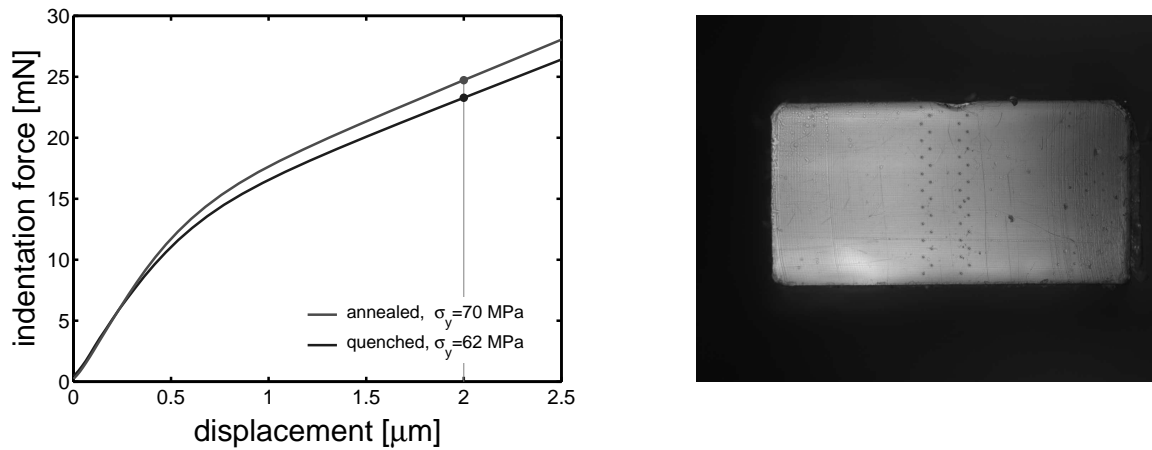
**Figure 4.9:** Left: Force versus indentation depth for a quenched and an annealed material. Right: Residual indents on a sample of mold temperature 130°C.
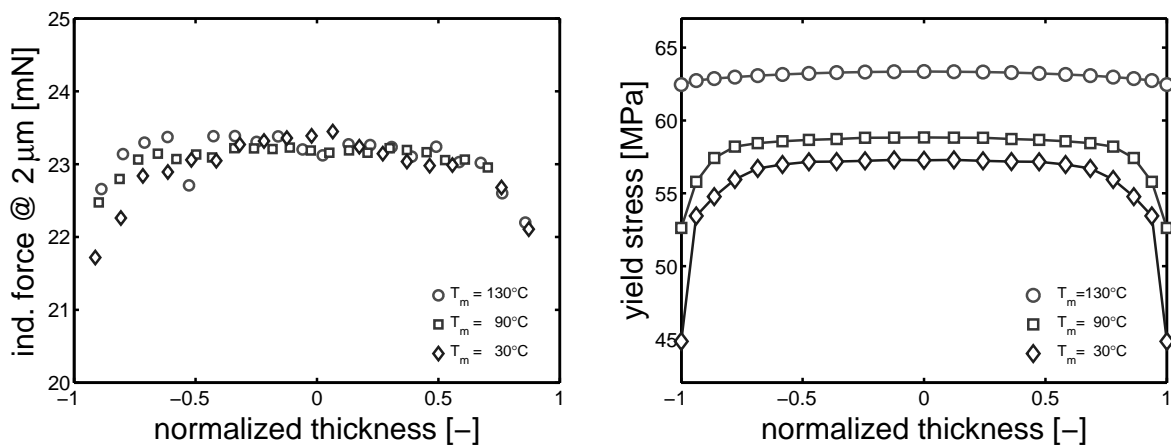


**Figure 4.10:** Left: Measured indentation force distributions over the thickness of samples with different thermal histories. Right: Calculated yield stress distributions over the thickness of samples with different thermal histories.

the influence of a local decrease in stiffness due to the presence of the surface.) The conclusion could be that, despite our precautions, sample preparation still influences the thermodynamic state of the surface, preventing to measure properties as they result from processing.

We therefore try to obtain samples that are prepared without the need of a post-processing machining operation, by stacking twelve (1 mm thick, vacuum dried) sheets of extruded polycarbonate ($200 \times 200mm^2$), separated by thin sheets of aluminium ($< 0.1$ mm thick) to prevent sticking. Two thermocouples are added, one at a surface sheet, one between the two middle sheets. The stack of sheets is placed in a hot press at 200°C for 10 minutes, to erase any previous thermal history and orientation from the sheets, and subsequently the stack is cooled in a cold press at 18°C. The stack is removed from the press once the center temperature is 18°C, and

**Table 4.3:** injection molded samples

| $T_m$ [°C] | $\sigma_y$ * [MPa] | $S_a$ [-] |
|:---:|:---:|:---:|
| 30 | 57.1 | 27.6 |
| 90 | 58.8 | 29.1 |
| 130 | 62.1 | 32.2 |

* measured at $\dot{\epsilon} = 1 \cdot 10^{-3} \text{s}^{-1}$

the sheets are separated. Subsequently tensile bars are machined from the center of the sheets with gauge sections of $33 \times 5 \times 1 \text{mm}^3$.

Figure 4.11 (left) shows the calculated and measured temperatures (heat capacities used as input for the numerical results were taken from the ATHAS Data Bank [53; 54]), and Figure 4.11 (right) shows the calculated, [30], and measured yield stress distributions. The calculated distribution overestimates the experimental one by approximately 2 MPa, i.e. a deviation of ~3%. When the predicted distribution is lowered by 2 MPa (dashed line), an excellent agreement between experimental and numerical distributions is obtained. In conclusion it proves to be difficult to measure yield stress distributions caused by inhomogeneous cooling via direct indentation measurements, due to errors induced by the sample preparation method. But by using samples that did not require any post-fabrication machining, the calculated distribution indeed can be measured, and the results are correct with an error of 3% only.
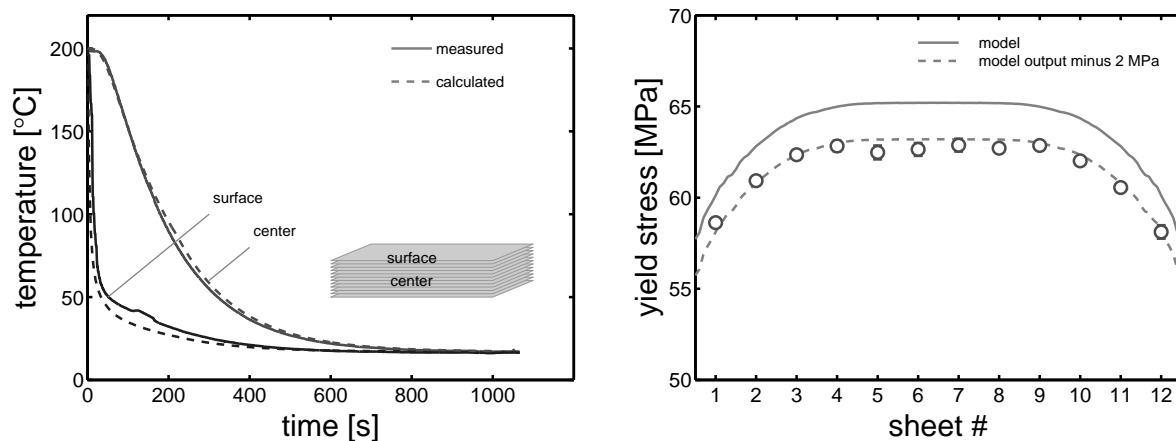


**Figure 4.11:** Left: Cooling histories as measured (-) and as calculated (–). Right: Measured (O) and predicted (solid drawn line) yield stress distributions.

## Influence of processing on the final properties of a product

The 3D constitutive framework of the predictive tool developed [55] allows to predict the performance for an arbitrary sample geometry under any loading condition [32]. To validate this, tensile experiments are performed at different strain rates and stresses for samples made using mold temperatures of 30℃ an d 120℃. Next a more complex geometry is analyzed, using a cup shaped product.
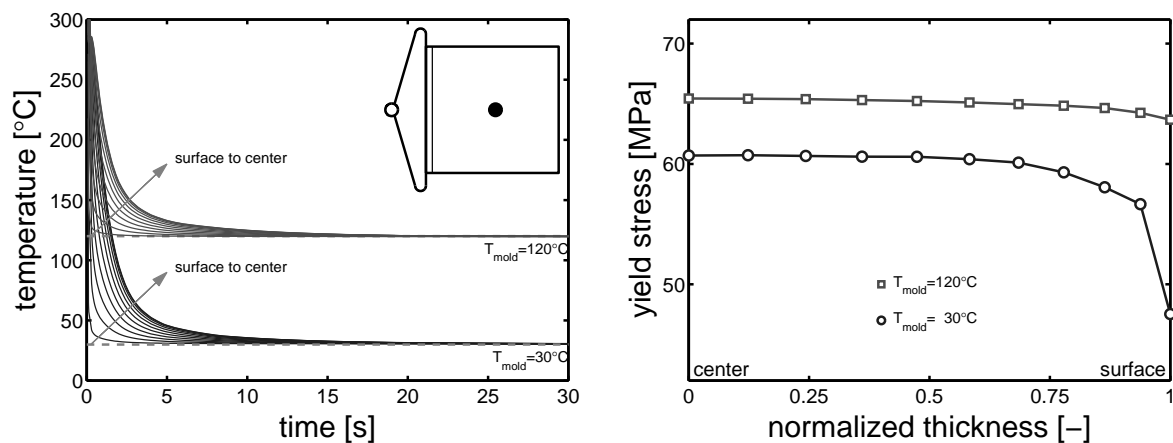


**Figure 4.12:** Left: Temperature versus time during the cooling of the injection molded samples. Right: Corresponding predicted yield stress distributions.

Figure 4.12 (left) shows the cooling profiles over the thickness in the center of square samples, see inset Figure 4.12 (left), as obtained from a numerical simulation of the injection molding process for mold temperatures of 30℃ and 120℃. Cooling is faster near the surface than at the center, and cooling rates are much higher for the low mold temperature. These differences in cooling history are reflected in the predicted yield stress distributions, see Figure 4.12 (right), lower near the surface, and higher in the center and for the higher mold temperature.

Tensile experiments were performed on the samples and the experimental and numerical results are compared in Figure 4.13. In the simulations an extension of the original 3D model constitutive model [55] is used applying multiple relaxation times [56]. Seventeen modes are used by fitting to the pre-yield region of an as-received tensile bar, and the resulting spectra of viscosities and shear moduli are given in Appendix A. Using this spectrum of relaxation times the stress responses up to yield are accurately predicted, while the post yield localization is stronger in the experiments than in the simulations. This can be attributed to sample preparation. The tensile bars are made by a machining operation and are not polished afterwards giving them a rather rough surface, resulting in strong localization, which is not captured by simulation. However, while it influences the width of the yield peak, the height is unaffected.
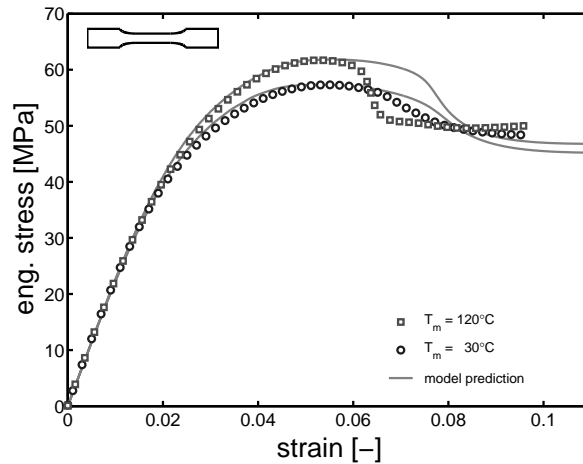
**Figure 4.13:** Experimental and numerical results of tensile tests at a strain rate of $10^{-3}s^{-1}$ for samples with mold temperatures 30°C and 120°C.

Figure 4.14 (left) shows the yield stress versus the strain rate for samples made with mold temperature 30°C and 120°C, and Figure 4.14 (right) the applied stress versus the time-to-failure in a creep experiment. Solid lines are predictions based on our modeling approach and they are in excellent agreement with experimental results. The difference in mold temperature of 90°C between the two sa mples, results in an increase in failure time of about a factor one hundred if the samples are loaded with the same stress. A similar effect was already found and predicted for a quenched versus an annealed material [55], but mind that here this effect is predicted based on the temperature history the material experienced during its fabrication in the injection molding process.
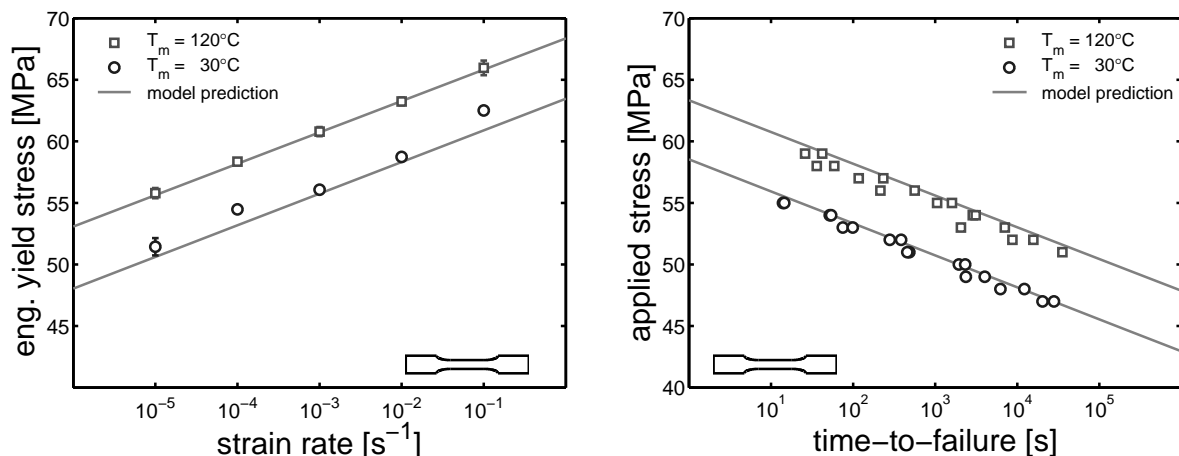


**Figure 4.14:** Left: Yield stress versus applied strain rate. Right: Applied stress versus time-to-failure. Both for samples with mold temperatures 30°C and 120°C.

The model thus far proves to predict the performance of simple tensile bars very well. Of course the question rises whether it will also perform well on a more complex product. To investigate this a cup shaped sample is chosen, as discussed in the experimental section, and shown in Figure 4.15 (middle). For the analysis of the injection molding process, a full 3D mesh is build, see Figure 4.15 (left), while for the structural analysis a 2.5D axi-symmetrical mesh proved to be sufficient, see Figure 4.15 (right). The dimensions of the mesh for the mold filling analysis are based on the dimensions of the mold, whereas the dimensions of the mesh for structural analysis are based on dimensions of actual samples, which however differ only slightly from the dimensions of the mold.
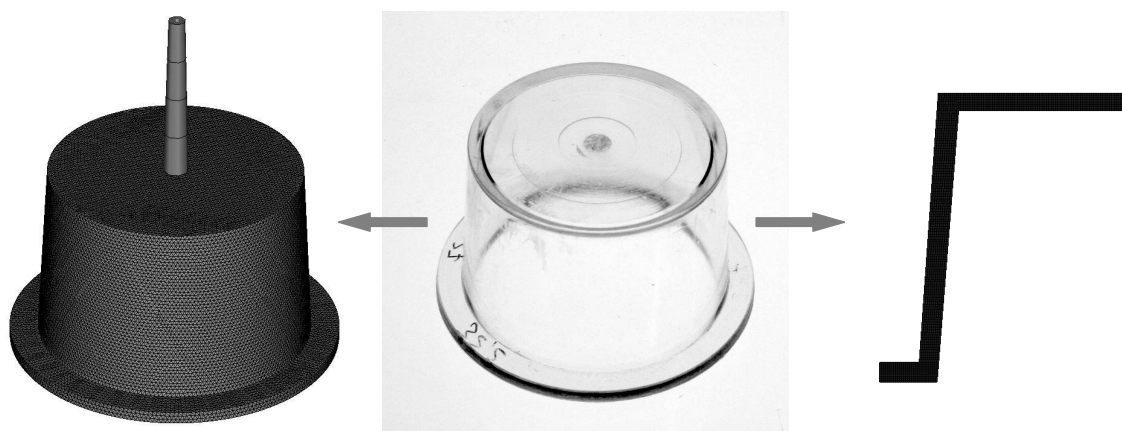


**Figure 4.15:** Cup shaped sample (middle) and injection molding analysis mesh (left) and structural analysis mesh (right) made thereof.

Analysis of the injection molding process is done with a commercial injection molding simulation package (MoldFlow MPI). A full 3D analysis is used with a mesh which has 8 elements over the thickness and a total of approximately 800.000 elements. The large amount of elements is necessary to obtain a sufficiently detailed temperature information over the thickness of the cup. In Figure 4.16 the distribution of the state parameter $S_a$ is given for a quarter cross-section taken from the center height of the cup. $S_a$ is used rather than yield stress, since we are dealing with a complex geometry, and a yield stress is related to a loading geometry and conditions, whereas $S_a$ uniquely defines the thermodynamic state of the material and is independent of loading details [30; 55]. As expected, the predicted values of $S_a$ are much higher for the 130℃ samples than for the 30℃ samples. The distributions a re, however, more pronounced for the last one. These findings correspond well with the results observed for the yield stress of the tensile bars molded at different mold temperatures, see Figure 4.12 (right).

As input for the structural analysis, an area mean value of $S_a$ is used, similar to what is done for the tensile bars. The calculated area mean values are $S_a \sim 25.0$ for the 30℃ mold temperature samples and $S_a \sim 34.9$ for the 130℃ samples. A value of 25 is, by experience, rather low and evaluation of the cooling profiles learns that
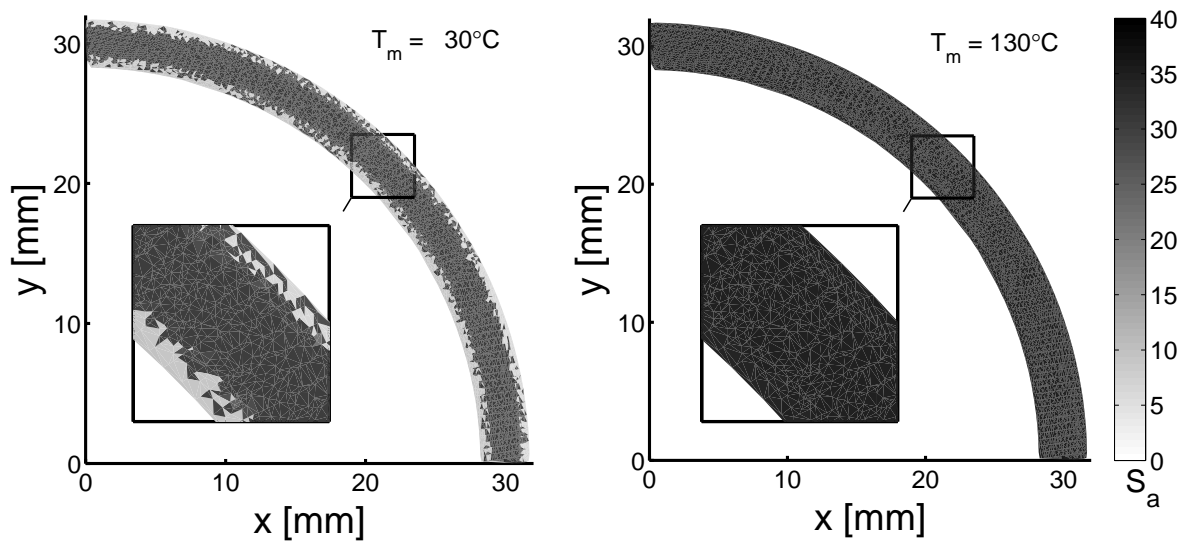
**Figure 4.16:** Distribution of $S_a$ over a quarter cross-section for $T_m = 30°C$ (left), and for $T_m = 130°C$ (right).

insufficient information is available for the surface nodes, i.e. the temperature at the first time increment is already below $T_g$, thereby giving an underestimation of the actual thermodynamic state. (See also the rough $S_a$ values at surfaces in the inset of Figure 4.16 (Left)). Therefore the surface nodes are excluded in calculating the area mean value of $S_a$, which results in a value of $S_a \sim 30.2$ for the 30°C sample and a negligible difference for the 130°C sample.
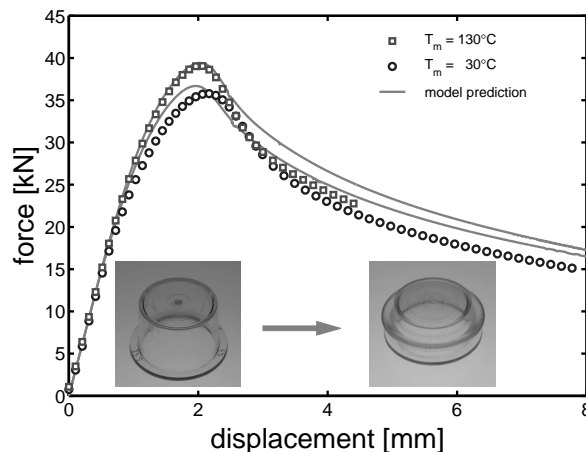


**Figure 4.17:** Experimental and numerical results of compression tests of a cup at a loading rate of 0.045mm/s for samples with mold temperatures 30°C and 130°C.

Results of the structural analysis are shown in Figure 4.17 and describe the exper-

imental data of force-displacement curves on the cup very well, including failure by buckling. Markers indicate experimental results, whereas solid drawn lines are the predictions. The predictions for different loading rates and different constant forces are presented in Figure 4.18 and also show excellent agreement with experiments.
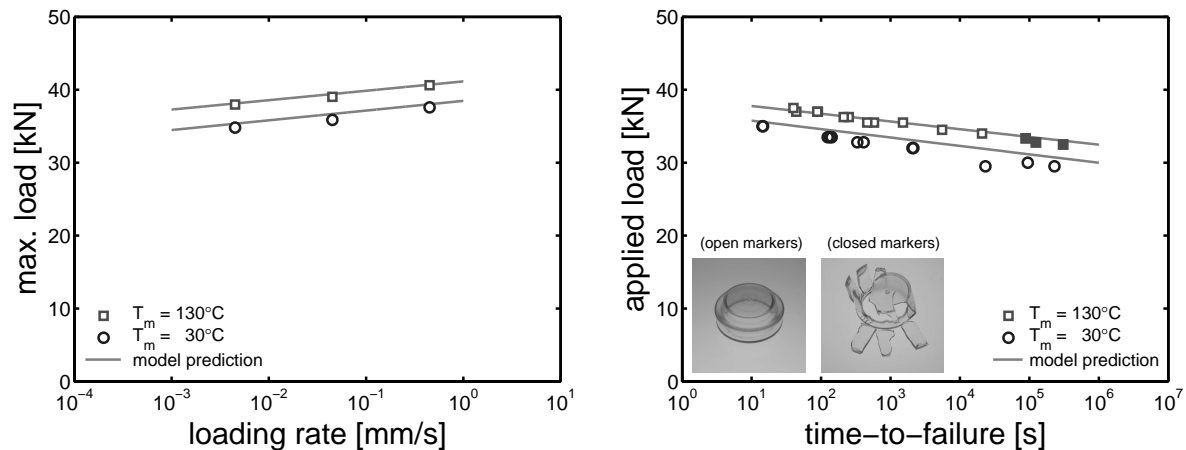


**Figure 4.18:** Left: Maximum load versus loading rate. Right: Applied load versus time-to-failure. Both for samples with mold temperatures 30℃ and 130℃.

The numerically calculated and experimentally observed failure modes were thus far all ductile. The cup shaped samples which were injection molded with a high mold temperature, and that consequently have a long time-to-failure (closed symbols Figure 4.18 (left)), display, however, a transition from a ductile to a brittle failure mode. The model still predicts the failure times accurately, since despite the change in failure mode, the deformation kinetics determine the onset to failure. This is in agreement with experiments on loaded poly(vinyl chloride) pipes [57] and on tensile bars of PC with different molecular weights [32].

# 4.4  Conclusions

The influence on properties of the flow- and the thermal history experienced during injection molding is investigated. The minor influence of anisotropy found in Chapter 3 [31] is investigated over a broader range of processing conditions and found to be small, and negligible in all cases, confirming the original assumption of isotropic behavior. The small anisotropic influence on the yield stress could be well described using a simple model based on the presence of an entropy elastic contribution and a viscous contribution to the yield stress. Also the influence of flow-induced orientation on the intrinsic behavior glassy polymers, as reflected in the strain hardening modulus, proved to be small. Only orienting samples below $T_g$ gives a distinct change in both yield (mechanical rejuvenation that lowers the yield stress) and post-yield

behavior (earlier upswing by strain hardening due to efficient pre-deformation).

The modeling approach which allows the prediction of the yield stress as it follows directly from the temperature history experienced during processing [30] is validated more extensively. Predicted yield stress distributions are experimentally validated, and show to be in good agreement. The predicted performance over a range of constant strain and deformation rates, and constant stresses and forces of simple tensile bars and a more complex product, like a cup, is in good agreement with the experimental results. Short- and long-term performance is predicted well, under different loading conditions and loading rates, including the tremendous influence of different mold temperatures, that can change the lifetime of polymer products with more than two orders of magnitude.

# References

[1] M.R. Kantz, H.D. Newman jr., and F.H. Stigale. The skin-core morphology and structure-property relationship in injection-molded polypropylene. *Journal of Applied Polymer Science*, 16:1249–1260, 1972.

[2] G. Menges, G. Wübken, and B. Horn. Einfluß der Verarbeitingsbedingungen auf die Kristallinität und Gefügestruktur teilkristalliner Spritzgußteile. *Colloid and Polymer Science*, 254:267–278, 1976.

[3] W.R. Hwang, G.W.M. Peters, M.A. Hulsen, and H.E.H. Meijer. Flow-induced crystallization of particle-filled polymers. *Macromolecules*, 39:8389–8398, 2006.

[4] R.J.A. Steenbakkers and G.W.M. Peters. Suspension-based rheological modeling of crystallizing polymer melts. *Rheologica Acta*, 47:643–665, 2008.

[5] B.A.G. Schrauwen, L.C.A. van Breemen, A.B. Spoelstra, L.E. Govaert, G.W.M. Peters, and H.E.H. Meijer. Structure, deformation, and failure of flow-oriented semicrystalline polymers. *Macromolecules*, 37:8618–8633, 2004.

[6] C.M. Hsiung and M. Cakmak. Effect of injection-molding conditons on the crystallinity, orientation gradients, and mechanical properties of poly(aryl ether ketone). II. Large dumbell parts. *Journal of Applied Polymer Science*, 47:149–165, 1993.

[7] M.A. Kennedy, A.J. Peacock, and L. Mandelkern. Tensile properties of crystalline polymers: linear polyethylene. *Macromolecules*, 27:5297–5310, 1994.

[8] R. Seguela. On the strain-induced crystalline phase changes in semi-crystalline polymers: mechanisms and incidence on the mechanical properties. *Journal of Macromolecular Science, Part C: Polymer Reviews*, 45:263–287, 2005.

[9] C. Stern, A. Frick, and G. Weickert. Relationship between the structure and mechanical properties of polypropylene: effects of the molecular weight and shear-induced structure. *Journal of Applied Polymer Science*, 103:519–533, 2007.

[10] J.C. Viana, A.M. Cunha, and N. Billon. Prediction of the tensile impact behavior

of injection molded samples from quasi-static data. *Polymer Engineering and Science*, 39(8):1463–1472, 1999.

[11] J.S. Godinho, A. Cunha, and R.J. Crawford. Prediction of the mechanical properties of polyethylene parts by different moulding methods. *Proceedings of the Institution of Mechanical Engineers, Part L: Journal of Materials: Design and Applications*, 216(L3):179–191, 2002.

[12] H. Zuidema, G.W.M. Peters, and H.E.H. Meijer. Development and validation of a recoverable strain-based model for flow-induced crystallization of polymers. *Macromolecular Theory and Simulation*, 10:447–460, 2001.

[13] R. Pantani, I. Coccorullo, V. Speranza, and G. Titomanlio. Modeling of morphology evolution in the injection molding process of thermoplastic polymers. *Progress in Polymer Science*, 30:1185–1222, 2005.

[14] Z. Tadmor. Molecular orientation in injection molding. *Journal of Applied Polymer Science*, 18:1753–1772, 1974.

[15] L.F.A. Douven, F.P.T. Baaijens, and H.E.H. Meijer. The computation of properties of injection-moulded products. *Progress in Polymer Science*, 20(3):403–457, 1995.

[16] Z. Bakerdjian and M.R. Kamal. Distribution of some physical properties in injection-molded thermoplastic parts. *Polymer Engineering and Science*, 17(2):98–100, 1977.

[17] A.I. Isayev. Orientation development in the injection molding of amorphous polymers. *Polymer Engineering and Science*, 23(5):271–284, 1983.

[18] R. Wimberger-Friedl. The assesment of orientation, stress and density distributions in injection-molded amorphous polymers by optical techniques. *Progress in Polymer Science*, 20(3):369–401, 1995.

[19] L.C.E. Struik. *Internal stresses, dimensional instabilities and molecular orientation in plastics*. John Wiley & Sons, 1990.

[20] R. Muller and J.J. Pesce. Stress-optical behaviour near the $T_g$ and melt flow-induced anisotropy in amorphous polymers. *Polymer*, 35(4):734–739, 1994.

[21] J.G. Rider and E. Hargreaves. Yielding of oriented poly(vinyl chloride). *Journal of Polymer Science: Part A-2*, 7:829–844, 1969.

[22] W. Retting. Orientierung, Orientierbarkeit und mechanische Eigenschaften von thermoplastischen Kunststoffen. *Colloid & Polymer Science*, 253:852–874, 1975.

[23] M. Takano and L.E. Nielsen. Effects of orientation and chemical structure on the strength properties of some polymers. *Polymer Engineering and Science*, 17(4):229–233, 1977.

[24] L.E. Govaert and T.A. Tervoort. Strain hardening of polycarbonate in the glassy state: Influence of temperature and molecular weight. *Journal of Polymer Science, Part B: Polymer Physics*, 42(11):2041–2049, 2004.

[25] G.B. McKenna. *Comprehensive Polymer Science, vol 2: Polymer Properties*, chapter Glass Formation and Glassy Behavior, pages 311–362. Pergamon Press, Oxford, 1989.

[26] A.J. Kovacs, J.J. Aklonis, J.M. Hutchinson, and R. Ramos. Isobaric volume and enthalpy recovery of glasses. (II). A transparent multiparameter theory. *Journal of Polymer Science: Polymer Physics Edition*, 17:1097–1162, 1979.

[27] G.W. Scherer. *Relaxation in glass and composites*. Krieger Publishing Company, 1986.

[28] I.M. Hodge. Enthalpy relaxation and recovery in amorphous materials. *Journal of Non-Crystalline Solids*, 169:211–266, 1993.

[29] S.L. Simon, J.W. Sobieski, and D.J. Plazek. Volume and enthalpy recovery of polystyrene. *Polymer*, 42:2555–2567, 2001.

[30] L.E. Govaert, T.A.P. Engels, E.T.J. Klompen, G.W.M. Peters, and H.E.H. Meijer. Processing induced properties in glassy polymers: Development of the yield stress in polycarbonate. *International Polymer Processing*, XX(2):170–177, 2005.

[31] T.A.P. Engels, L.E. Govaert, G.W.M. Peters, and H.E.H. Meijer. Processing induced properties in glassy polymers: Application of structural relaxation to yield stress development. *Journal of Polymer Science: Part B: Polymer Physics*, 44(8):1212–1225, 2006.

[32] E.T.J. Klompen, T.A.P. Engels, L.C.A. van Breemen, P.J.G. Schreurs, L.E. Govaert, and H.E.H. Meijer. Quantitative prediction of long-term failure of polycarbonate. *Macromolecules*, 38(16):7009–7017, 2005.

[33] B.H. Bersted and T.G. Anderson. Influence of molecular weight and molecular weight distribution on the tensile properties of amorphous polymers. *Journal of Applied Polymer Science*, 39:499–514, 1990.

[34] T.A. Tervoort, J. Visjager, and P. Smith. On abrasive wear of polyethylene. *Macromolecules*, 35:8467–8471, 2002.

[35] L.C.A. van Breemen, T.A.P. Engels, C.G.N. Pelletier, L.E. Govaert, and J.M.J. den Toonder. Numerical simulation of flat-tip micro-indentation of glassy polymers: Influence of loading speed and thermodynamic state. *Philosophical Magazine*, accepted, 2008.

[36] C.G.N. Pelletier, E.C.A. Dekkers, L.E. Govaert, J.M.J. den Toonder, and H.E.H. Meijer. The influence of indenter-surface misalignment on the results of instrumented indentation tests. *Polymer Testing*, 26:949–959, 2007.

[37] R. Haward and G. Thackray. The use of a mathematical model to describe isothermal stress-strain curves in glassy thermoplastics. *Proceedings of the Royal Society of London, Series A: Mathematical, Physical and Engineering Sciences*, 302:453–472, 1968.

[38] H.G.H. van Melick, L.E. Govaert, and H.E.H. Meijer. On the origin of strain hardening in glassy polymers. *Polymer*, 44:2493–2502, 2003.

[39] H.G.H. van Melick, L.E. Govaert, and H.E.H. Meijer. Localisation phenomena in glassy polymers: influence of thermal and mechanical history. *Polymer*, 44:3579–3591, 2003.

[40] E.J. Kramer. Open questions in the physics of deformation of polymer glasses. *Journal of Polymer Science, Part B: Polymer Physics*, 43:3369–3371, 2005.

[41] M. Wendlandt, T.A. Tervoort, and U.W. Suter. Non-linear, rate-dependent strain-hardening behavior of polymer glasses. *Polymer*, 46:11786–11797, 2005.

[42] M. Wendlandt, T.A. Tervoort, J.D. van Beek, and U.W. Suter. Segmental orientation in plastically deformed glassy PMMA. *Journal of the Mechanics and Physics of Solids*, 54:589–610, 2006.

[43] A.V. Lyulin, B. Vorselaars, M.A. Mazo, N.K. Balabaev, and M.A.J. Michels. Strain softening and hardening of amorphous polymers: atomistic simulation of bulk mechanics and local dynamics. *Europhysics Letters*, 71:618–624, 2005.

[44] R.S. Hoy and M.O. Robbins. Strain hardening of polymers glasses: effect of entanglement density, temperature , and rate. *Journal of Polymer Science, Part B: Polymer Physics*, 44:3487–3500, 2006.

[45] R.S. Hoy and M.O. Robbins. Strain hardening in polymers glasses: limitations of network models. *Physical Review Letters*, 99:117801, 2007.

[46] R.S. Hoy and M.O. Robbins. Strain hardening of polymers glasses: entanglements, energetics, and plasticity. *Physical Review E*, 77:031801, 2008.

[47] L.R.G. Treloar. *The physics of rubber elasticity*. Clarendon, Oxford, England, 3rd edition, 1975.

[48] R.N. Haward. Strain hardening of thermoplastics. *Macromolecules*, 26:5860–5869, 1993.

[49] M.C. Boyce, D.M. Parks, and A.S. Argon. Large inelastic deformation of glassy polymers. Part I: Rate dependent constitutive model. *Mechanics of Materials*, 7(1):15–33, 1988.

[50] P.D. Wu and E. van der Giessen. On improved network models for rubber elasticity and their applications to orientation hardening in glassy polymers. *Journal of the Mechanics and Physics of Solids*, 41(3):427–456, 1993.

[51] E.M. Arruda, M.C. Boyce, and H. Quintus-Bosz. Effects of initial anisotropy on the finite strain deformation behavior of glassy polymers. *International Journal of Plasticity*, 9:783–811, 1993.

[52] L.E. Govaert, H.G.H. van Melick, and H.E.H. Meijer. Temporary toughening of polystyrene through mechanical pre-conditioning. *Polymer*, 42:1271–1274, 2001.

[53] Athas data bank: http://athas.prz.edu.pl/.

[54] U. Gaur, S. Lau, and B. Wunderlich. Heat capacity and other thermodynamic properties of linear marcomolecules. IX. Final group of aromatic and inorganic polymers. *Journal of Physical and Chemical Reference Data*, 12(1):91–108, 1983.

[55] E.T.J. Klompen, T.A.P. Engels, L.E. Govaert, and H.E.H Meijer. Modelling of the post-yield response of glassy polymer: Influence of thermomechanical history. *Macromolecules*, 38(16):6997–7008, 2005.

[56] L.C.A. van Breemen, T.M. den Hartog, L.E. Govaert, and H.E.H. Meijer. Constitutive modeling of polymer glasses: A multi-mode approach. in preparation, 2008.

[57] H. Niklas and H.H. Kaush von Schmeling. Molekularstruktur und mechanische Eigenschaften von Polyvinylchloride III. Mitteilung: Ursachen zeitabhängiger Festigkeitseigenschaften von PVC-Rohren. *Kunstoffe*, 53:886–891, 1963.

## 4.A  Appendix: Relaxation time spectrum

**Table 4.4:** Relaxation time spectrum

| mode | $\eta_0 [\mathrm{Pa} \cdot \mathrm{s}]$ | $G [\mathrm{MPa}]$ |
|------|------|------|
| 1 | $2.10 \cdot 10^{17}$ | $3.50 \cdot 10^{2}$ |
| 2 | $3.48 \cdot 10^{16}$ | $5.55 \cdot 10^{1}$ |
| 3 | $2.95 \cdot 10^{14}$ | $4.48 \cdot 10^{1}$ |
| 4 | $2.84 \cdot 10^{13}$ | $4.12 \cdot 10^{1}$ |
| 5 | $2.54 \cdot 10^{12}$ | $3.50 \cdot 10^{1}$ |
| 6 | $2.44 \cdot 10^{11}$ | $3.20 \cdot 10^{1}$ |
| 7 | $2.20 \cdot 10^{10}$ | $2.75 \cdot 10^{1}$ |
| 8 | $2.04 \cdot 10^{9}$ | $2.43 \cdot 10^{1}$ |
| 9 | $1.83 \cdot 10^{8}$ | $2.07 \cdot 10^{1}$ |
| 10 | $1.68 \cdot 10^{7}$ | $1.81 \cdot 10^{1}$ |
| 11 | $1.51 \cdot 10^{6}$ | $1.55 \cdot 10^{1}$ |
| 12 | $1.40 \cdot 10^{5}$ | $1.37 \cdot 10^{1}$ |
| 13 | $1.27 \cdot 10^{4}$ | $1.19 \cdot 10^{1}$ |
| 14 | $1.10 \cdot 10^{3}$ | $9.80 \cdot 10^{0}$ |
| 15 | $1.23 \cdot 10^{2}$ | $1.04 \cdot 10^{1}$ |
| 16 | $2.62 \cdot 10^{0}$ | $2.11 \cdot 10^{0}$ |
| 17 | $2.14 \cdot 10^{0}$ | $1.64 \cdot 10^{1}$ |

# Predicting age-induced embrittlement of glassy polymers[1]

## Abstract

Upon physical aging the yield stress of tough amorphous polymers, like polycarbonate, increases, as does the polymer's resistance to static and dynamic fatigue loading expressed in the time-to-failure, but in the end embrittlement results. A direct correlation is found between the time evolution of the yield stress in an unnotched tensile bar, and that of impact energy measured using a notched tensile bar. In both cases a master curve can be constructed with an Arrhenius type shift function, using the same activation energy. To identify the cause of embrittlement, numerical simulations on notched bars are performed. A maximum in hydrostatic stress proves to be a good criterion to predict the onset of failure. However, to quantitatively describe the loss in energy take-up in notched tensile bars after embrittlement this simple criterion proves to be insufficient for the higher molecular weight polymers, since these maximal take up an extra 30% energy during craze extension and crack propagation. Finally an alternative criterion is proposed that could also serve for optimization in the design process: a critical value of the evolving yield stress. This value predicts a products sensitivity to damage. To be more precise it predicts whether a notched test bar, taken from a product that experienced aging in use, would break ductile or brittle.

# 5.1 Introduction

Below their glass transition temperature, $T_g$, amorphous polymers are in a non-equilibrium state and, as a result, their physical and mechanical properties are subject to change over time. This is called physical aging [1; 2]. During annealing, which is a heat treatment at elevated temperatures still below $T_g$, aging is accelerated and a marked increase in yield stress is achieved in short times [3–6]. Simultaneously the lifetime under static and dynamic loading conditions improves [7–11]. A drawback is that upon aging, strain softening increases with the increasing yield value and a stronger tendency to localize strain results [12], finally leading to complete brittle failure [13–17]. Annealing thus results in enhanced long-term properties, but diminished impact properties and finally leads to a change in failure mode.

Failure is, of course, an unwanted event in the application of any structural material. If failure has to occur, a predictable ductile mode of failure is desired, characterized by a considerable amount of energy dissipation prior to breakage, combined with an absence of debris causing extra damage. Some polymers always fail macroscopically brittle, e.g. polystyrene (PS) and poly(methyl methacrylate) (PMMA), while others like polycarbonate (PC) are tough. Despite, also in brittle PS on a local scale, inside craze fibrils, the deformations are very large [18; 19], while, on the other hand, notching ductile PC can result in craze formation and embrittlement. The apparent discrepancy between deformations on microscopic and macroscopic scales, can be explained based upon the polymer's intrinsic deformation kinetics [12; 20]. Key for toughness is the material's ability to delocalize strain, and it is hindered by strain softening and promoted by strain hardening. PS is brittle only because its strain softening is significant and strain hardening much too moderate, whereas PC is ductile since its strain softening is moderate and strain hardening is significant [21]. And where strain hardening is unaffected by physical aging, strain softening is, in a negative way.

The influence of the presence of low temperature secondary relaxation processes on embrittlement has long been subject of discussion. Where for some polymers, indeed, a correlation is found, mostly based on relaxation processes related to main-chain mobility [22], it is not the only explanation, simply because accelerated physical aging by annealing has a negligible effect on the secondary relaxation peak [23; 24]. However, secondary relaxation processes start to contribute to the stress response leading to an increase in yield stress at high deformation rates as occur e.g. under impact conditions. This increased yield stress gives a stronger strain softening [25], resulting in a stronger tendency to localize deformation and strain and therefore inducing brittleness.

Other influences on the embrittlement of polymers include strain rate [15; 26; 27], molecular weight [15; 16; 26; 28], thermal history [13–15; 23; 29–31], temperature [15], notch radius [15; 16; 23; 32], sample thickness (in notched specimen) [14; 23; 30] and the presence of solvents, know as Environmental Stress Cracking (ESC) [33; 34]. Molecular weight, thermal history and ESC influence the polymers intrinsic behavior, whereas the other parameters can be interpreted as changing conditions

of the experiment, which once the polymer's intrinsic behavior is known, can be taken into account accurately in predictive numerical modeling. In conclusion, all influences on the occurrence of brittleness in polymer's can be captured by either the material's intrinsic behavior, or the loading geometry and conditions.

Embrittlement that occurs in the presence of a notch [35; 36], called notch sensitivity, can be attributed to the buildup of a strong positive hydrostatic stress underneath the notch. The preferred mode of deformation for polymers is by shear yielding, but when large positive hydrostatic stresses are present the only option for the material to deform by flow to relieve the stress is by voiding followed by crazing. This was convincingly shown experimentally by gradually shifting the deformation mode of a notched bar from mode I bending to mode II bending, reducing the hydrostatic stress contribution finally to zero and enforcing a transition from brittle to ductile failure [37]. The critical hydrostatic stress at which voiding, followed by crazing, sets in is material dependent and related to network density. For polystyrene a value of around 40 MPa is found [38; 39], whereas for polycarbonate the values range between 81 and 95 MPa [40–42]. Since the critical hydrostatic stress is a local value, it can not be measured directly, but is determined in a combined experimental-numerical approach. The values for PC are found using different numerical approaches, such as slip-line field theory [43], and 3D elasto-plastic finite element analysis [42]. Although the material models used in these approaches do take yield into account, albeit not time dependent, they neglect characteristic polymer behavior such as strain softening and strain hardening and, very importantly, the evolution of the yield stress with time and temperature.

In our group a full 3D large-strain visco-plastic constitutive model has been developed over the years that accurately describes the large strain deformation behavior of glassy polymers over a broad range of loading conditions [6; 44]. This model not only captures the instantaneous material behavior, but also describes the evolution of the yield stress in time, as accelerated by temperature and stress, and can predict the enhanced long-term properties which are a result of the increase in yield stress [7]. To do so, a state parameter, $S_a$ has been introduced, which uniquely identifies the thermomechanical state of the material [6]. In this paper this model is applied to analyze changes in macroscopic mechanical behavior and local stress fields that occur upon aging of notched tensile bars, and to identify of a possible critical hydrostatic stress criterion related to the embrittlement of polycarbonate. Embrittlement is, in contrast to the yield behavior and evolution of yield [6], molecular weight dependent [15; 16; 26; 28] and, therefore, any criterion should also take molecular weight dependence into account. If such a criterion can be identified, it would proof valuable in polymer design and engineering as a safety limit to ensure a ductile mode of deformation upon final failure.

## 5.2 Experimental

### Materials

Materials used are injection molding grades of polycarbonate (PC): Lexan 121R, 141R and 101R, supplied as granules by Sabic Innovative Plastics (Bergen op Zoom, the Netherlands). The molecular weights, and molecular weight distributions, of the grades are listed in Table 5.1: PC-LM (121R), PC-MM (141R) and PC-HM (101R). Table 5.1 also lists the number-average molecular weight corrected for the fraction of short chains which do not contribute to the connectivity in the material and act as a diluent, multiplied by the volume fraction of 'effective' polymer, $\phi\bar{M}_n^*$ [45; 46].

**Table 5.1:** Polycarbonate molecular weights

|         | grade      | $\bar{M}_n$ [kg/mol] | $\bar{M}_w$ [kg/mol] | PDI  | $\phi\bar{M}_n^*$ [kg/mol] |
|---------|------------|------|------|------|------|
| PC-LM   | Lexan 121R | 9.8  | 23.4 | 2.38 | 13.6 |
| PC-MM   | Lexan 141R | 9.2  | 25.8 | 2.82 | 14.9 |
| PC-HM   | Lexan 101R | 16.1 | 30.7 | 1.91 | 16.6 |

Tensile bars are injection molded according to ISO 527 using an Arburg 320S 500-150 Allrounder. Processing conditions are kept the same for all grades. Notched specimen are obtained by notching tensile bars by a machining operation at room temperature. The radius of the notch is 0.4 mm, and the included angle 35°.

Annealing treatments are performed using hot air circulating ovens at various temperatures. Prior to testing samples are allowed to slowly cool to room temperature for at least 15 minutes.

### Methods

Tensile tests are performed on a Zwick Z010 universal tensile tester at ambient temperature (23℃). Experiments are performed by applying cons tant engineering strain rates or stresses. Unless indicated otherwise, a standard constant rate of $10^{-3}$s$^{-1}$ is used. In case of applied stresses, the time-to-failure is taken as the time-to-onset of localization.
Impact tests are performed on a servo-hydraulic MTS 831 Elastomer Testing System. Experiments are done at ambient temperature (23℃) at a const ant displacement rate of 100 mm/s [47].
All tensile yield stresses listed in the results section are engineering yield stresses. The impact results are taken as the mean value of 5 experiments; 68.3% confidence intervals are calculated.

# 5.3  Results

## Deformation kinetics and yield-stress evolution

Figure 5.1 displays the deformation kinetics of the three different molecular weight polycarbonates, showing the yield stress as a function of the strain rate applied (left), and the time-to-failure as a function of the stress applied (right). The kinetics are identical for all three polycarbonates, a result of the fact that they received exactly the same thermal history during processing, and therefore are apparently independent of molecular weight. Differences in thermal history are expressed in an increase in the absolute level of the stresses, whereas the slopes stay unaffected [6].
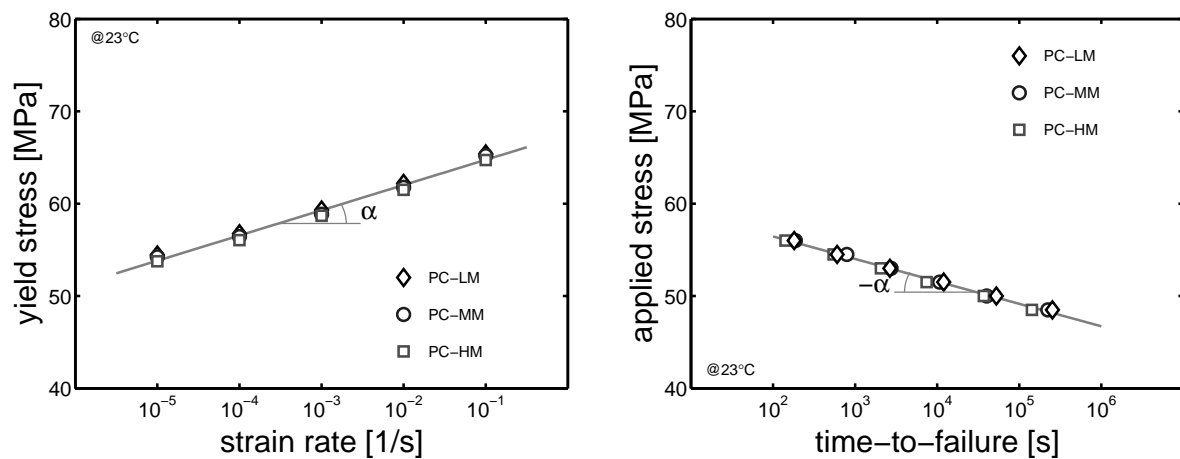


**Figure 5.1:** Deformation kinetics of polycarbonate. Left: yield stress versus strain rate. Right: Time-to-failure versus applied stress.
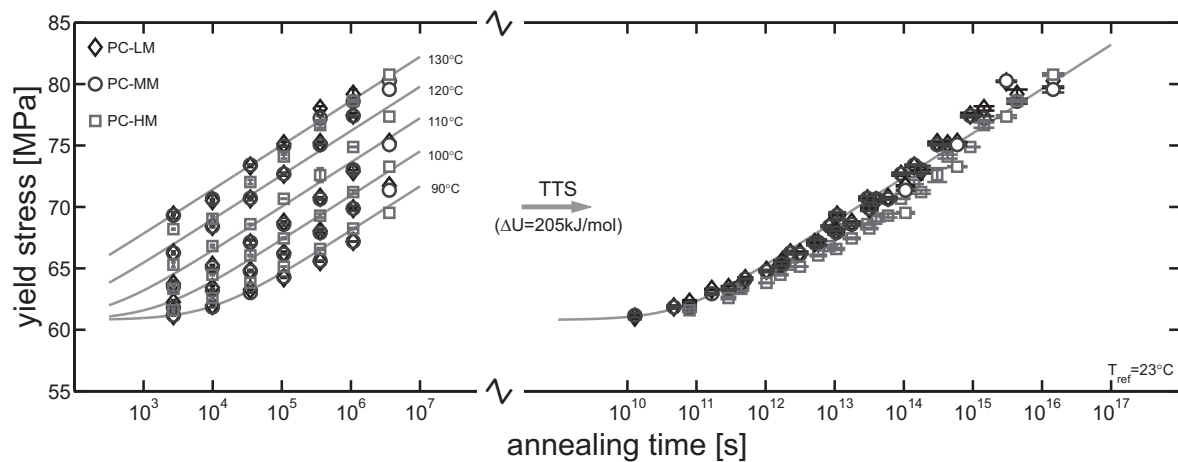


**Figure 5.2:** Yield stress versus annealing time for different annealing temperatures, and the master curve constructed thereof.

Results of the evolution of yield stress with time and temperature for all molecular weights are presented in Figure 5.2. Yield stresses increase with time for all temperatures investigated, no leveling off is observed. Therefore no equilibrium is reached, as might happen at high temperatures, just below $T_g$, for long annealing times [48; 49]. The master curve on the right-hand-side is constructed by Time-Temperature-Superposition (TTS), under the assumption of thermorheological simple behavior, using an Arrhenius type of temperature dependence resulting in a shift-factor, $a_T$, given by [6]:

$$a_T(T) = \exp\left(\frac{\Delta U}{R}\left(\frac{1}{T} - \frac{1}{T_{ref}}\right)\right) \tag{5.1}$$

where $\Delta U$ is the activation energy, R the universal gas constant, T the annealing temperature, and $T_{ref}$ a reference temperature (here taken as room temperature: 23°C).

The yield stress evolution with time is described by Equation 5.2, using the parameters from Table 5.2, and is shown as the solid drawn line in Figure 5.2 (right):

$$\sigma_y(t, T) = \sigma_{y,0} + c \cdot \log\left(\frac{t_{eff}(t, T) + t_a}{t_0}\right) \tag{5.2}$$

where the two constants $\sigma_{y,0}$ and c give the intersection of the curve with the vertical axis at $t = 1$ s, and the slope of yield stress with (the logarithm of) time in the linear relation, respectively, while $t_a$ is the initial age of the material. The scaling constant $t_0 = 1$s, and the effective time, $t_{eff}$, is defined as:

$$t_{eff}(t, T) = \int_0^t a_T^{-1}(T(t'))dt' \tag{5.3}$$

with $a_T$ the shift function, defined in Equation 5.1.

**Table 5.2:** Master curve parameters

|     | $\sigma_{y,0}$ [MPa] | c [MPa] | $t_a$ [s] |
|-----|------|------|------|
| PC* | 22.00 | 3.60 | $5.0 \cdot 10^{10}$ |

*taken from [6]; corrected for strain rate
and engineering stress

Master curves for all three molecular weights coincide within experimental error. Therefore also the evolution of the yield stress is, as expected, molecular weight in-

dependent. The activation energy related to the kinetics of aging ($\Delta U = 205$kJ/mol), corresponds well to the value found in a previous publication [6] that uses another molecular weight polycarbonate.

## Embrittlement upon aging

As a result of an increase in yield stress, embrittlement can occur, being a result of an enhanced tendency to strain localization [12]. This is illustrated in Figure 5.3 (results taken from [12]) where for an optical grade, thus low molecular weight, polycarbonate, $\bar{M}_n = 8100$ g/mol and $\bar{M}_w = 18700$ g/mol, the stress-strain curves for normal tensile bars are given for an as-received and an annealed sample (120 hours at 120℃). The first showing stable neck formation, while the second breaks brittle. In the present study the molecular weights are higher and all samples displayed necking, even after annealing for 1000 hours at 130℃, albeit that the neck be came instable for the longer annealing times. This is attributed to the pronounced molecular weight dependence of the tensile strength, the stress at which the deformed entanglement network breaks [45; 50; 51].
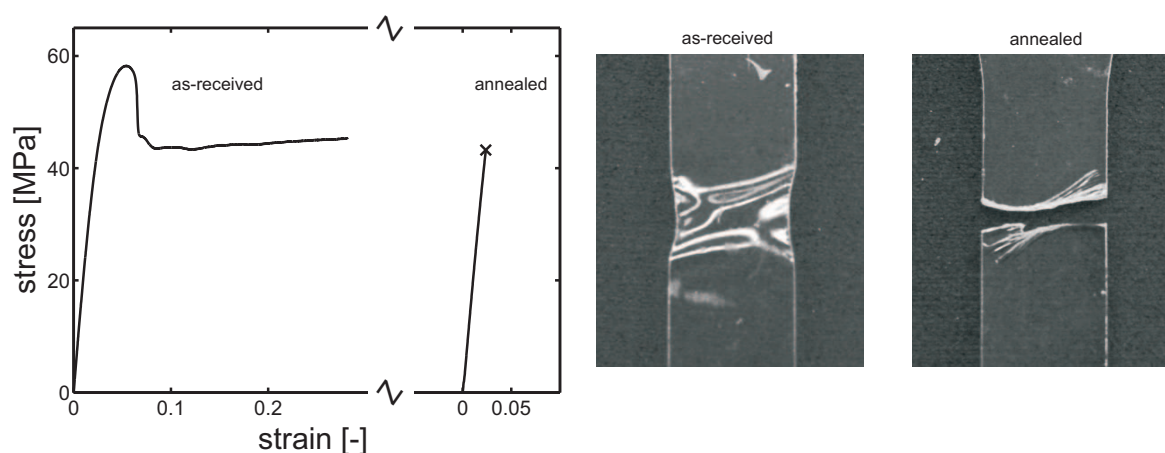


**Figure 5.3:** Embrittlement of an un-notched tensile bar, taken from [12]

To study the influence of increasing yield stress on ductility, notched samples are used [13; 31]. Figure 5.4 (left) shows embrittlement upon aging, changing annealing time and temperature. Higher annealing temperatures lead to embrittlement on shorter time-scales, and after annealing at 125℃ polyca rbonate becomes brittle even within an hour. As tensile strength, embrittlement is molecular weight dependent, see Figure 5.4 (right), where, after annealing at the same temperature (T = 120℃), the higher molecular weight material shows embritt lement on a significantly longer timescale. (All data of Figure 5.4 are taken from LeGrand [13].)
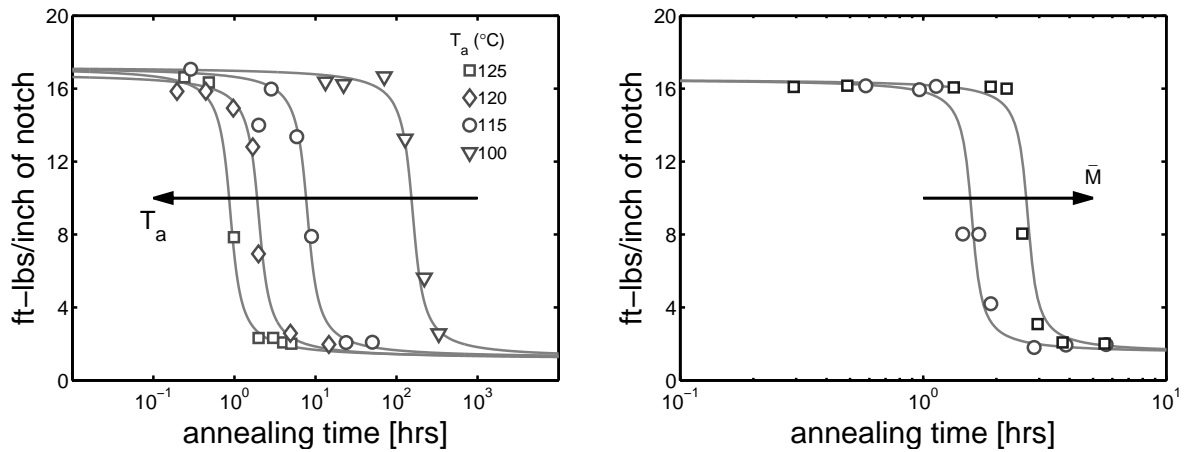
**Figure 5.4:** Embrittlement after aging of notched polycarbonate. Left: Influence of annealing temperature. Right: Influence of molecular weight. (Data reproduced from [13]).

## Numerical investigation of notch sensitivity

Failure is initiated at a local (microscopic) scale, near a stress concentrator. We prefer better defined conditions and study the local stress state under a notch, as it is influenced by physical aging. Rather than using the aging dependent value of the yield stress, we go one step back in the constitutive modeling to use the aging dependent value of the state parameter, $S_a$, since that is, in contrast to the yield stress, independent of loading conditions like strain rate, temperature and notch geometry. $S_a$ was introduced to uniquely define the thermomechanical state of a material [6]. It is directly proportional to the yield stress and it captures the ageing kinetics. It is the only parameter in our constitutive model which changes with thermal history, and it is given by:

$$S_a(t, T) = c_0 + c_1 \cdot \log\left(\frac{t_{eff}(t, T) + t_a}{t_0}\right) \tag{5.4}$$

where $c_0$ and $c_1$ are two constants with for PC values of -4.41 and 3.3, respectively, again $t_0 = 1s$, and the effective time is again determined from Equation 5.2.

Figure 5.5 gives the results obtained with a numerical simulation of the deformation of a notched tensile bar with $S_a = 40$, which corresponds to a tensile engineering yield stress of approximately 71 MPa if measured at a strain rate of $10^{-3}s^{-1}$. The notch radius used (0.4 mm) is chosen somewhat larger than those normally used in tests like the Izod impact test, ISO 108A: 0.25 mm, to facilitate the numerical investigations (smaller notch radii require extremely more refined meshes, thus severely more computational effort). The force increases with displacement until a maximum is reached, where we find plastic deformation over the complete cross-section of the
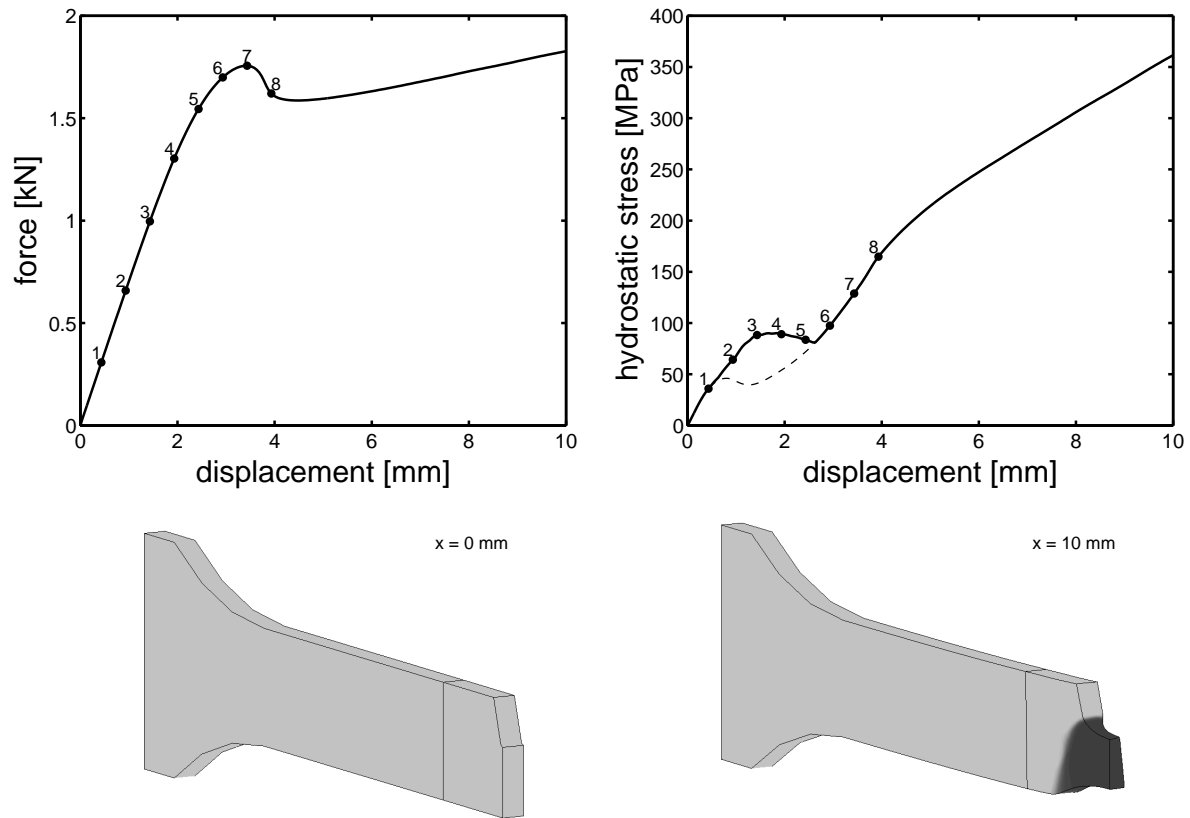
**Figure 5.5:** Top left: Force versus displacement for a notched tensile bar. Top right: Maximum hydrostatic stress underneath the notch (dashed line represents the hydrostatic stress close to the surface of the notch.) Bottom left: Initial geometry of the notched bar, and, right, after deformation (gray-scale indicates plastic deformation). Note: because of symmetry only a quarter of the actual geometry is used.

test bar. A detailed analysis of all numerical data reveals the value and position of the maximum in hydrostatic stress somewhere under the notch in the sample. (The hydrostatic stresses are stored for each integration point per displacement increment). A maximum in hydrostatic stress (top-right) is found before the maximum in force (top-left), correlating to the start of spreading of plastic deformation over the cross-section of the bar. Before this maximum (stages 1-3), plastic deformation is restricted to a small area directly underneath the notch. The maximum value of the hydrostatic stress starts at the surface of the notch, moves inwards to finally return to the surface again at large deformation (indicated by the dashed line in Figure 5.5).

This is further illustrated in Figure 5.6, where the plastic deformation (left) and the hydrostatic stress (right) are given at increasing loadings indicated with the corresponding numbers in Figure 5.5. The maximum hydrostatic stress builds up at the surface underneath the notch until plastic deformation starts to evolve (stages 1-2). The area of maximum hydrostatic stress is then pushed in front of the plastic deformation zone, moving towards a position away from the notch (stages 3-4-5).

## plastic deformation | hydrostatic stress
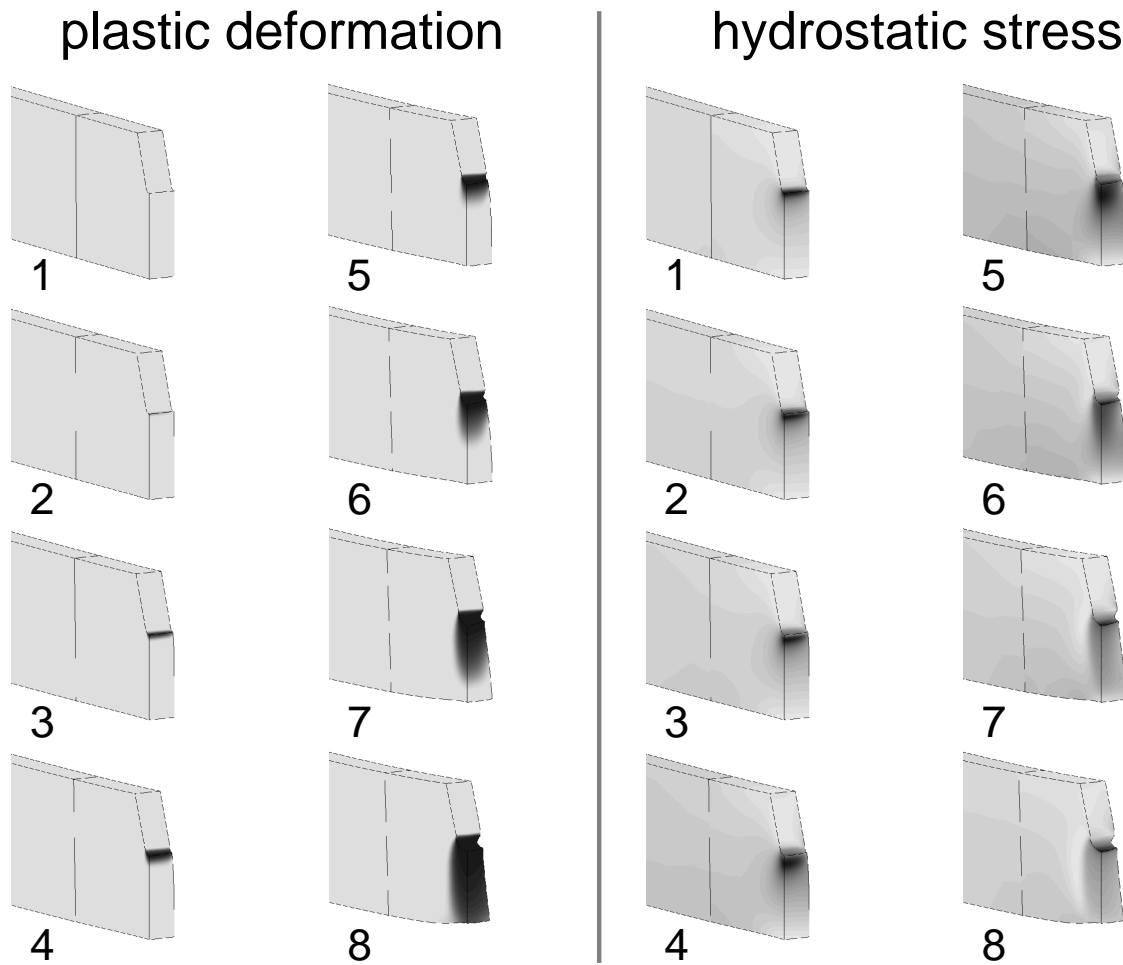


**Figure 5.6:** Left: Evolution of the plastic deformation underneath the notch. Right: Evolution of the hydrostatic stress underneath the notch. Numbers correspond to the positions as indicated in Figure 5.5.

When plastic deformation starts to evolve over the whole cross-section of the bar, the maximum returns to the surface of the notch (6-8). The results agree well, at least qualitatively, with those of other numerical investigations [40; 42]. Since the constitutive model does not incorporate a failure criterion, deformation in the simulation continues indefinitely. Experimentally, however, complete failure of the notched bar would long be observed.

Now we start to investigate the influence of physical aging on embrittlement. To do so we change the thermomechanical state of the material, by choosing different values of $S_a$. Varying its value over a large range from $S_a = 20, 30, 40$ to $50$ (corresponding to yield stresses of $\sigma_y \simeq 49, 60, 71$ and $82$ MPa, respectively) we find different force-displacement curves and different evolutions of the maximum hydrostatic stress, see Figure 5.7. Both the force (left) and the maximum hydrostatic stress (right) increase significantly with increasing the value of $S_a$. Upon increasing $S_a$, the plastic deformation zone is more stronger localized underneath the notch for longer loading stages,
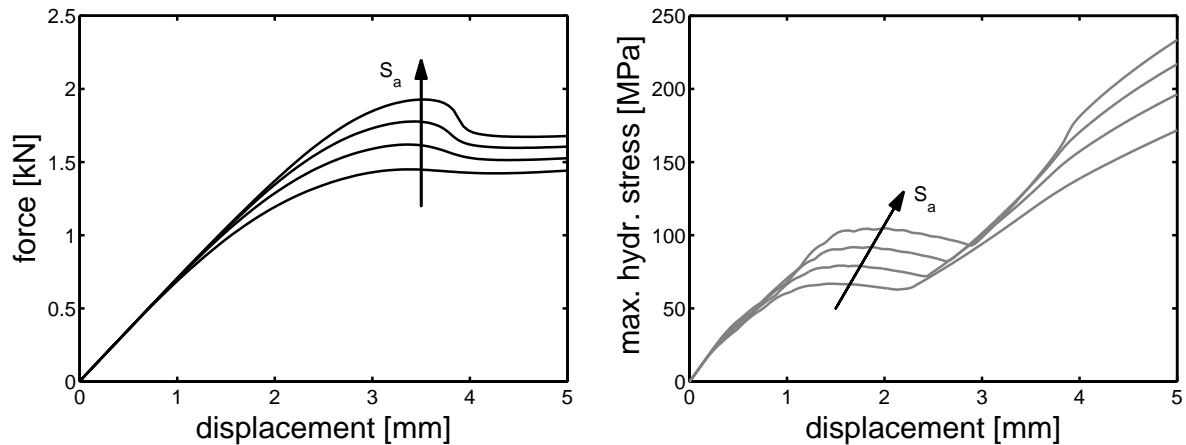
**Figure 5.7:** Influence of physical aging on the response of a notched tensile bar. Left: Force versus displacement. Right: Maximum hydrostatic stress versus displacement. (note: $S_a$ is a measure for the thermodynamic state of the material and larger values indicate an increase in age.)

which causes an increase with $S_a$ in the hydrostatic stress observed, from a value of $\simeq 67$ MPa for $S_a = 20$, to $\simeq 100$ MPa for $S_a = 50$, well above the value of the hydrostatic stress which is indicated as being critical, for PC between 81 and 95 MPa [40–42].

## A criterion for embrittlement

By combining numerical and experimental results, we can judge the applicability of a hydrostatic stress criterion with respect to embrittlement of notched samples. Figure 5.8 shows the notched impact energy versus annealing time for three molecular weights (LM, MM and HM) at five different annealing temperatures, 90-130℃, with their master curves shown at the right-hand-sid e of the figure. Time-to-embrittlement decreases with increasing annealing temperature and embrittlement occurs on shorter timescales for lower molecular weights, which is in agreement with the observations of LeGrand [13]. Remarkably, if Time-Temperature-Superposition (TTS) is applied, using the same activation energy as found for the yield stress (205kJ/mol), smooth master curves can be constructed, see Figure 5.8 (right). This indicates that the evolution of the yield stress is determining for the observed evolution of embrittlement. The time-to-embrittlement (for a given reference temperature and here taken as room temperature) is molecular weight dependent in a unique way, as are the initial value and especially the final value (after embrittlement) of the impact energy. The highest molecular weight material shows a factor two higher impact values after annealing. The vertical dashed lines in Figure 5.8 indicate the time at which half of the initial impact energy for each material remains, and is taken as the representative time-to-embrittlement for the different molecular weights.

Using Equation 5.4, the corresponding values of $S_a$ for each molecular weight can be determined at these characteristic times, and the results are given in Table 5.3
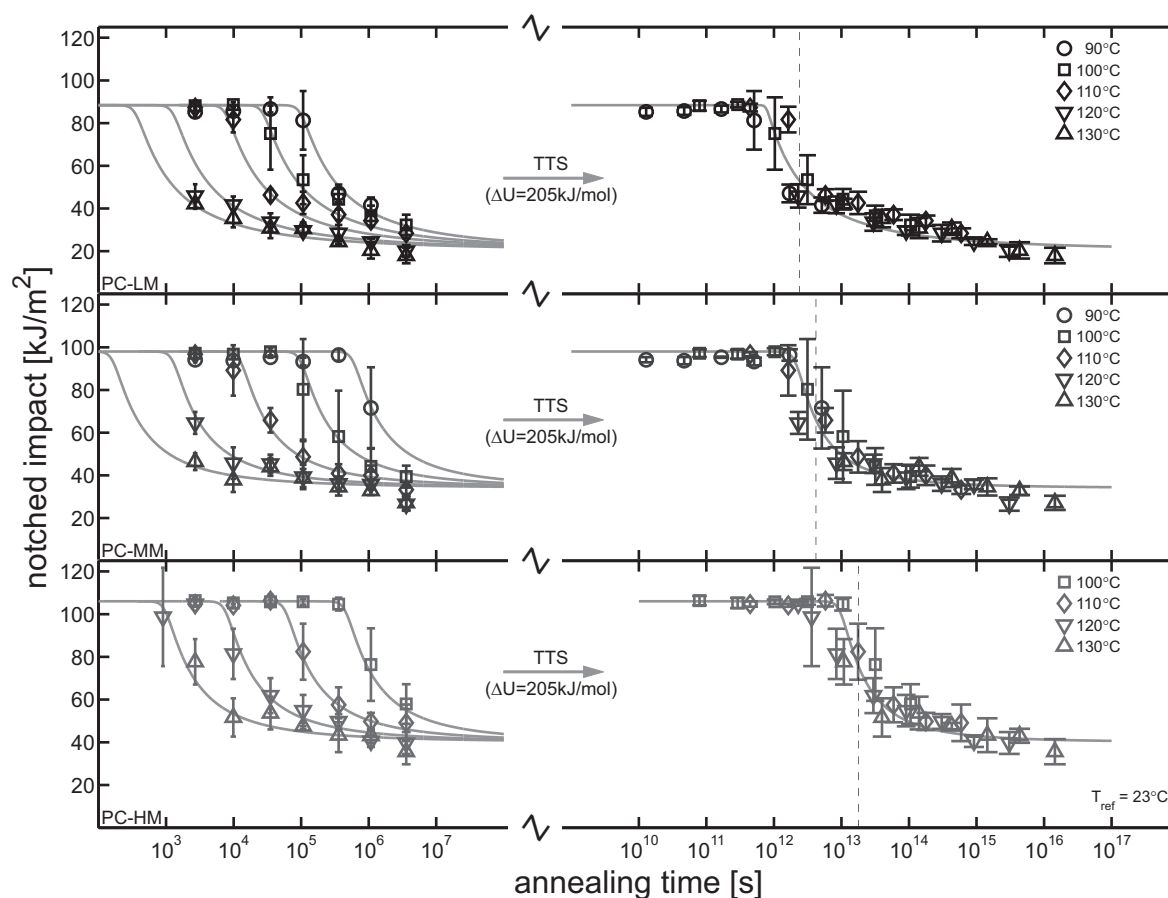
**Figure 5.8:** Notched impact energy versus annealing time and master curves con-
structed thereof, for all three molecular weights used from top to bottom
PC-LM, PC-MM and PC-HM. In shifting of the curves the same activation
energy is used as in Figure 5.2.

together with the corresponding yield stresses. Higher molecular weights give longer
timescales, and therefore higher values for the state parameter, $S_a$, and for the yield
stress, $\sigma_y$. The calculated values of $S_a$ can now be used as input for our con-
stitutive model to investigate the local stress state under the notch at the time-to-
embrittlement.

**Table 5.3:** Values of the state parameter corresponding to the time-to-embrittlement
of Figure 5.8 and corresponding yield stresses.

|              | PC-LM | PC-MM | PC-HM |
|--------------|-------|-------|-------|
| $S_a$[-]     | 35.8  | 36.7  | 38.6  |
| $\sigma_y^*$ [MPa] | 66.1  | 67.0  | 69.1  |

$^*$ eng. yield stress at $\dot{\epsilon} = 10^{-3}s^{-1}$.

Before investigating the embrittlement on a local scale, it is verified whether the constitutive model gives proper descriptions of the macroscopic response. Figure 5.9 (left) shows the results of unnotched tensile bars that neck. For both states, the as-received and the one annealed (for 1000 hours at 120°C), t he stress-strain response, including necking, is described well by the model, where only $S_a$ is changed. In Figure 5.9 (right) the force versus displacement curves are shown for the corresponding notched tensile bars (for clarity the annealed curve is shifted horizontally). Prior to failure again excellent agreement is found in predicted and measured force-displacement curves, although the simulations continue, where experimentally samples fail. For the as-received sample a ductile failure mode is observed, whereas the annealed sample fails in a brittle manner.
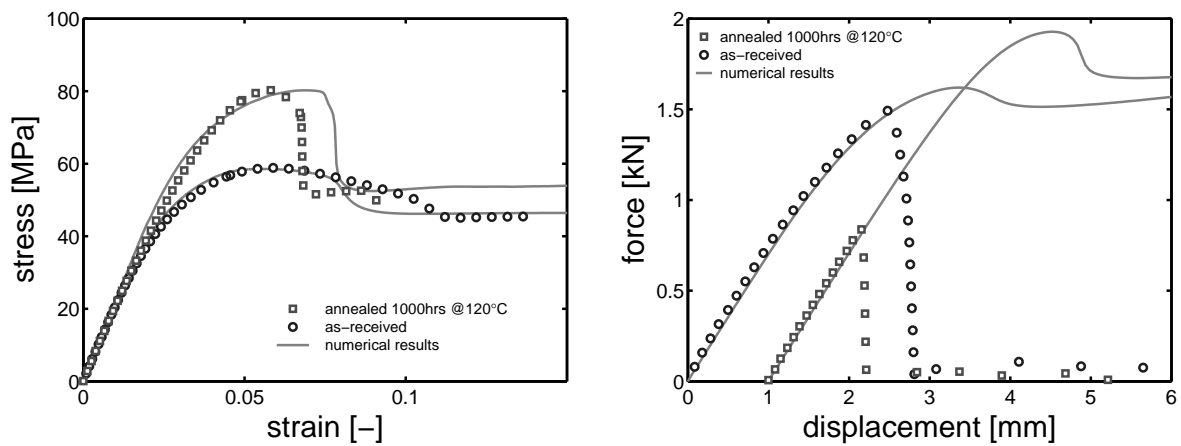


**Figure 5.9:** Experimental versus numerical results for as-received samples and annealed samples. Left: Stress versus strain for unnotched bars. Right: Load versus displacement for notched bars.

Because the macroscopic response of as-received and annealed samples is accurately predicted, we now turn to the local analyses at the time-of-embrittlement for all three molecular weights, using the $S_a$ values of Table 5.3, see Figure 5.10 (top). Apart from the force versus displacement curves (solid lines, left vertical axis), also the maximum hydrostatic stress versus displacement (dashed lines, right vertical axis) is shown. The maximum in the maximum hydrostatic stress increases with $S_a$, as was observed in Figure 5.7. Its increase with increasing molecular weight is only minor: 86.5, 87.6 and 90.0 MPa, respectively, see Figure 5.10 (top). The markers on the load-displacement curves indicate where experimentally the maximum in force is observed and failure occurs. Only for the lowest molecular weight material this point coincides with the maximum in maximum hydrostatic stress underneath the notch. For the higher molecular weight materials, macroscopic failure occurs at forces that are increasingly larger than the force that corresponds to the maximum in hydrostatic stress. From the predicted force-displacement curves impact energies can be calculated corresponding to the maximum in hydrostatic stress as well as to the experimental failure point (markers Figure in 5.8). Results are given in Table 5.4 and for

PC-LM agreement is found within 10%, whereas values using the critical hydrostatic stress criterion are underestimated compared to the experimental ones for PC-MM and PC-HM by 25% and 30%, respectively. Also the experimental impact energies at the characteristic times-to-embrittlement and after embrittlement are given.

**Table 5.4:** Impact energies calculated from predicted and experimental force-displacement curves.

|  | impact energy [kJ/m$^2$] | | | |
|---|---|---|---|---|
|  | max. $\sigma^h$ | max. force ($\star$) | time-to-embrittlement | after embrittlement |
| PC-LM | 42.7 | 45.6 | 48.2 | 17.3 |
| PC-MM | 43.7 | 56.7 | 61.5 | 25.4 |
| PC-HM | 45.2 | 62.5 | 70.1 | 33.5 |
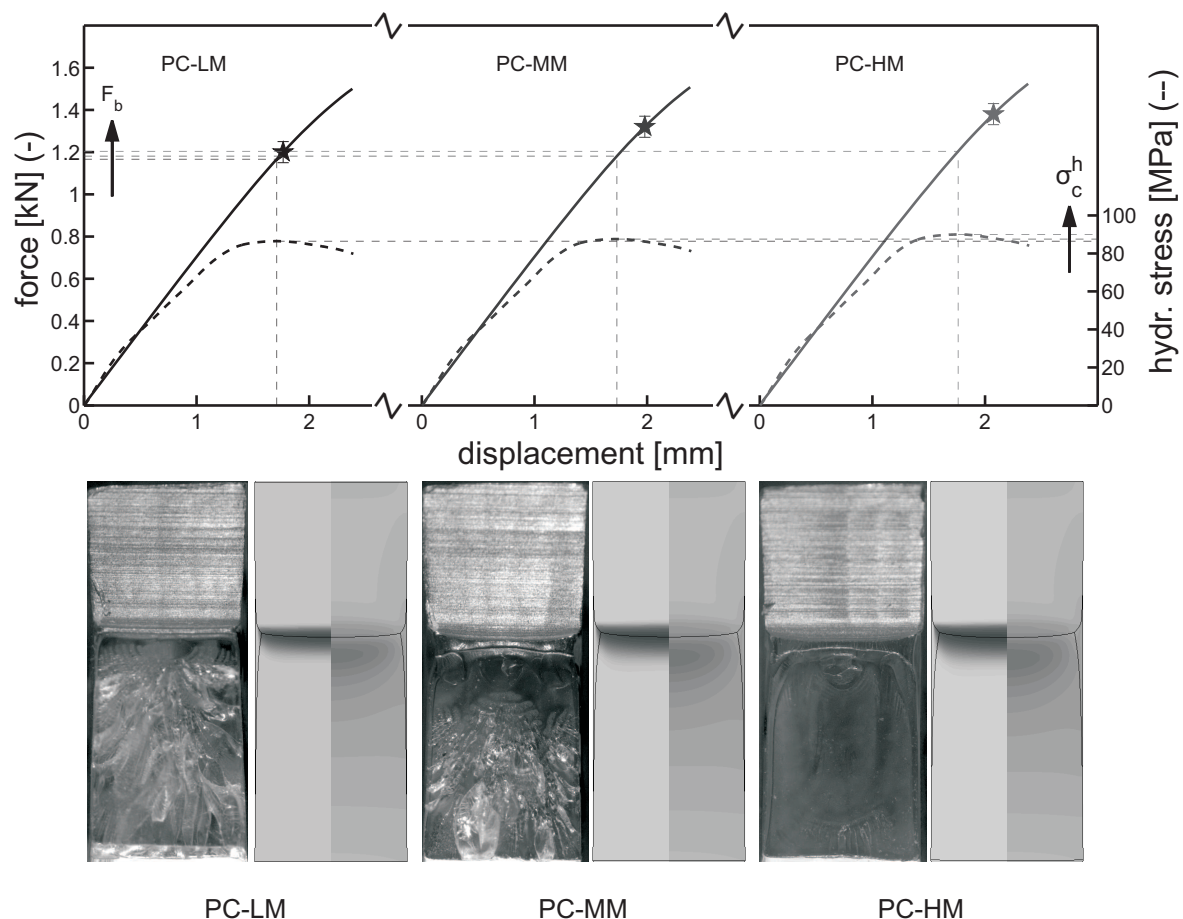


**Figure 5.10:** Top: Numerically determined force and maximum hydrostatic stress versus displacement for three molecular weights at their respective times-to-embrittlement. Bottom: Corresponding fracture images and their numerical equivalents of plastic deformation (left) and hydrostatic stress (right).
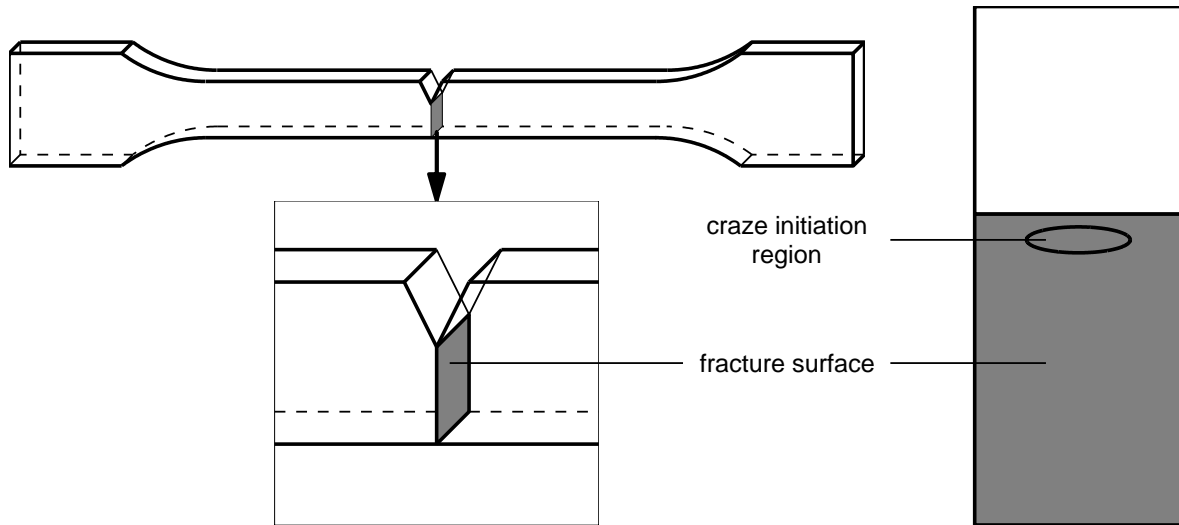
**Figure 5.11:** Notched tensile sample and illustration of the fracture surface.

Figure 5.10 (bottom) displays images of the fracture surface, taken from fractured samples that failed at a loading force indicated by the markers in the top of the figure. For clarity, Figure 5.11 illustrates the indicated surface. Next to the images, the numerically calculated plastic deformations (left half of the simulation results) and hydrostatic stress (right half of the simulation results) at the respective breaking forces, marked with a ☆ in Figure 5.10 (top), are shown. The differences in results for different molecular weights in the calculated results are minor. The experimental images reveal larger differences, correlating to the extra absorbed energy, after initiation of embrittlement, that change with molecular weight, see Figure 5.8.

Closer examination of the fracture surfaces near the notch, see Figure 5.12, reveals different shapes and sizes of the crazes formed underneath the notch [40], and that eventually evolve into a propagating crack in the middle of the test bar. For PC-LM, a craze is initiated, just below the surface of the notch, that almost immediately transforms into a unstable propagating crack, witnessed by the rough fracture surface. For the PC-MM and PC-HM extended, stable, crazes are observed before unstable propagation of the crack occurs through this crazed surface [52; 53]. For PC-MM the crazed surface covers one third of the fracture surface, adjacent to the initiation region, whereas for PC-HM it covers almost the entire fracture surface (and only at the very last can a small truly brittle fracture surface be observed). Since a craze is load bearing also in polycarbonate [54], the experimental force can still increase after craze initiation. It therefore appears that craze initiation starts at loads below the maximum in force (e.g. at a critical hydrostatic stress) observed in the experiments for the PC-MM and PC-HM, in complete correspondence to the results in [40]. A critical value of the hydrostatic stress therefore appears to be a good indicator of the initiation of failure only, but the molecular weight apparently has an influence on the propagation of crazes and cracks up to failure. So although surpassing a critical hydrostatic stress thus is a prerequisite for the occurrence of brittle failure, and

PC–LM                          PC–MM                          PC–HM
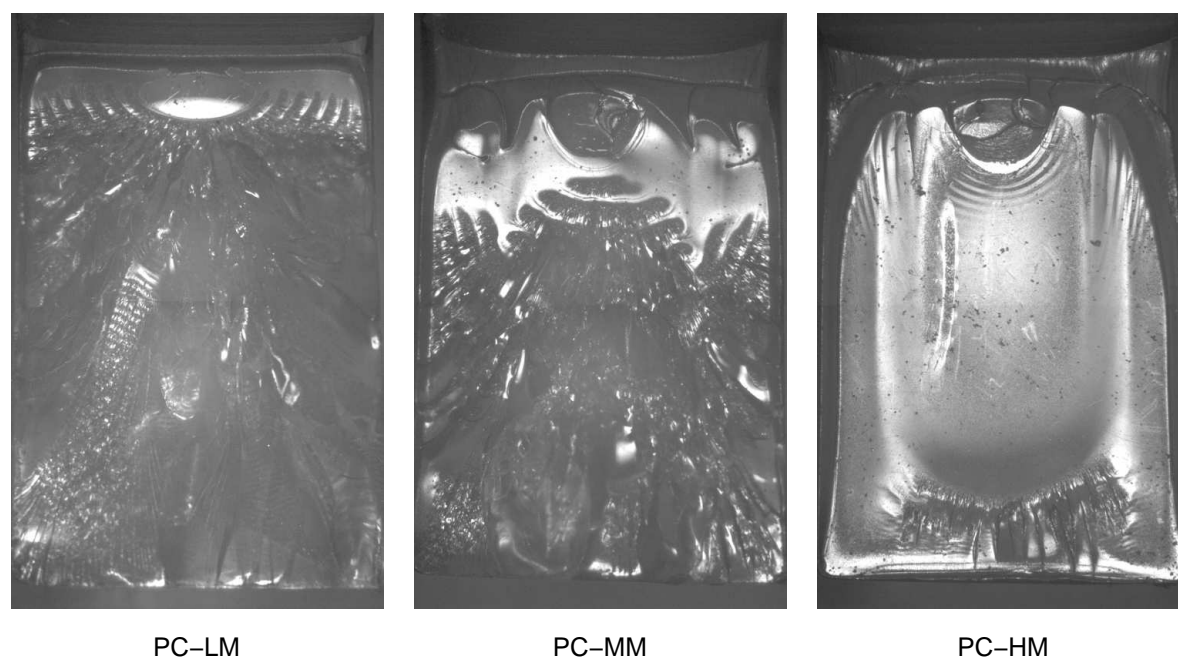
**Figure 5.12:** Images of fracture surfaces: crack propagates from top to bottom.

a good criterion for its initiation (in our experiments the critical value for PC samples was ca. 85 MPa), it appears that hydrostatic stress alone is an insufficient criterion for a quantitative description of a transition in failure mode, and some more details about craze growth and crack propagation should be included. At least if for the HM grade also the last 30% of the energy absorption upon break should be predicted quantitatively.

A final difficulty in predicting embrittlement is that it also can occur without a notch being present, see e.g. Figure 5.3. Instead of a (relatively well defined) notch, a more undefined stress concentrator like e.g. an impurity in the material or a surface scratch or flaw, can act as initiator of failure. A hydrostatic stress criterion can only be used in combination with a well defined defect geometry. Rather then trying to obtain a typical characteristic defect, scratch or flaw, geometry, we try the concept of a critical yield stress. The choice is inspired by that (i) the yield stress determines the softening, and thus the severeness of strain localization, and by (ii) that we found a strong relation between the evolution of yield stress with annealing time and the impact energy with annealing time, since both sets of data can be shifted using exactly the same activation energy, compare Figures 5.2 and 5.8. We chose the yield stress at the (molecular weight dependent) time-to-embrittlement, as listed in Table 5.3. Figure 5.13 repeats the data from Figure 5.2, and adds with dashed lines the computed yield stresses for the molecular weights at the time-to-embrittlement from Table 5.3. It can be determined when the critical yield stress is reached for any annealing temperature, or alternatively the maximum allowable Continuous Use Temperature (CUT) can be determined for a desired life-time ($t_{CUT}$), by combining Equations 5.1, 5.2 and 5.3:

$$CUT = \left( \frac{1}{T_{ref}} - \frac{R}{\Delta U} \ln \left( \frac{t_0}{t_{CUT}} 10^{((\sigma_{y,c} - \sigma_{y,0})/c)} - \frac{t_a}{t_{CUT}} \right) \right)^{-1} \qquad (5.5)$$
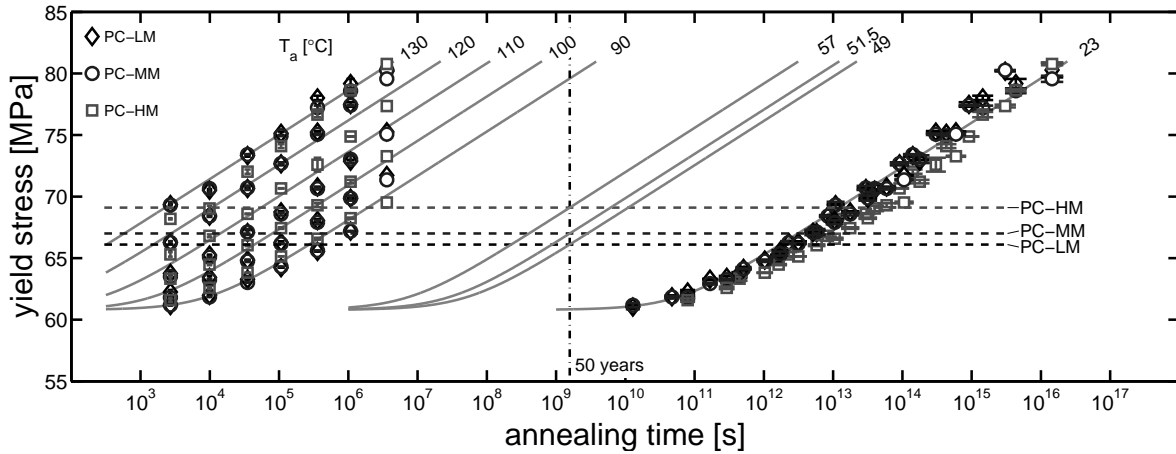


**Figure 5.13:** Evolution of yield stress versus annealing time for different annealing temperatures, and the critical yield stresses for the molecular weights investigated.

As an example, a life-time of 50 years is taken: the vertical dash-dot line at ~ $10^9$ seconds. The maximum allowable application temperatures range from 49°C for the lowest molecular weight, to 57°C for the highest molecular w eight PC. These limits do not indicate actual embrittlement, but rather that a polymer of this age put under this temperature would fail brittle under notched impact conditions as defined in this paper. Of course, such a critical yield stress can also be related to a standardized notched impact test, such as Izod impact according to ISO or ASTM.

## 5.4 Conclusions

The embrittlement of polycarbonate upon aging in notched tensile bars is investigated. The evolution of the yield stress with annealing time and temperature in unnotched bars is found to be independent of the molecular weight. In contrast, both the impact energy and time-to-embrittlement depend in notched bars on the molecular weight. Evolution of yield stress and evolution of impact energy can be shifted to master curves using the same activation energy, indicating that the evolution of yield stress determines embrittlement.

A molecular weight dependent critical hydrostatic stress is found to be a good criterion to predict the initiation of failure, but it appears to be insufficient for an exact quantitative description of embrittlement because craze and crack propagation after

cavitation contribute somewhat (in the order of 30%) to the load bearing capacity of the higher molecular weight polymers. As an alternative indicator for embrittlement, a critical value of the yield stress is proposed. Application of this criterion does not provide a quantitative value of impact energies after embrittlement, but rather indicates when a material with a given age used at a given temperature would fail in a brittle manner would it be tested under notched impact conditions.

# References

[1] L.C.E. Struik. *Physical aging of amorphous polymers and other materials*. Elsevier, Amsterdam, 1978.

[2] J.M. Hutchinson. Physical aging of polymers. *Progress in Polymer Science*, 20:703–760, 1995.

[3] A. Aref-Azar, F. Biddlestone, J.N. Hay, and R.N. Haward. The effect of physical ageing on the properties of poly(ethylene terephthalate). *Polymer*, 24:1245–1251, 1983.

[4] D.J. Kemmish and J.N. Hay. The effect of physical ageing on the properties of amorphous PEEK. *Polymer*, 26:905–912, 1985.

[5] O.A. Hasan, M.C. Boyce, X.S. Li, and S. Berko. An investigation of the yield and postyield behavior and corresponding structure of poly(methyl methacrylate). *Journal of Polymer SCience: Part B: Polymer Physics*, 31:185–197, 1993.

[6] E.T.J. Klompen, T.A.P. Engels, L.E. Govaert, and H.E.H Meijer. Modelling of the post-yield response of glassy polymer: Influence of thermomechanical history. *Macromolecules*, 38(16):6997–7008, 2005.

[7] E.T.J. Klompen, T.A.P. Engels, L.C.A. van Breemen, P.J.G. Schreurs, L.E. Govaert, and H.E.H. Meijer. Quantitative prediction of long-term failure of polycarbonate. *Macromolecules*, 38(16):7009–7017, 2005.

[8] R.P.M. Janssen, D. de Kanter, L.E. Govaert, and H.E.H. Meijer. Fatigue life predictions for glassy polymers: a constitutive approach. *Macromolecules*, 41:2520–2530, 2008.

[9] I. Narisawa, M. Ishikawa, and H. Ogawa. Delayed yielding of polycarbonate under constant load. *Journal of Polymer Science: Polymer Physics Edition*, 16:1459–1470, 1978.

[10] J.M. Crissman and G.B. McKenna. Relating creep and creep rupture in PMMA using a reduced variable approach. *Journal of Polymer Science: Part B: Polymer Physics*, 25:1667–1677, 1987.

[11] J.M. Crissman and G.B. McKenna. Physical and chemical aging in PMMA and their effects on creep and creep rupture behavior. *Journal of Polymer Science: Part B: Polymer Physics*, 28:1463–1473, 1990.

[12] H.G.H. van Melick, L.E. Govaert, and H.E.H. Meijer. Localisation phenomena in glassy polymers: influence of thermal and mechanical history. *Polymer*, 44:3579–3591, 2003.

[13] D.G. Legrand. Crazing, yielding, and fracture of polymers. I. Ductile brittle transition in polycarbonate. *Journal of Applied Polymer Science*, 13:2129–2147, 1969.

[14] G.A. Adam, A. Cross, and R.N. Haward. The effect of thermal pretreatment on the mechanical properties of polycarbonate. *Journal of Materials Science*, 10:1582–1590, 1975.

[15] J.T. Ryan. Impact and yield properties of polycarbonate as a function of strain rate, molecular weight, thermal history and temperature. *Polymer Engineering and Science*, 18(4):264–267, 1978.

[16] G.L. Pitman, I.M. Ward, and R.A. Duckett. The effects of thermal pre-treatment and molecular weight on the impact behaviour of polycarbonate. *Journal of Materials Science*, 13:2092–2104, 1978.

[17] R.A. Bubeck, S.E. Bales, and H.D. Lee. Changes in yield and deformation of polycarbonates caused by physical aging. *Polymer Engineering and Science*, 24(10):1142–1148, 1984.

[18] A.M. Donald and E.J. Kramer. Deformation zones and entanglements in glassy polymers. *Polymer*, 23(8):1183–1188, 1982.

[19] A.M. Donald, E.J. Kramer, and R.A. Bubeck. The entanglement network and craze micromechanics in glassy polymers. *Journal of Polymer Science, Polymer Physics Edition*, 20(7):1129–1141, 1982.

[20] H.E.H. Meijer and L.E. Govaert. Multi-scale analysis of mechanical properties of amorphous polymer systems. *Macromolecular Chemistry and Physics*, 204:274–288, 2003.

[21] R.J.M. Smit, W.A.M. Brekelmans, and H.E.H. Meijer. Predictive modelling of the properties and toughness of polymeric materials, Part I, Why is polystyrene brittle and polycarbonate tough? *Journal of Materials Science*, 35:2855–2867, 2000.

[22] J. Heijboer. Dynamic mechanical properties and impact strength. *Journal of Polymer Science: Part C*, 16:3755–3763, 1968.

[23] G. Allen, D.C.W. Morley, and T. Williams. The impact strength of polycarbonate. *Journal of Materials Science*, 8:1449–1452, 1973.

[24] M.G. Wyzgoski and G.S.Y. Yeh. Origin of impact strength in polycarbonate: II. Effect of thermal treatment. *International Journal of Polymeric Materials*, 3:149–163, 1974.

[25] E.T.J. Klompen. *Mechanical properties of solid polymers: constitutive modelling of long and short term behavior. Chapter 4: Post-yield response of glassy polymers: influence of thermorheological complexity*. PhD thesis, Eindhoven University of Technology, 2005.

[26] J.H. Golden, B.L. Hammant, and E.A. Hazell. Effects of molecular weight and strain rate on the flexural properties of polycarbonate. *Journal of Applied Polymer Science*, 12:557–569, 1968.

[27] R.J. Gaymans, M.J.J. Hamberg, and J.P.F. Inberg. The brittle-ductile transition temperature of polycarbonate as a function fo test speed. *Polymer Engineering*

*and Science*, 40(1):256–262, 2000.

[28] J.H. Golden and E.A. Hazell. Degradation of a polycarbonate by ionizing radiation. *Journal of Polymer Science: Part A*, 1:1671–1686, 1963.

[29] J.H. Golden, B.L. Hammant, and E.A. Hazell. The effect of thermal pretreatment on the strenght of polycarbonate. *Journal of Applied Polymer Science*, 11:1571–1579, 1967.

[30] L.J. Broutman and S.M. Krishnakumar. Impact strength of polymers: 1. The effect of thermal treatment and residual stress. *Polymer Engineering and Science*, 16(2):74–81, 1976.

[31] T.W. Cheng, H. Keskkula, and D.R. Paul. Thermal aging of impact-modified polycarbonate. *Journal of Applied Polymer Science*, 45:531–551, 1992.

[32] E. Plati and J.G. Williams. Effect of temperature on the impact fracture toughness of polymers. *Polymer*, 16:915–920, 1975.

[33] C.H.M. Jacques and M.G. Wyzgoski. Prediction of environmental stress cracking of polycarbonate from solubility considerations. *Journal of Applied Polymer Science*, 23:1153–1166, 1979.

[34] J.C. Arnold. Craze initiation during the environmental stress cracking of polymers. *Journal of Materials Science*, 30:655–660, 1995.

[35] M. Takano and L.E. Nielsen. The notch sensitivity of polymeric materials. *Journal of Applied Polymer Science*, 20:2193–2207, 1976.

[36] R.A.W. Fraser and I.M. Ward. The impact fracture behaviour of notched specimens of polycarbonate. *Journal of Materials Science*, 12:459–468, 1977.

[37] Y. Kuriyama and I. Narisawa. Fracture behaviour of ductile polymer under mixed mode loading. *Annual Tehnical Conference - Society of Plastics Engineers*, 3:3235–3237, 1994.

[38] I. Narisawa and A.F. Yee. Crazing and fracture of polymers. In R.W. Cahn, P. Haasen, and E.J. Kramer, editors, *Materials science and technology: a comprehensive treatment. Structure and properties of polymers*, volume 12, chapter 15, pages 699–765. VCH Publishers Inc., New York, 1993.

[39] H.G.H. van Melick, O.F.J.T. Bressers, J.M.J. den Toonder, L.E. Govaert, and H.E.H. Meijer. A micro-indentation method for probing the craze-initiation stress in glassy polymers. *polymer*, 44:2481–2491, 2003.

[40] M. Ishikawa, I. Narisawa, and H. Ogawa. Criterion for craze nucleation in polycarbonate. *Journal of Polymer Science: Polymer Physics Edition*, 15:1791–1804, 1977.

[41] R.P. Kambour and E.A. Farraye. Crazing beneath notches in ductile glassy polymers: a materials correlation. *Polymer Communications*, 25(12):357–360, 1984.

[42] R.P. Nimmer and J.T. Woods. An investigation of brittle failure in ductile notch-sensitive thermoplastics. *Polymer Engineering and Science*, 32(16):1126–1137, 1992.

[43] R. Hill. *The mathematical theory of plasticity*. Oxford University Press, Oxford, 1950.

[44] L.C.A. van Breemen, T.M. den Hartog, L.E. Govaert, and H.E.H. Meijer. Constitutive modeling of polymer glasses: A multi-mode approach. in preparation, 2008.

[45] B.H. Bersted and T.G. Anderson. Influence of molecular weight and molecular weight distribution on the tensile properties of amorphous polymers. *Journal of Applied Polymer Science*, 39:499–514, 1990.

[46] T.A. Tervoort, J. Visjager, and P. Smith. On abrasive wear of polyethylene. *Macromolecules*, 35:8467–8471, 2002.

[47] At high deformation/strain rates, the secondary relaxation process in PC contributes to the stress. The deformation rate was chosen such that the maximum strain rates in a specimen stay clear of this high strain rate regime. Typically the secondary process starts to contribute at strain rates of $10^0 - 10^1$ s$^{-1}$ for PC, and the transition to the high strain rate regime occurs gradually over a number of decades. The macroscopic strain rate chosen here is $10^0$ s$^{-1}$, which will be amplified under the notch by a factor of ~6, but still below the high strain rate regime.
Rather than using an Izod impact test, a notched tensile bar is chosen, since tensile testing allows instrumented testing and recording of the complete load-displacement curves, rather than a single impact energy.

[48] C. Bauwens-Crowet and J.C. Bauwens. Annealing of polycarbonate below the glass transition temperature up to equilibrium: A quantitative interpretation of enthalpy relaxation. *Polymer*, 27:709–713, 1985.

[49] T.A.P. Engels, L.E. Govaert, G.W.M. Peters, and H.E.H. Meijer. Processing induced properties in glassy polymers: Application of structural relaxation to yield stress development. *Journal of Polymer Science: Part B: Polymer Physics*, 44(8):1212–1225, 2006.

[50] P.J. Flory. Tensile strength in relation to molecular weight of high polymers. *Journal of the American Chemical Society*, 67:2048–2050, 1945.

[51] P.I. Vincent. The tough-brittle transition in thermoplastics. *Polymer*, 1:425–444, 1960.

[52] D. Hull and T.W. Owen. Interpretation of fracture surface features in polycarbonate. *Journal of Polymer Science: Polymer Physics Edition*, 11:2039–2055, 1973.

[53] C.M. Agrawal and G.W. Pearsall. The fracture morphology of fast unstable fracture in polycarbonate. *Journal of Materials Science*, 26:1919–1930, 1991.

[54] R.P. Kambour and R.W. Kopp. Cyclic stress-strain behavior of the dry polycarbonate craze. *Journal of Polymer Science: Part A-2*, 7:183–200, 1969.

# Improvement of the long-term performance of impact-modified polycarbonate by selected heat treatments[1]

## Abstract

The influence of impact modification by rubber-toughening on the strength of polycarbonate as reflected in its yield stress and time-to-failure is investigated. Next to a significant increase in impact toughness with respect to its unfilled counterpart, a strong decrease in strength as measured under constant imposed strain rates and stresses is observed. With annealing this decrease in strength can be compensated, giving the impact modified materials equal properties to their unfilled counterpart, while the impact properties are still far superior.

Extending the existing modeling of short- and long-term mechanical properties of glassy polymers using a scaling rule based on the volume percentage of rubber filler, the influence of impact modification can be described. Combining the scaling rule with the evolution of properties during processing even allows the direct prediction of mechanical performance of impact modified polycarbonate as it results from the thermal history experienced by the polymer during processing.

---

[1] Reproduced from: T.A.P. Engels, B.A.G. Schrauwen, L.E. Govaert and H.E.H. Meijer, Improvement of the long-term performance of impact-modified polycarbonate by selected heat treatments, Macromolecular Materials and Engineering, *submitted*, (2008)

# 6.1  Introduction

Polymers are frequently used as structural materials partly due to the ease with which complex geometrical parts can be produced. Not all polymers are suited and, for instance, polystyrene (PS) and poly(methyl methacrylate) (PMMA) show brittle behavior, whereas polycarbonate (PC) is tough. However, also PC can, under certain conditions, fail in a brittle manner, e.g. after prolonged exposure to high temperatures still below the glass transition temperature ($T_g$) [1–6] or when high (positive) triaxial stress states are reached as for instance observed under a notch [7–9]. The intricate interplay between strain softening and strain hardening determines a materials ability to delocalize strain, and it was shown that they are indeed the parameters governing the macroscopic behavior of all glassy polymers [6; 10–12].

A common route to increase the toughness of brittle polymers is the addition of a rubber phase [13]. High impact polystyrene (HIPS) is toughened by the introduction of a co-continuous polybutadiene phase[14–16], where multiple cavitation and crazing intermediately contributes to energy dissipation [14]. A similar effect can be found for carboxyl-terminated butadiene acrylonitrile (CTBN) rubber modified epoxies [17; 18] where multiple cavitation and shear yielding is observed. Polystyrene is extremely sensitive to stress triaxiality: a positive hydrostatic stress level of ±40 MPa polystyrene will lead to brittle failure, whereas in compression yield stresses in excess of two times that value can be easily reached [19]. PC shows large plastic deformation and ductile failure in a normal tensile test. But, in the presence of a notch, hydrostatic stress builds up, resulting in a change to brittle failure via crazing [7]. In contrast to PS, the hydrostatic stress at which brittle failure is expected for PC is much higher: ±90 MPa [20; 21]. As a result of this stronger resistance to cavitation, even a simple voided structure suffices in toughening polycarbonate [22], which in practise can be accomplished by using easy cavitating methyl methacrylate-butadiene-styrene (MBS) core-shell impact modifiers [23–26].

Addition of impact modifiers enhances the impact behavior, but frequently causes a loss in transparency and, more importantly, negatively affects the load-bearing capacity of the polymer, by reduction of the yield stress [15; 23; 27; 28]. A decrease in yield stress can be termed a short-term material property, but also a decrease in the static and dynamic fatigue strength is found, which clearly are long-term properties. This negative effect on short- and long-term properties has been shown for HIPS [29; 30] and acrylonitrile-butadiene-styrene (ABS) [31; 32], with respect to their unfilled counterparts PS and styrene-acrylonitrile (SAN), respectively.

A possible solution to correct this negative effect on long-term strength may be found in selected heat treatments. Amorphous polymers below $T_g$ are in a state of non-equilibrium and, as a result, their physical and mechanical properties are subject to change over time, a phenomenon known as physical aging [33; 34]. During annealing, a heat treatment at elevated temperature below $T_g$, the aging process is accelerated, and a marked increase in yield stress can be achieved in relative short time [35–39]. Simultaneously the lifetime under static and dynamic loading will also im-

prove [40–44]. A drawback of these treatments is that polymers will show a stronger tendency to localize [6], resulting in more brittle behavior under impact conditions [1–5]. Annealing thus leads to enhanced short- and long-term properties, but diminished impact properties.

Here we will investigate both experimentally and theoretically whether an impact modified polymer can be given identical long-term strength as the unfilled polymer, by increasing the yield stress by annealing, while maintaining improved impact properties.

## 6.2  Experimental

### Materials

Materials used are an injection molding grade PC, Lexan 141R (Sabic Innovative Plastics, Bergen op Zoom, the Netherlands); $\bar{M}_n$ = 9200 g/mol and $\bar{M}_w$ = 25800 g/mol and a low temperature impact modifier, Paraloid EXL-2600 (Rohm&Haas), a methacrylate/butadiene/styrene (MBS) core-shell copolymer with a diameter of 100nm.  Three blends were prepared on a Werner&Pfleiderer ZSK 28 extruder, containing 0%, 4.5% and 9% by volume MBS.

Tensile bars were injection molded according to ASTM 638 type I using an Arburg 320S 500-150 Allrounder.  Izod impact bars with dimensions $80{\times}10{\times}4$ mm$^3$ were molded according to ISO 180/A using an Engel 75 ton injection molding machine. Rectangular plates with dimensions $70{\times}70{\times}1$ mm$^3$ were molded using an Arburg 320S 500-150 Allrounder.  The mold (Axxicon Mould Technology) guaranteed uniform filling of the cavity, demonstrated by short shot experiments.  Different thermal histories were realized to investigate the influence of temperature history during processing on the resulting mechanical properties by changing the mold temperature in three steps (30℃, 90℃ and 120℃). From the plates, bars o f $70{\times}10$ mm$^2$ were cut in flow direction and perpendicular to flow direction, applying gauge sections of $33{\times}5$mm$^2$, see Figure 6.1.



parallel        perpendicular
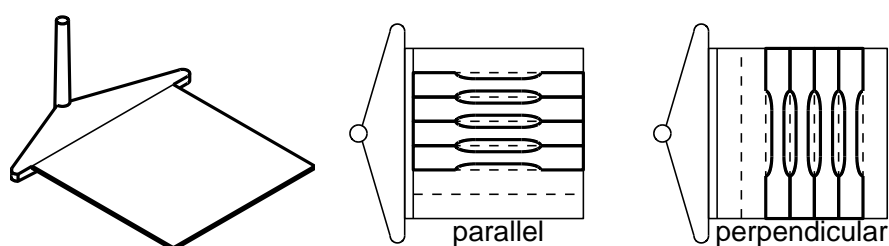
**Figure 6.1:** Injection molded samples and tensile bars made thereof

## Annealing treatments

Annealing treatments were performed in air circulated ovens at the temperatures as indicated in the respective figures. Equilibration time to the annealing temperatures was determined to be approximately 15 minutes. After the required annealing period, samples were removed from the ovens and allowed to slowly cool to room temperature prior to testing.

## Methods

Tensile tests were performed on a Zwick Z010 tester applying either a constant linear strain rate or a constant engineering stress. A default strain rate of $10^{-3}s^{-1}$ was used. Moduli were measured on a servo-hydraulic MTS 831 Elastomer Testing System equipped with an Instron strain gage extensometer type 2620-620. Izod impact tests were performed on a Zwick pendulum impact tester, according to ISO 180. Differential Scanning Calorimetry (DSC) experiments were performed on a Mettler Toledo DSC823e equipped with a FRS5 sensor. Calibration was performed by melting peaks of indium, lead, tin, zinc, benzophenone and benzoic acid. Scans were performed from 20 to 280°C with a heating rate of 10°C/min. Sta ndard 40 $\mu$l aluminium crucibles were used and samples weighed approximately 20 mg. Nitrogen was used as a purge gas.

# 6.3 Results

Figure 6.2 shows the results of notched impact tests performed at different temperatures: Polycarbonate is brittle even at room temperature, whereas the 4.5% and 9% MBS modified PC samples show ductile behavior (order 5 times higher impact than pure PC) and ductile to brittle transitions at -31°C and -46°C , respectively. Note that the ductile to brittle temperature is taken to be the temperature at which half the initial impact energy remains.

Along with the increase in absorbed impact energy, a decrease in strength of the materials, expressed in their yield stress (Figure 6.3 left) and time to failure (Figure 6.3 right), is observed. The 9% impact modified PC shows a reduction in yield stress of almost 10 MPa and a reduction in time-to-failure of more than two decades, a factor of 350, with respect to its unfilled counterpart. The 4.5% impact modified PC shows a decrease in yield stress of 5 MPa and in time to failure of a factor 15. This decrease in strength of MBS impact modified PC is similar to those observed in HIPS [29; 30] and ABS [31; 32].

The tensile, Figure 6.3 (left) and creep, Figure 6.3 (right), behavior of glassy polymers was shown to be governed by the same deformation process [40; 45]. It follows Eyring's flow rule [45–47], and the yield stress as a function of strain rate under
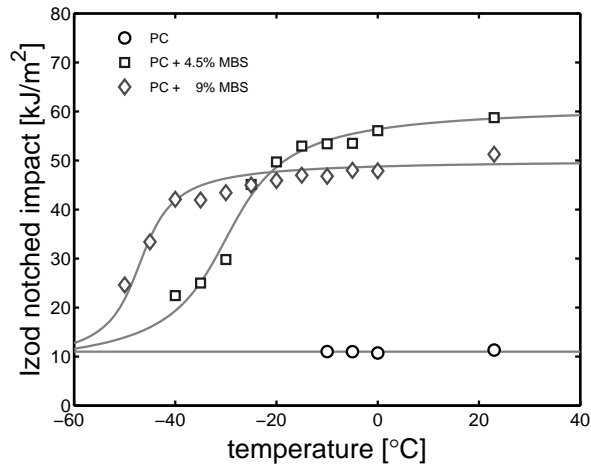
**Figure 6.2:** Izod impact energy of 0% (○), 4.5% (□) and 9% (◊) impact modified polycarbonate versus temperature.
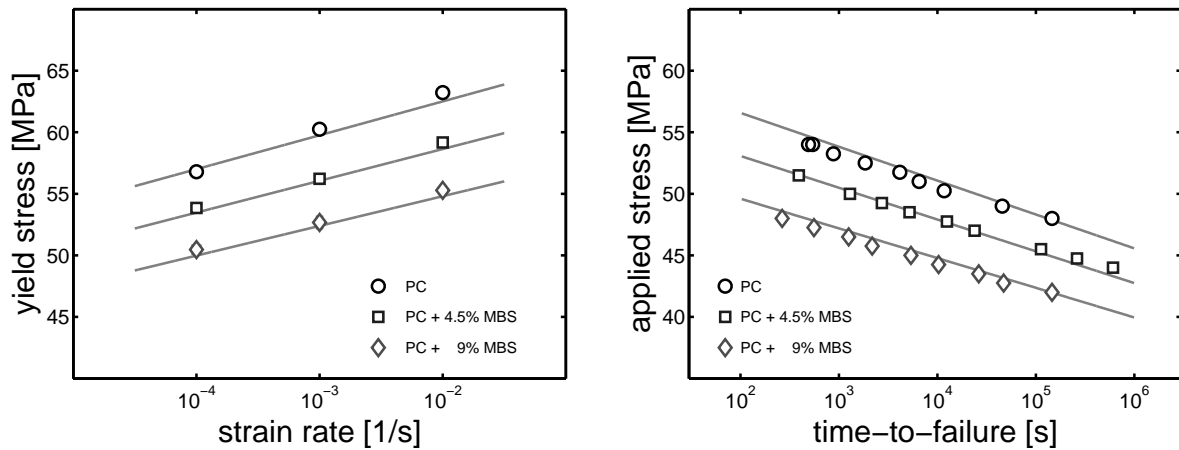


**Figure 6.3:** Left: Yield stress versus strain rate. Right: Applied stress versus time-to-failure. For the 0% (○), 4.5% (□) and 9% (◊) impact modified polycarbonate.

isothermal conditions is given by:

$$\sigma_{\text{y}}(\dot{\epsilon}) = \sigma_0 \cdot \sinh^{-1}\left(\frac{\dot{\epsilon}}{\dot{\epsilon}_0}\right) \tag{6.1}$$

with $\sigma_{\text{y}}$ is the yield stress, $\dot{\epsilon}$ the strain rate applied, $\sigma_0$ a characteristic stress and $\dot{\epsilon}_0$ a rate constant, and with the introduction of a critical plastic strain, $\epsilon_{\text{cr}}$ [48], the time-to-failure, $t_{\text{f}}$, as a function of applied stress, $\sigma_{\text{a}}$, is given by:

$$t_f(\sigma_a) = \frac{\epsilon_{cr}}{\dot{\epsilon}_0} \cdot \sinh\left(\frac{\sigma_a}{\sigma_0}\right)^{-1} \tag{6.2}$$

The solid lines for pure PC are obtained by using Equations 6.1 and 6.2, taking the parameters from [48], see Table 6.1, and adapting the rate constant, $\dot{\epsilon}_0$ (which depends on the specific thermal history of the samples) to fit the data in Figure 6.3.

**Table 6.1:** Eyring parameters [48]

| $\sigma_0$ [MPa] | $\dot{\epsilon}_0$ [s$^{-1}$] | $\epsilon_{cr}$ [%] |
|---|---|---|
| 1.19 | $3.9 \cdot 10^{-25}$ | 0.7 |

The line drawn through the 4.5% and 9% modified PC of Figure 6.3 (left) is obtained by scaling Equation 6.1 by using:

$$\sigma_{y,IM}(\phi) = \sigma_{y,ref} \cdot (1 - 1.375\phi) \tag{6.3}$$

with $\sigma_{y,IM}$ the yield stress of the impact modified PC, $\sigma_{y,ref}$ the yield stress of the unmodified PC and $\phi$ is the volume fraction impact modifier.

Equation 6.3 is taken from reference [49] and is based on the results obtained with rubber-toughened PMMA [28; 50]. In Figure 6.4 we verify its applicability on experimental data of rubber-toughened materials taken from literature: PMMA [28; 50], PC [23; 24; 51], and a PC/PET blend [27]. The scaling rule proposed is empirical by nature, and not based on any theory of deformation processes involved like is done for elastic moduli of two-phase systems [52–54], or for the influence of voids or rigid fillers on compressive yield [55].

The scaling describes our short-term data well, see Figure 6.3 (left). In an equivalent manner the long-term data, Figure 6.3 (right), can be described according to:

$$t_f(\sigma_a, \phi) = \frac{\epsilon_{cr}}{\dot{\epsilon}_0} \cdot \sinh\left(\frac{\sigma_a \cdot (1 - 1.375\phi)}{\sigma_0}\right)^{-1} \tag{6.4}$$

which also gives an excellent description of our experimental data, using the same parameters as for the unmodified PC.

From the data presented so far it can be concluded that although the addition of a MBS impact modifier significantly increases the impact toughness of PC, the strength of the material is severely diminished, i.e. a decrease in yield stress of 5 and 10 MPa and a decrease in time-to-failure of one and two orders of magnitude for the 4.5% and
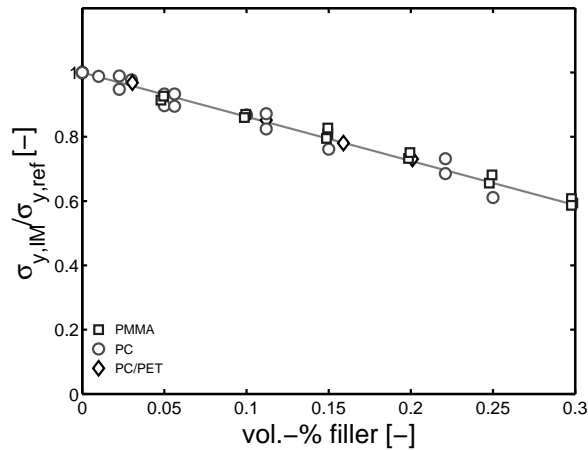
**Figure 6.4:** Decrease in normalized yield stress with volume percentage filler; solid
line according to Equation (6.3).

9% impact modified material, respectively. The yield stress of all polymers, including
PC, can be significantly increased by annealing [35–39; 56–58], and indeed the same
increase can be realized for impact modified PC. This is demonstrated in Figure 6.5,
where the yield stress is plotted as a function of annealing time for different annealing
temperatures and increases linear with the logarithm of the annealing time. From
Figure 6.5 it was estimated that annealing treatments of 1.5 hours at 110°C for 4.5%
MBS and 8.5 hours at 120°C for 9% MBS are required to increase the yield stresses
to the level of the unmodified PC.
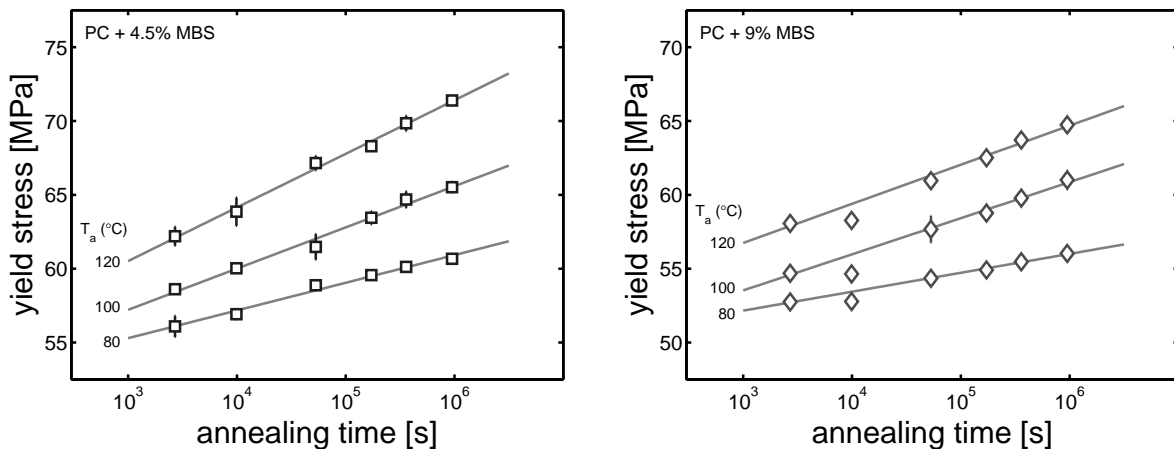


**Figure 6.5:** Left: Increase in yield stress upon annealing for 4.5% impact modified
polycarbonate. Right: Increase in yield stress upon annealing for 9%
impact modified polycarbonate. Annealing temperatures as indicated in
figures.

The results of these treatments are presented in Figure 6.6, where it is shown that the
strain-rate dependence of the yield stress (left), as well as the lifetime under applied
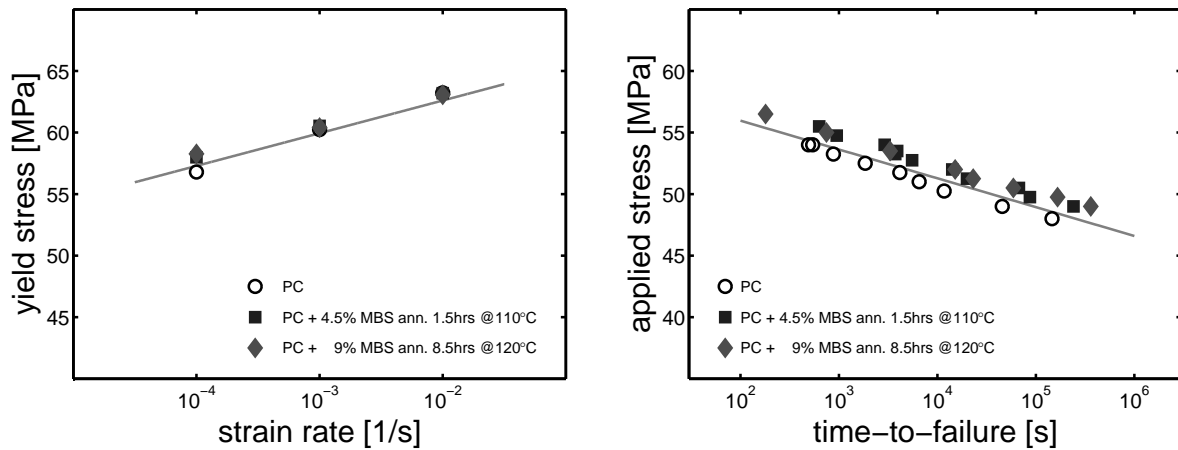
**Figure 6.6:** Left: Yield stress versus strain rate. Right: Applied stress versus time-to-failure. For the 0% (O), annealed 4.5% (■) and annealed 9% (♦) impact modified polycarbonate.

stress (right), can be restored to the level of the unmodified PC.

The question now rises to what extend the annealing treatment has influenced the impact properties. Figure 6.7 shows the Izod impact energy versus test temperature for the two annealed impact modified PC's and the pure PC. It is clear that the impact modified materials, although having received annealing treatments, still have a considerably enhanced impact toughness. Compared to their un-annealed counterparts (Figure 6.2), a small increase in the ductile-to-brittle temperature of 3°C for the 4.5% and 7°C for the 9% impact modified materials is found. An upper limit in effectiveness of annealing treatments, however, does exist, since annealing at too high temperature (135°C) leads to degradation of MBS and formation of active radical species that cause molecular weight reduction in the PC [24].
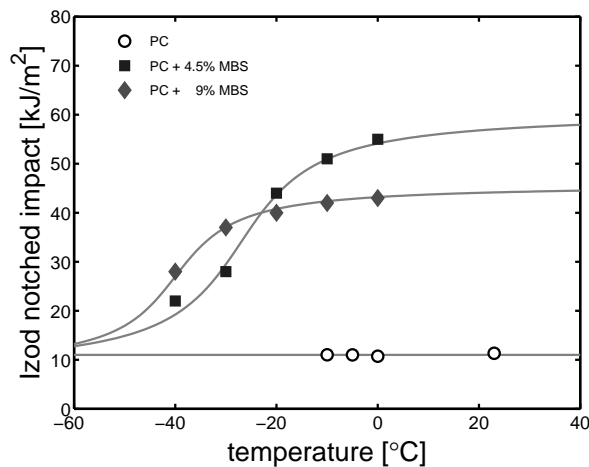


**Figure 6.7:** Izod impact energy of 0% (O), annealed 4.5% (■) and annealed 9% (♦) impact modified polycarbonate versus temperature.

Where annealing treatments unambiguously lead to an increase in yield stress and a decrease in impact toughness, the modulus of annealed polymers can either increase [33], or decrease [2; 59], depending on the relaxation of possible frozen-in orientation [60]. The moduli for the pure PC and impact modified PC's are given in Figure 6.8 (right) and are seen to decrease on annealing, both for the pure PC as for the modified PC's. The decrease in modulus for the modified PC's is ~4%, and for the unmodified PC maximum ~6%, and therefore not significant. The initial moduli can be described by a modified Halpin-Tsai relation [61; 62], the solid drawn line in Figure 6.8:

$$E_c = E_m \frac{1 + \zeta\eta\phi}{1 - \eta\phi\psi} \tag{6.5}$$

$$\eta = \frac{(E_f/E_m) - 1}{(E_f/E_m) + \zeta} \tag{6.6}$$

$$\psi = 1 + \frac{1 - \phi_m}{\phi_m^2}\phi \tag{6.7}$$

with $E_c$ the modulus of the composite, $E_m$ the modulus of the matrix, $\zeta = 1.5$, $\phi$ the volume percentage filler, $E_f$ the modulus of the filler, and $\phi_m$ the maximum packing fraction of filler (0.637 for randomly packed spherical particles, all of the same diameter).
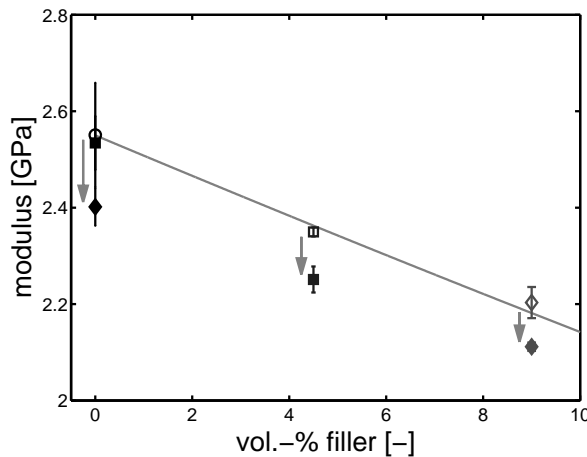


**Figure 6.8:** Decrease in elastic modulus with annealing. Open symbols are for the as-received materials; closed symbols for the annealed materials. Solid drawn line according to Equation (6.5).

Summarizing, annealing improves the long-term properties of impact modified polycarbonate, while maintaining the its improved impact properties. It should be noted, however, that property modification by thermal treatments is not limited to annealing,

but can also be accomplished during processing. For pure PC the yield stress as it results from the thermal history experienced during processing can even be predicted based on an approach using Time-Temperature-Superposition to calculate the evolution of effective time during the cooling stage [63; 64]. This approach is also applied to the impact modified PC's, and the evolution of yield stress with time and temperature, as measured after annealing below $T_g$ (see Figure 6.5), from which the evolution of the effective time is derived, is shown in Figure 6.9. These master curves were constructed using an Arrhenius type of temperature shift, with an activation energy of 205 kJ/mol, and can be described by [39]:
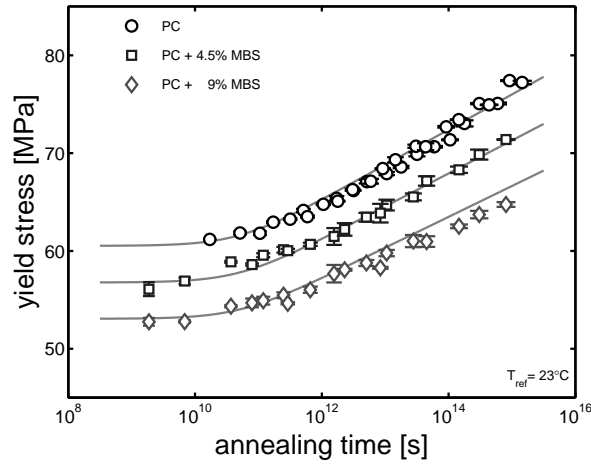


**Figure 6.9:** Master curves of the increase in yield stress with aging time, for the 0% (O), 4.5% (□) and 9% (◊) impact modified polycarbonates. (measured at $\dot{\epsilon} = 10^{-3}\text{s}^{-1}$)

$$\sigma_y(t, T, \phi) = (\sigma_{y,0} + c \cdot \log((t_{eff}(t, T) + t_a)/t_0)) \cdot (1 - 1.375\phi) \tag{6.8}$$

with $\sigma_y$ the yield stress, $t_{eff}$ the effective time, $t$ the time, $T$ the temperature, $\sigma_{y,0}$, $c$ and $t_a$ are fit parameters, $t_0 = 1$ s, and:

$$t_{eff}(t, T) = \int_0^t a_T^{-1}(T(t'))dt' \tag{6.9}$$

$$a_T(T(t)) = \exp\left(\frac{\Delta U_a}{R} \cdot \left(\frac{1}{T(t)} - \frac{1}{T_{ref}}\right)\right) \tag{6.10}$$

with $\Delta U_a$ the activation energy, $R$ the universal gas constant and $T_{ref}$ a reference temperature.

The solid drawn line describing the master curves in Figure 6.9 are obtained by eval-

uating Equation 6.8 with parameters taken from a previous study [39], see Table 6.2. The master curves describe the experiments rather accurate, although at long annealing times the 9% impact modified yield stress is slightly over-predicted.

**Table 6.2:** Master curve parameters

|      | $\sigma_{y,0}$ [MPa] | c [MPa] | $t_a$ [s]          |
|------|----------------------|---------|--------------------|
| PC*  | 22.00                | 3.60    | $5.0 \cdot 10^{10}$ |

*taken from [39]; corrected for strain rate
and engineering stress
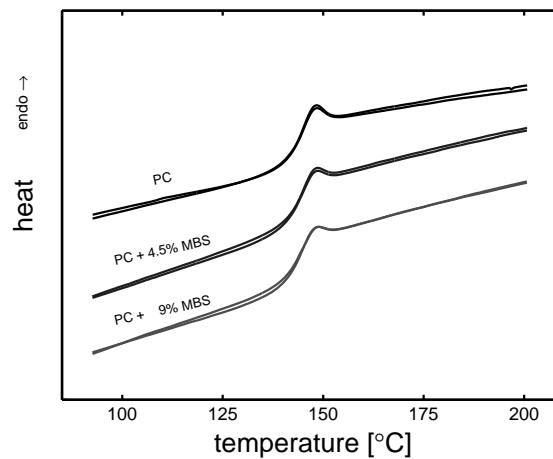


**Figure 6.10:** DSC heating scans of the 0% , 4.5% and 9% impact modified polycarbonates.

The parameter $t_a$ in Equation 6.8 can be regarded as the initial age of the material, i.e. the effective (aging) time obtained during processing, $t_{eff,c}$. Aging during use only leads to an increase in yield stress when the effective time becomes of the same order of, or greater than, the initial age. By evaluating Equations 6.9 and 6.10 already during the cooling stage of the injection molding process, $t_{eff,c}$ can be calculated, and thus $t_a$ predicted. This will be demonstrated. Thermal histories are obtained by numerical simulation of the injection molding process. Analysis of the thermal behavior of the modified PC's indicates that the presence of the MBS filler has no significant influence on either $T_g$ nor on specific energy, see Figure 6.10, and we therefore apply the temperature information obtained from the analysis of the unmodified material also to the impact modified materials.

Figure 6.11 shows the results of the directly predicted yield stresses versus the experimentally determined ones. Please note these predictions were obtained without the need of any additional mechanical testing. Clearly an excellent agreement is found between the experimental and numerical results for mold temperatures below 100°C.

At higher mold temperatures the predicted yield stresses overshoot the experimental values. No clear explanation was found for this deviation, but from a practical point of view the range of (high) mold temperatures, where we see a deviation, is not used in commercial polymer processing. The influence of anisotropy is found to be negligible for the experiments performed here; difference between experiments performed parallel and perpendicular to flow show only small (<1.5 MPa; <3%) differences.

If we now compare the yield stress of the 4.5% impact modified polycarbonate injection molded at 120℃ with the unmodified polycarbonate injec tion molded at 30℃, there is only a difference of 1 MPa. This indicates that the performance of these two materials is almost identical when evaluating tensile or creep behavior, whereas the impact modified material still shows far superior impact behavior.
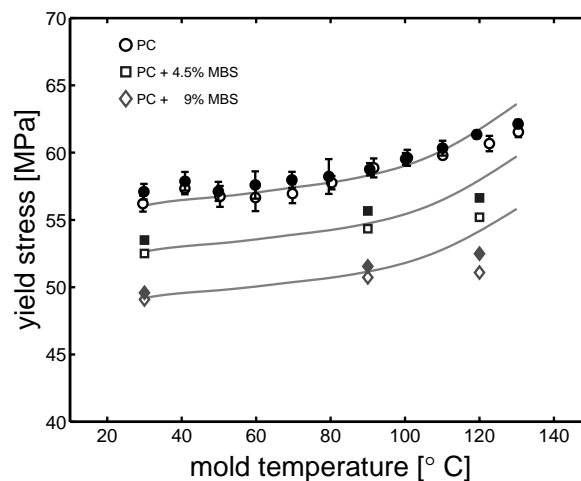


**Figure 6.11:** Yield stress versus mold temperature for the 0% (○), 4.5% (□) and 9% (◊) impact modified polycarbonates. Closed symbols represent experiments performed parallel to flow, whereas open symbols represent experiments performed perpendicular to flow.

## 6.4  Conclusions

Rubber modification of polycarbonate leads to significant improvement in impact performance, while the strength of the material under constant strain rates and stresses is dramatically decreased. The addition of 4.5% and 9% impact modifier leads to a decrease in static fatigue behavior of more than one and two orders of magnitude in time, respectively. Application of short annealing treatments well below the glass transition temperature (<10 hours at temperatures ≤ 120℃), gives rise to an increase in yield properties, and the tensile and creep performance of modified polycarbonates can be made to match that of unfilled PC, while a superior impact strength is maintained.

Using a modeling approach based on the classical Eyring flow theory in combination with an empirical scaling rule, enables the description of the deformation behavior of impact modified polycarbonate as a function of volume percentage impact modifier. The properties of modified PC after processing are predicted based on the combination of a previously developed modeling approach capturing the evolution of yield stress during processing and the aforementioned scaling rule. The combination of these modeling approaches form a powerful tool to predict and adapt the overall performance of impact modified polycarbonate based on the desired low temperature notched impact strength that determines the volume percentage impact modifier needed.

# References

[1] D.G. Legrand. Crazing, yielding, and fracture of polymers. I. Ductile brittle transition in polycarbonate. *Journal of Applied Polymer Science*, 13:2129–2147, 1969.

[2] G.A. Adam, A. Cross, and R.N. Haward. The effect of thermal pretreatment on the mechanical properties of polycarbonate. *Journal of Materials Science*, 10:1582–1590, 1975.

[3] J.T. Ryan. Impact and yield properties of polycarbonate as a function of strain rate, molecular weight, thermal history, and temperature. *Polymer Engineering and Science*, 18(4):264–267, 1978.

[4] G.L. Pitman, I.M. Ward, and R.A. Duckett. The effects of thermal pre-treatment and molecular weight on the impact behaviour of polycarbonate. *Journal of Materials Science*, 13:2092–2104, 1978.

[5] R.A. Bubeck, S.E. Bales, and H.D. Lee. Changes in yield and deformation of polycarbonates caused by physical aging. *Polymer Engineering and Science*, 24(10):1142–1148, 1984.

[6] H.G.H. van Melick, L.E. Govaert, and H.E.H. Meijer. Localisation phenomena in glassy polymers: Influence of thermal and mechanical history. *Polymer*, 44:3579–3591, 2003.

[7] M. Takano and L.E. Nielsen. The notch sensitivity of polymeric materials. *Journal of Applied Polymer Science*, 20:2193–2207, 1976.

[8] R.A.W. Fraser and I.M. Ward. The impact fracture behaviour of notched specimens of polycarbonate. *Journal of Materials Science*, 12:459–468, 1977.

[9] I. Narisawa, M. Ishikawa, and H. Ogawa. Notch brittleness of ductile glassy polymers under plane strain. *Journal of Materials Science*, 15:2059–2065, 1980.

[10] L.E. Govaert, H.G.H. van Melick, and H.E.H. Meijer. Temporary toughening of polystyrene through mechanical pre-conditioning. *Polymer*, 42:1271–1274, 2001.

[11] H.E.H. Meijer and L.E. Govaert. Multi-scale analysis of mechanical proper-

ties of amorphous polymer systems. *Macromolecular Chemistry and Physics*, 204:274–288, 2003.

[12] H.E.H. Meijer and L.E. Govaert. Mechanical performance of polymer systems: The relation between structure and properties. *Progress in Polymer Science*, 30:915–938, 2005.

[13] C.B. Bucknall. *Toughened Plastics*. Applied Science Publishers Ltd., 1977.

[14] C.B. Bucknall and R.R. Smith. Stress-whitening in high-impact polystyrenes. *Polymer*, 6:437–446, 1965.

[15] S.G. Turley and H. Keskkula. Effect of rubber-phase volume fraction in impact polystryrene on mechanical behaviour. *Polymer*, 21:466–468, 1980.

[16] A.M. Donald and E.J. Kramer. Internal structure of rubber particles and craze break-down in high-impact polystyrene (HIPS). *Journal of Materials Science*, 17:2351–2358, 1982.

[17] A.F. Yee and R.A. Pearson. Toughening mechanisms in elastomer-modified epoxies. Part 1. Mechanical studies. *Journal of Materials Science*, 21:2462–2474, 1986.

[18] R.A. Pearson and A.F. Yee. Toughening mechanisms in elastomer-modified epoxies. *Journal of Materials Science*, 21:2475–2488, 1986.

[19] H.G.H. van Melick, O.F.J.T. Bressers, J.M.J. den Toonder, L.E. Govaert, and H.E.H. Meijer. A micro-indentation method for probing the craze-initiation stress in glassy polymers. *Polymer*, 44:2481–2491, 2003.

[20] M. Ishikawa, I. Narisawa, and H. Ogawa. Criterion for craze nucleation in polycarbonate. *Journal of Polymer Science: Polymer Physics Edition*, 15:1791–1804, 1977.

[21] T. Kuriyama and I. Narisawa. Fracture behavior of ductile polymer under mixed mode loading. *52nd Annual Technical Conference - Society of Plastics Engineers*, 3:3235–3237, 1994.

[22] R.J.M. Smit, W.A.M. Brekelmans, and H.E.H. Meijer. Prediction of the large-strain mechanical response of heterogeneous polymer systems: Local and global deformation behaviour of a representative volume element of voided polycarbonate. *Journal of the Mechanics and Physics of Solids*, 47:201–221, 1999.

[23] Feng-Chih Chang, Jiann-Shing Wu, and Line-Hwa Chu. Fracture and impact properties of polycarbonates and MBS elastomer-modified polycarbonates. *Journal of Applied Polymer Science*, 44:491–504, 1992.

[24] T.W. Cheng, H. Keskkula, and D.R. Paul. Thermal aging of impact-modified polycarbonate. *Journal of Applied Polymer Science*, 45:531–551, 1992.

[25] C. Cheng, N. Peduto, A. Hiltner, E. Baer, P.R. Soskey, and S.G. Mylonakis. Comparison of some butadiene-based impact modifiers for polycarbonate. *Journal of Applied Polymer Science*, 53:513–525, 1994.

[26] V. Tanrattanakul, E. Baer, A. Hiltner, R. Hu, V.L. Dimone, M.S. El-aasser, L.H. Sperling, and S.G. Mylonakis. Toughening polycarbonate with core-shell structured latex particles. *Journal of Applied Polymer Science*, 62:2005–2013, 1996.

[27] Zhi-Li Liao and Feng-Chih Chang. Rubber-toughened polymer blends of poly-carbonate (PC) and poly (ethylene terephthalate) (PET). *Journal of Polymer Research*, 1(2):197–203, 1994.

[28] J.M. Gloaguen, P. Heim, P. Gaillard, and J.M. Lefebvre. Plasticity of rubber-toughened poly(methyl methacrylate): Effect of rubber particle size. *Polymer*, 33(22):4741–4746, 1992.

[29] Der-Jin Woan, M. Habibullah, and J.A. Sauer. Fatigue characteristics of high impact polystyrene. *Polymer*, 22:699–701, 1981.

[30] J.A. Sauer, J. Trent, and C.C. Chen. Influence of rubber content on static and dynamic properties of polystyrene. *Polymer Engineering and Science*, 29(1):69–76, 1989.

[31] J.A. Sauer and C.C. Chen. Deformation modes and fatigue behavior in styrene-acrylonitrile and acrylonitrile-butadiene-styrene copolymers. *Polymer Engineering and Science*, 24(10):786–797, 1984.

[32] C.C. Chen and J.A. Sauer. Yield and fracture mechanisms in ABS. *Journal of Applied Polymer Science*, 40:503–521, 1990.

[33] L.C.E. Struik. *Physical aging of amorphous polymers and other materials*. Elsevier, Amsterdam, 1978.

[34] J.M. Hutchinson. Physical aging of polymers. *Progress in Polymer Science*, 20:703–760, 1995.

[35] A. Aref-Azar, F. Biddlestone, J.N. Hay, and R.N. Haward. The effect of physical ageing on the properties of poly(ethylene terephthalate). *Polymer*, 24:1245–1251, 1983.

[36] D.J. Kemmish and J.N. Hay. The effect of physical ageing on the properties of amorphous PEEK. *Polymer*, 26:905–912, 1985.

[37] P.Y. Jar, H.H. Kausch, W.J. Cantwell, P. Davies, and H. Richard. The effect of annealing on the short and long term behavior of PEEK. *Polymer Bulletin*, 24:657–664, 1990.

[38] O.A. Hasan, M.C. Boyce, X.S. Li, and S. Berko. An investigation of the yield and postyield behavior and corresponding structure of poly(methyl methacrylate). *Journal of Polymer SCience: Part B: Polymer Physics*, 31:185–197, 1993.

[39] E.T.J. Klompen, T.A.P. Engels, L.E. Govaert, and H.E.H Meijer. Modelling of the post-yield response of glassy polymer: Influence of thermomechanical history. *Macromolecules*, 38(16):6997–7008, 2005.

[40] E.T.J. Klompen, T.A.P. Engels, L.C.A. van Breemen, P.J.G. Schreurs, L.E. Govaert, and H.E.H. Meijer. Quantitative prediction of long-term failure of polycarbonate. *Macromolecules*, 38(16):7009–7017, 2005.

[41] R.P.M. Janssen, D. de Kanter, L.E. Govaert, and H.E.H. Meijer. Fatigue life predictions for glassy polymers: a constitutive approach. *Macromolecules*, 41:2520–2530, 2008.

[42] I. Narisawa, M. Ishikawa, and H. Ogawa. Delayed yielding of polycarbonate under constant load. *Journal of Polymer Science: Polymer Physics Edition*, 16:1459–1470, 1978.

[43] J.M. Crissman and G.B. McKenna. Relating creep and creep rupture in PMMA using a reduced variable approach. *Journal of Polymer Science: Part B: Polymer Physics*, 25:1667–1677, 1987.

[44] J.M. Crissman and G.B. McKenna. Physical and chemical aging in PMMA and their effects on creep and creep rupture behavior. *Journal of Polymer Science: Part B: Polymer Physics*, 28:1463–1473, 1990.

[45] C. Bauwens-Crowet, J-M. Ots, and J-C. Bauwens. The strain-rate and temperature dependence of yield of polycarbonate in tension, tensile creep and impact tests. *Journal of Materials Science Letters*, 9:1197–2101, 1974.

[46] H. Eyring. Viscosity, plasticity, and diffusion as examples of absolute reaction rates. *Journal of Chemical Physics*, 4:283–291, 1936.

[47] C. Bauwens-Crowet, J-C. Bauwens, and G. Homés. Tensile yield-stress behavior of glassy polymers. *Journal of Polymer Science, Part A-2 Polymer Physics*, 7:735–742, 1969.

[48] R.P.M. Janssen, L.E. Govaert, and H.E.H. Meijer. An analytical method to predict fatigue life of thermoplasics in uniaxial loading: Sensitivity to wave type, frequency and stress amplitude. *Macromolecules*, 41:2531–2540, 2008.

[49] C.B. Bucknall. *The physics of glassy polymers*, chapter 8, pages 363–412. Chapman & Hall, London, 2 edition, 1997.

[50] J.M. Gloaguen, P. Steer, P. Gaillard, C. Wrotecki, and J.M. Lefebvre. Plasticity and fracture initiation in rubber-toughened poly(methyl methacrylate). *Polymer Engineering and Science*, 33(12):748–753, 1993.

[51] E. Parsons, M.C. Boyce, and D.M. Parks. An experimental investigation of the large-strain tensile behavior of neat and rubber-toughened polycarbonate. *Polymer*, 45:2665–2684, 2004.

[52] E.H. Kerner. Elastic and thermoelastic properties of composite media. *Proceedings of the Physical Society, London*, 69B:808–813, 1956.

[53] L.E. Nielsen. Simple theory of stress-strain properties of filled polymers. *Journal of Applied Polymer Science*, 10:97–103, 1966.

[54] S. Uemura and M. Takayanagi. Application of the theory of elasticity and viscosity of two-phase systems to polymer blends. *Journal of Applied Polymer Science*, 10:113–125, 1966.

[55] O. Ishai and L.J. Cohen. Effect of fillers and voids on compressive yield of epoxy composites. *Journal of Composite Materials*, 2(3):302–315, 1968.

[56] D.M. Gezovich and P.H. Geil. Deformation and aging of quenched polypropylene. *Polymer Engineering and Science*, 8(3):210–215, 1968.

[57] I. Schwarz, M. Stranz, M. Bonnet, and J. Petermann. Changes of mechanical properties in cold-crystallized syndiotactic polypropylene during aging. *Colloid and Polymer Science*, 279:506–512, 2001.

[58] E.El. Shafee. Effect of aging on the mechanical properties of cold-crystallized poly(trimethylene terephthalate). *Polymer*, 44:3727–3732, 2003.

[59] B.S. Thakkar and L.J. Broutman. Impact strength of polymers. 3: The effect of

annealing on cold worked polycarbonates. *Polymer Engineering and Science*, 21(3):155–162, 1981.

[60] Z. Tadmor. Molecular orientation in injection molding. *Journal of Applied Polymer Science*, 18:1753–1772, 1974.

[61] J.C. Halpin and J.L. Kardos. The Halpin-Tsai equations: A review. *Polymer Engineering and Science*, 16(5):344–352, 1976.

[62] T.B. Lewis and L.E. Nielsen. Dynamic mechanical properties of particulate filled composites. *Journal of Applied Polymer Science*, 14:1449–1471, 1970.

[63] L.E. Govaert, T.A.P. Engels, E.T.J. Klompen, G.W.M. Peters, and H.E.H. Meijer. Processing induced properties in glassy polymers: Development of the yield stress in polycarbonate. *International Polymer Processing*, XX(2):170–177, 2005.

[64] T.A.P. Engels, L.E. Govaert, G.W.M. Peters, and H.E.H. Meijer. Processing induced properties in glassy polymers: Application of structural relaxation to yield stress development. *Journal of Polymer Science: Part B: Polymer Physics*, 44(8):1212–1225, 2006.

# Conclusions and recommendations

## 7.1  Main conclusions

This thesis focussed on the prediction of the mechanical performance of products made of polymer glasses based on the evolution of their structural state during processing and service life.  Two methods were presented which predict yield stress distributions throughout a product based on the thermal history it experienced during processing, and good agreement was found with experiments. Since the yield stress not only determines the short-term performance of a material but also its long-term failure under static and dynamic loading conditions, this ultimate behavior can also be predicted, as was validated for an actual product finding again good agreement between prediction and experiment.  To predict embrittlement of polymer glasses, both a critical maximum hydrostatic stress and a critical yield stress were introduced as criteria. Where the first can be used to identify the failure mode for an arbitrary geometry and loading conditions, the second indicates at what time, during the service life of a product, the material becomes notch sensitive, and would fail in a brittle manner were it tested in a notched impact test. Finally, in case embrittlement is prevented by impact modification, considerably enhancing impact properties but negatively affecting the long-term performance of polymer glasses, shortening their life time by orders of magnitude, this negative effect could be compensated for by applying selected heat treatments while maintaining superior impact properties.

The modeling approaches presented in this thesis are important tools for the design and optimization process of products made of polymer glasses. As a result they are currently being implemented in the commercial injection molding simulation package MoldFLow MPI. An example of the added functionality is demonstrated in Figure 7.1, where the results of the first implementation of our modeling approach (chapter 2) are shown. The yield stress, and corresponding value of the state parameter $S_a$, is calculated for a cup shaped sample, the same as used in chapter 4 of this thesis.

Where in chapter 4 a custom build interface (Matlab) was still used to extract the temperature profiles calculated by the injection molding simulation package, and to perform the post-molding calculation of the evolution of structural state, here this is all done by the simulation package itself. The calculated values can be exported to a linked finite element package to evaluate the mechanical performance of the product without doing a single mechanical test.
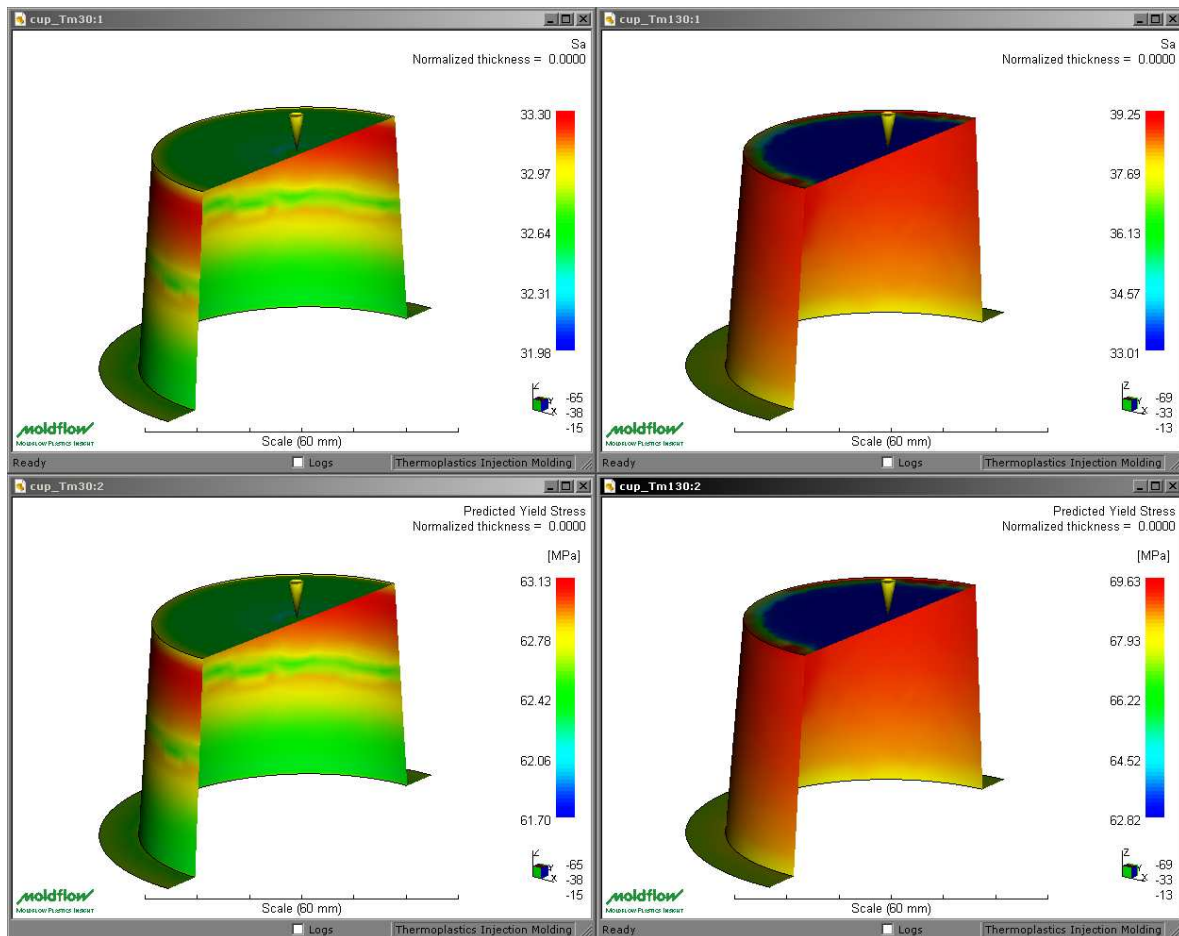


**Figure 7.1:** Predicted values for the state parameter, $S_a$ (top), and the yield stress (bottom) in the midplane of the product for two mold temperatures: 30℃ (left) and 130℃ (right).

## 7.2  Recommendations

This thesis is concerned with the mechanical properties of polymer glasses with an emphasis on their yield stress. Polycarbonate (PC) was chosen as the model system to investigate, mainly due to its intrinsic ductility, allowing yield stresses to be measured in tension, which is not always possible for polymer glasses e.g. poly(methyl

methacrylate) (PMMA) and polystyrene (PS). Most, not to say all, polymer glasses have one or more secondary relaxation mechanisms present at temperatures below their primary glass transition, $T_g$. The temperature at which these secondary processes reveal themselves and their magnitudes depend strongly on molecular architecture, mobility, and cooperativity, of the polymer chains involved [1; 2]. Figure 7.2 (left) presents the loss angle versus temperature for PC and PMMA, and indeed for both materials a broad secondary ($\beta$) loss peak is observed well below the primary ($\alpha$) relaxation e.g. at -100℃ for PC and 25℃ for PMMA. These second ary relaxation mechanisms also affect the deformation kinetics, and at high deformation rates they start to contribute to the stress response, see Figure 7.2 (right) where the change of slope at high strain rates for PMMA can be attributed to the secondary relaxation mechanism. The rate at which they start to contribute again depends on the molecular structure and the molecular motions involved, resulting in a pronounced contribution for PMMA already at moderate strain rates, whereas for PC only at high rates ($> 10^0$ s$^{-1}$) a contribution is observed. Since long-term properties such as the life time under static loading conditions are dominated by low deformation rates they are governed by the primary relaxation mechanism.
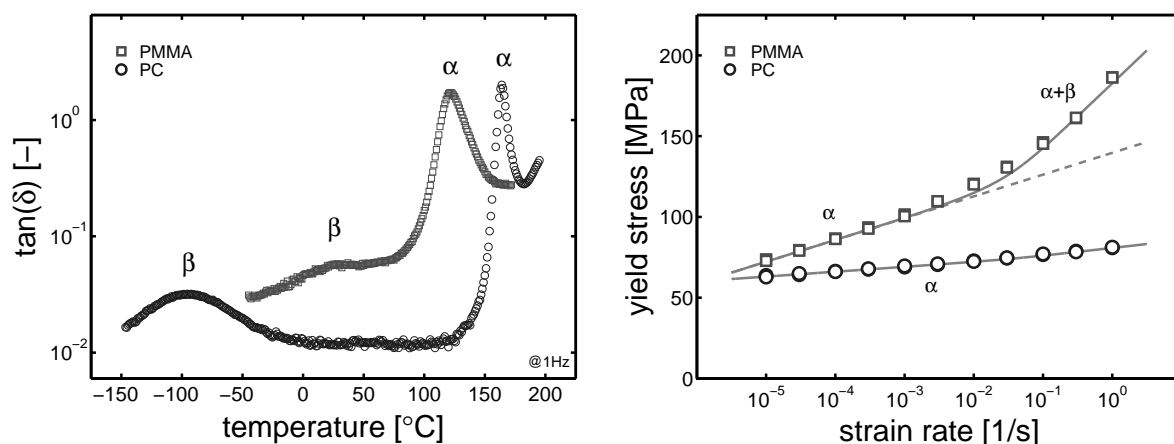


**Figure 7.2:** Left: Loss angle versus temperature. Right: Compressive yield stress versus strain rate.

Throughout this thesis care was taken that the assumption of thermorheological simple behavior was valid throughout the experiments performed, and the behavior could indeed be described using a model with a single stress-activated spectrum of relaxation times, with a single stress dependence, or a single stress-activated viscosity. Only when going to high deformation rates or low temperatures, see Figure 7.3 (left), it becomes necessary to add a second stress-activated spectrum of relaxation times, with its own stress-dependence, or a second stress-activated viscosity [3–6]. For PMMA such an approach is almost always necessary, see Figure 7.3 (right) where even at relatively high temperatures a pronounced contribution of the $\beta$ process is observed.
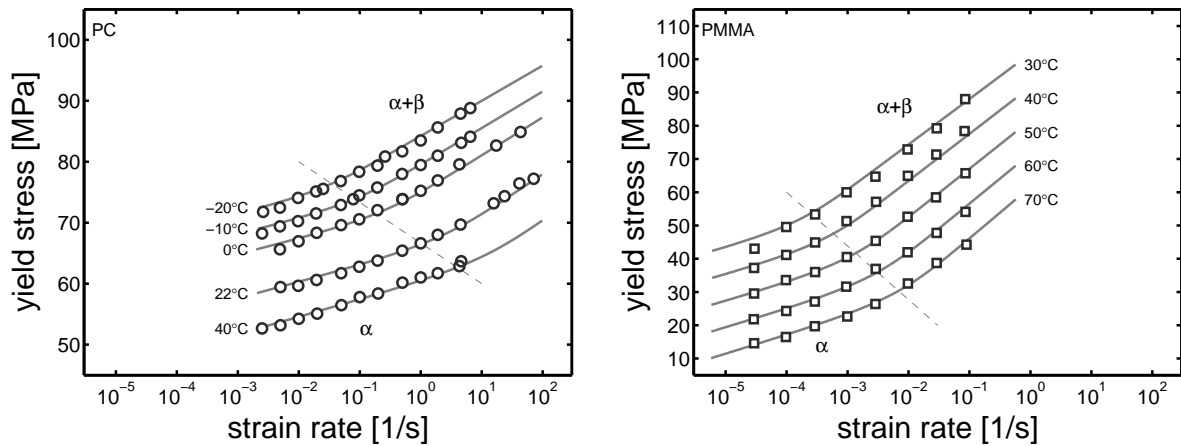
**Figure 7.3:** Tensile yield stress versus strain rate for various temperatures. Left: Polycarbonate. Right: Poly(methyl methacrylate).

Since the kinetics of the $\beta$ process with respect to stress and temperature are similar to the kinetics of the $\alpha$ process, with its own set of governing parameters, it is expected that the $\beta$ process also displays aging behavior. For PC the $\beta$ process is completely relaxed at room temperature and in equilibrium, leading to a constant contribution to the yield stress independent of aging time [7; 8]. This is demonstrated in Figure 7.4 (left) where the deformation kinetics are shown for four different thermo-mechanical histories. Clearly an increase in the low strain rate $\alpha$-regime is observed, whereas the high strain rate $\beta$-contribution is constant (if the secondary process would show ageing during the thermal treatments, and stress additivity holds, the transition from the low to high strain-rate regime, which is dominated by both the $\alpha$ and $\beta$ processes, would shift towards lower strain rates).
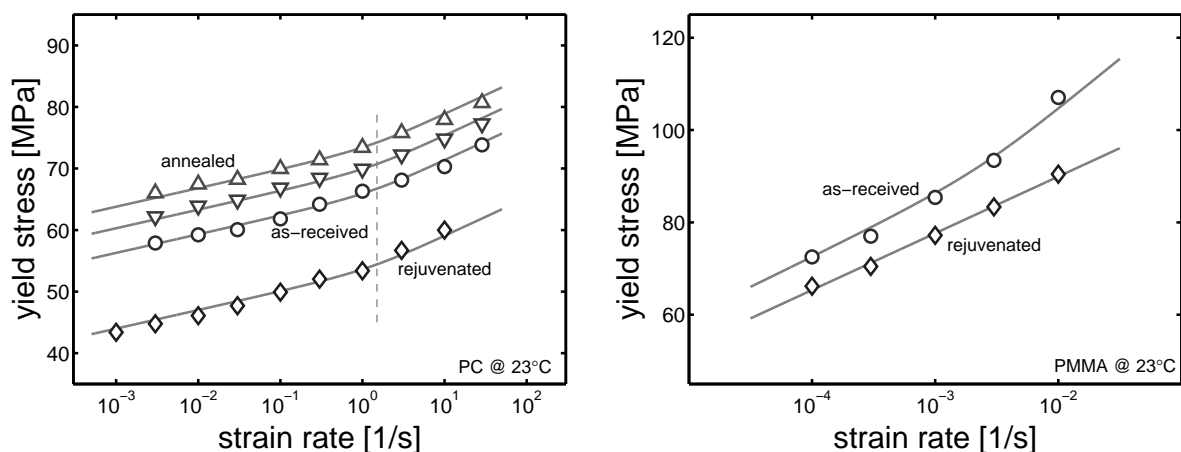


**Figure 7.4:** Yield stress versus strain rate for different thermo-mechanical histories. Left: Tensile results for polycarbonate. Right: Compressive results for poly(methyl methacrylate).

For PMMA, however, the $\beta$ contribution is found to shift towards higher deformation rates in the mechanically rejuvenated state, see Figure 7.4 (right), where the yield stress versus strain rate is shown for as-received and mechanically-rejuvenated samples. The rejuvenated samples were tested 10 seconds after being mechanically rejuvenated and show no transition towards a higher strain-rate dependence, indicating that the $\beta$ process has softened and not yet returned to equilibrium. When the modeling approaches presented in this thesis are used for polymer glasses with a pronounced secondary relaxation process at relatively high temperatures (around or above room temperature), the description of the aging kinetics has to be extended to take into account aging of this secondary process.

## 7.3  Challenges

The two main aspects of the mechanical behavior of polymers with which this thesis is concerned are *deformation kinetics* and *aging kinetics*, see Figure 7.5.  Proper knowledge of the kinetics of these phenomena is essential for an accurate prediction of the mechanical performance of polymer products.  Predictions based on the modeling tools presented in this thesis require an elaborate characterization of the polymer's behavior before they can be used. True predictive capabilities should, however, be based on direct knowledge of the polymer's molecular structure.  Even if direct and absolute, ab-initio, predictions are impossible, given the existing problems with length and timescales, it would be desirable to understand how local chemical modifications influence the kinetics of these two processes. This would open routes to design guidelines to modify polymers in their main-chain backbone and/or in their pending side groups to considerably improve their mechanical performance.
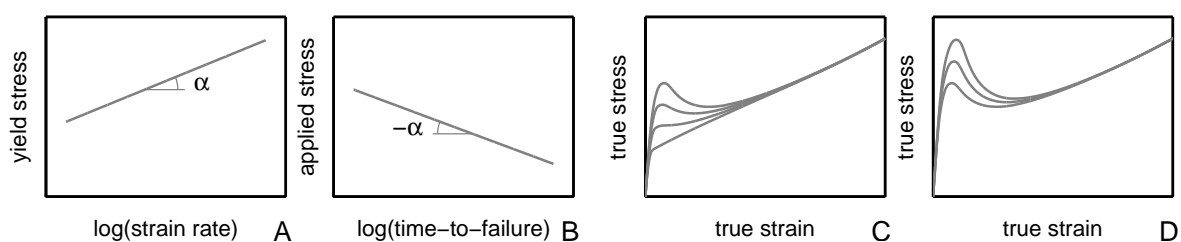


**Figure 7.5:** *Deformation kinetics*:  constant strain rate (A) and constant stress (B), and *Aging kinetics*: during processing (C) and during service life (D).

Numerous studies have been devoted to the *aging kinetics* of a large variety of polymers. Almost always it concerned molecularly very different materials. In the studies of *deformation kinetics* usually only a single structural state of the polymer at hand is investigated.  In all cases modeling is phenomenological and no sound physical basis concerning the governing processes that occur at the molecular scale is available.  Spectroscopic techniques and ab-initio modeling approaches have so far not been able to answer questions as to what determines the *kinetics of aging* and the

*kinetics of deformation* on that scale. X-ray scattering experiments show an increase in the local structural order in amorphous polystyrene upon aging, but no explanation as to what embodies this local order has been given [9]. Another study on PS suggests stacking of phenyl groups to occur, that has in contrast to a crystalline phase no long-range order [10]. For polycarbonate also an indication of increasing local order with annealing time has been found and attributed to an increasing level of interlocking of neighboring chain segments, although at long annealing times the effect is lost [11]. Fourier Transform Infrared spectroscopy on atactic PVC reveals conformational changes upon annealing below $T_g$ and the formation of a more extended structure, distinctly different from that upon annealing above $T_g$ [12]. A similar FTIR study focussing on physical aging of polycarbonate also reports conformational changes upon annealing, resulting in a more favored low energy *trans-trans* conformation [13]. However, in both cases changes are small and no conclusive molecular interpretation is presented. Low-frequency Raman scattering and inelastic neutron scattering at low temperatures show that the intensity of the Boson peak decreases when comparing quenched and annealed PMMA samples [14; 15]. The effects observed, however, are small, given the considerable annealing periods at temperatures not to far below $T_g$, and no connection to changes in conformation are made.

Spectroscopic techniques and ab-initio moleculair modeling are based on a bottom up approach. Phenomenological models work from the top down. Although it is, of course, not possible to directly acces the relevant molecular length scales involved with methods that probe the macroscopic behavior e.g. using mechanical tests, this approach might provide insight into aspects of the molecular structure that play a role. A systematic investigation into the effects of molecular architecture on *deformation kinetics* and *aging kinetics* could be a first step towards understanding of the underlying physics.
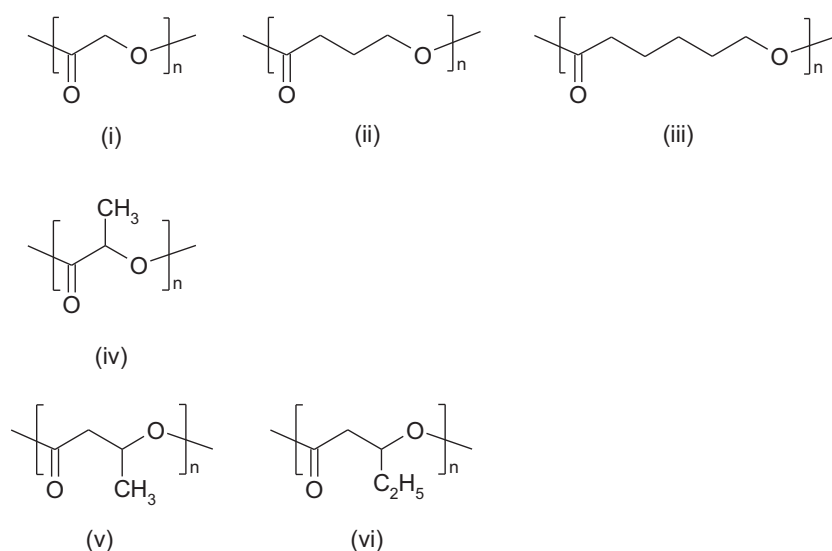


**Figure 7.6:** Different degradable polyesters

An interesting family of polymers for such an investigation could be that of degradable polyesters. The main chain can be extended in discrete steps by going from polyglycolic acid (PGA) to poly(4-hydroxybutyrate) (P4HB) to polycaprolactone (PCL), see Figure 7.6 (i), (ii) and (iii) respectively. The influence of a methyl sidegroup can be investigated by comparing polyglycolic acid (PGA) with polylactic acid (PLA) , see Figure 7.6 (i) and (iv). The influence of an extra carbon in the main chain can be investigated by comparing polylactic acid (PLA) with poly(3-hydroxybutyrate) (P3HB), see Figure 7.6 (iv) and (v). The influence of the length of the sidegroup can be investigated by comparing poly(3-hydroxybutyrate) (P3HB) with poly(3-hydroxyvalerate) (P3VA) where a methyl sidegroup is substituted by a ethyl sidegroup, see Figure 7.6 (v) and (vi). However, the glass transition temperatures of these polymers range from -60℃ (PCL) to +60℃ (PLA) [16] and crystallization rates can be considerable, making this family of materials less suited to be investigated in the glassy state. Other complicating factors are the fact that the stereo-regularity of PLA leads to a marked difference in the glass transition temperature and ability of the material to crystallize [17], posing a question to be answered in itself.
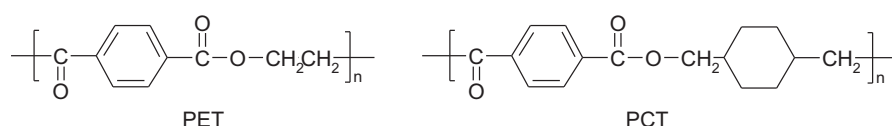


**Figure 7.7:** Left: Poly(ethylene terephthalate) (PET). Right: poly(1,4-cyclohexylene-dimethylene terephthalate) (PCT) [18].
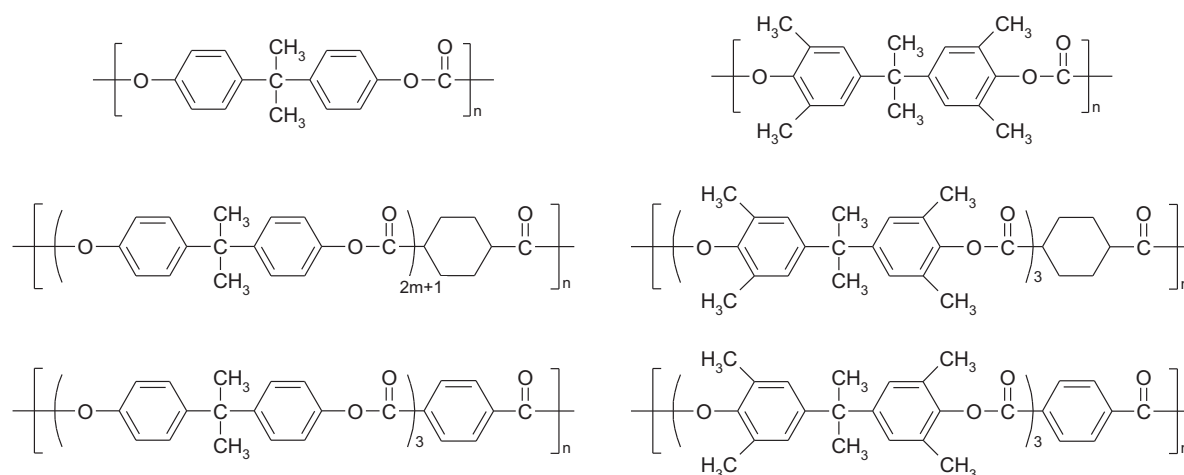


**Figure 7.8:** A selection of polycarbonate copolymers as used by Yee et al. [19; 20]

A second example of a limited but nevertheless systematic study can be found in the work of Yee et al. [18–21], which mainly focusses on the relation between mobility and ductile-to-brittle transitions. Copolymerization of slightly different monomer units, which add main-chain mobility e.g. cyclohexylene groups, see Figure 7.7 [18], or the addition of pending side groups, or the combination of both, see Figure 7.8

[19; 20], are used to gain understanding in the relation between chain mobility and embrittlement. Only a selection of the many polymer systems used by Yee et al. is shown in Figures 7.7 and 7.8, but the common factor in the chemistry used is that it builds on polycarbonates, polyesters and poly(ester carbonate)s. Their studies confirm the initial notion of Heijboer [1] that main chain mobility is a prerequisite for ductile behavior, but that it also needs to facilitate cooperative conformational changes. However, Yee's work solely focusses on correlations between chain mobility and ductile versus brittle behavior, neglecting the important aspect of the influence of intrinsic strain softening and strain hardening [22], which play a determining role in the macroscopic failure behavior of polymers as we know now. Yee studied indeed *deformation kinetics* depending on copolymer composition and an increase in activation volume is found, increasing the content main chain C-ring concentration [18; 21]. Whether such a main-chain secondary relaxation mechanism always leads to a higher activation volume would be an interesting question to answer.

In studies like these the use of small amounts of material is preferred. Techniques that measure bulk thermodynamic properties, like enthalpy and dilatometry, indeed use small sample volumes and a vast body of literature is available on volume and enthalpy relaxation of polymers glasses upon aging. However, these can not be used to characterize the *aging kinetics* as observed by mechanical tests. Generally good qualitative correlations are found between aging phenomena measured by the different techniques, however, the quantitative time-scales are found to vary [23; 24]. But even this qualitative agreement is not always valid, as was shown for a family of substituted polystyrenes where no difference in enthalpy relaxation was found, but did differ when evaluating the mechanical aging rate [25; 26]. Therefore, the evaluation of the *aging kinetics* for the purpose of mechanical performance prediction still has to be done mechanically, requiring considerable amounts of material (~ kg's). Naturally when the molecular origin is known, it should be possible to make a quantitative connection between all physical aging phenomena.

To complete the understanding of the performance of polymer glasses from a molecular point of view, an experimental approach as proposed here should also attend to the question of the origin of strain hardening [27; 28]. Where *deformation kinetics* and *aging kinetics* determine the time of failure under dynamic and static loading conditions, it is the interplay between intrinsic strain softening and strain hardening which determines the mode of failure [22], e.g. ductile or brittle. Moreover, the experimental correlation found between the *deformation kinetics* and strain-hardening behavior of polymer glasses suggests that their elementary processes are at least partially related [29].

Trying to influence the *deformation kinetics* and *aging kinetics* by intervening on the level of the molecular structure of the polymer is a challenging exercise which can lead to new polymers. Ideally, however, one would like to modify the properties of existing polymers. Upon mechanical rejuvenation, initially brittle polystyrene can be made tough by reducing the post-yield softening drop (PYSD), albeit that this effect is only temporarily since aging leads to an increase in yield stress, and thus the PYSD

[30]. If the reduced PYSD could be frozen in, a permanently ductile polystyrene is obtained. But rather than bringing a material to a state with a strongly reduced PYSD by means of mechanical rejuvenation, reaching this state by a reduced rate of evolution of the yield stress during processing is preferred.

One approach is to reduce the rate of aging by introducing anti-plasticizers [31; 32]. Anti-plasticization has been related to a reduced mobility on a molecular scale, leading to an increased yield strength and modulus, while exhibiting a depressed glass transition temperature. This reduced mobility thus affects the *aging kinetics* and in case of polystyrene results in a reduced rate of aging [33]. The addition of anti-plasticizers, however, also leads to a dilution of the entanglement network, leading to a material with a reduced strain hardening modulus, which, on a macroscopic level [28], results in a material that behaves more brittle [33]. The effect of anti-plasticizers on the evolution of the yield stress during processing also showed not to lead to the desired results [32], e.g. an increase in yield stress is observed after processing, rather than a decrease.

A second approach is that followed by the group of Torkelson, who study the effect of nanoconfinements on the glass transition temperature, $T_g$, of polymer thin films [34–37]. Polar interactions between polymer and silica nanocomposites can lead to a considerable increase in the glass transition temperature, $T_g$, while this increase also leads to a reduced rate of aging at a given aging temperature [35; 37]. In case of a 0.4 vol% silica-poly(2-vinyl pyridine) (P2VP) nanocomposite, the $T_g$ was increased by 10°C while the aging rate was dramatically reduced with re spect to an unfilled bulk reference sample [36]. However, these studies focus on polymer thin films and mechanical properties are not evaluated.

All in all, unraveling the processes that occur at the molecular scale and govern the macroscopic *deformation kinetics* and *aging kinetics* is a challenging task which requires a multi-disciplinary approach, combining chemistry, physics and mechanics, but in the end can lead to new insights and, ideally, tools to optimize new and existing polymers.

# References

[1] J. Heijboer. Dynamic mechanical properties and impact strength. *Journal of Polymer Science: Part C*, 16:3755–3763, 1968.

[2] R.F. Boyer. Dependence of mechanical properties on molecular motion in polymers. *Polymer Engineering and Science*, 8(3):161–185, 1968.

[3] T. Ree and H. Eyring. Theory of non-Newtonian flow. I. Solid plastic system. *Journal of Applied Physics*, 26:793–800, 1955.

[4] J.A. Roetling. Yield stress behaviour of poly(methyl methacrylate). *Polymer*, 6:311–317, 1965.

[5] C. Bauwens-Crowet, J-C. Bauwens, and G. Homès. Tensile yield-stress behavior of glassy polymers. *Journal of Polymer Science. Part A-2*, 7:735–742, 1969.

[6] E.T.J. Klompen and L.E. Govaert. Nonlinear viscoelastic behaviour of thermorheologically complex materials: A modelling approach. *Mechanics of Time-Dependent Materials*, 3:49–69, 1999.

[7] C. Bauwens-Crowet and J-C. Bauwens. Effect of thermal history on the tensile yield stress of polycarbonate in the $\beta$ transition range. *Polymer*, 24:921–924, 1983.

[8] C. Ho Huu and T. Vu-Khanh. Effects of physical aging on yielding kinetics of polycarbonate. *Theoretical and Applied Fracture Mechanics*, 40:75–83, 2003.

[9] H.H. Song and R.J. Roe. Structural change accompanying volume change in amorphous polystyrene as studied by small and intermediat angle X-ray scattering. *Macromolecules*, 20:2723–2732, 1987.

[10] G.R. Mitchell and A.H. Windle. Structure of polystyrene glasses. *Polymer*, 25:906–920, 1984.

[11] G.R. Mitchell and A.H. Windle. The effect of annealing on the local structure of glassy polycarbonate. *Colloid & Polymer Science*, 263:280–285, 1985.

[12] J.L. Koenig and M.K. Antoon. Thermally induced conformational changes in poly(vinyl chloride). *Journal of Polymer Science: Polymer Physics Edition*, 15:1379–1395, 1977.

[13] J. Lu, Y. Wang, and D. Shen. Infrared spectroscopic and modulated differential scanning calorimetric study of physical aging in bisphenol A polycarbonate. *Polymer Journal*, 32(7):610–615, 2000.

[14] E. Duval, L. Saviot, L. David, S. Etienne, and J.F. Jal. Effect of physical aging on the low-frequency vibrational density of states of a glassy polymer. *Europhysics Letters*, 63:778–784, 2003.

[15] A. Wypych, E. Duval, A. Mermet, G. Boiteux, L. David, J. Ulanski, and S. Etienne. Kovacs effect in PMMA observed by low-frequency Raman scattering (boson peak). *Journal of Non-Crystalline Solids*, 352:4562–4567, 2006.

[16] L.S. Nair and C.T. Laurencin. Biodegradable polymers as biomaterials. *Progress in Polymer Science*, 32:762–798, 2007.

[17] C.A.P. Joziasse, H. Veenstra, D.W. Grijpma, and A.J. Pennings. On the chain stiffness of poly(lactide)s. *Macromolecular Chemistry and Physics*, 197:2219–2229, 1996.

[18] L.P. Chen and A.F. Yee. The molecular basis for the relationship between the secondary relaxation and mechanical properties os a series of polyester copolymer glasses. *Macromolecules*, 32:5944–5955, 1999.

[19] J. Liu and A.F. Yee. Effect of local conformational transition on craze initiation in polyestercarbonates containing cyclohexylene linkages. *Macromolecules*, 33:1338–1344, 2000.

[20] C.L. Soles, R.M. Dimeo, D.A. Neumann, A. Kisliuk, A.P. Sokolov, J. Liu, A.F. Yee, and W. Wu. Correlations of the Boson peak with positron annihilation in series of polycarbonate copolymers. *Macromolecules*, 34:4082–4088, 2001.

[21] X. Li and A.F. Yee. Design of mechanically robust high-Tg polymers: mechanical properties of glassy poly(ester carbonate)s with cyclohexylene rings in the

backbone. *Macromolecules*, 37:7231–7239, 2004.

[22] H.G.H. van Melick, L.E. Govaert, and H.E.H. Meijer. Localisation phenomena in glassy polymers: influence of thermal and mechanical history. *Polymer*, 44:3579–3591, 2003.

[23] J.M. Hutchinson. Physical aging of polymers. *Progress in Polymer Science*, 20:703–760, 1995.

[24] J.M. Hutchinson, S. Smith, B. Horne, and G.M. Gourlay. Physical aging of polycarbonate: enthalpy relaxation, creep response, and yielding behavior. *Macromolecules*, 32:5046–5061, 1999.

[25] A. Brunacci, J.M.G. Cowie, R. Ferguson, and I.J. McEwen. Enthalpy relaxation in glassy polystyrenes: 1. *Polymer*, 38(4):865–870, 1997.

[26] A. Brunacci, J.M.G. Cowie, R. Ferguson, and I.J. McEwen. Enthalpy relaxation in glassy polystyrenes. Part 3. Stress and enthalpy relaxation in poly(4-methylstyrene) and poly(4-chlorostyrene). *Journal of the Chemical Society. Faraday Transactions*, 94(8):1105–1109, 1998.

[27] E.J. Kramer. Open questions in the physics of deformation of polymers glasses. *Journal of Polymer Science: Part B: Polymer Physics*, 43:3369–3371, 2005.

[28] H.G.H. van Melick, L.E. Govaert, and H.E.H. Meijer. On the origin of strain hardening in glassy polymers. *Polymer*, 44:2493–2502, 2003.

[29] J. Ho, L. Govaert, and M. Utz. Plastic deformation of glassy polymers: correlation between shear activation volume and entanglement density. *Macromolecules*, 36:7398–7404, 2003.

[30] L.E. Govaert, H.G.H. van Melick, and H.E.H. Meijer. Temporary toughening of polystyrene through mechanical pre-conditioning. *Polymer*, 42:1271–1274, 2001.

[31] W.J. Jackson and J.R. Caldwell. Antiplasticization. II. Characteristics of antiplasticizers. *Journal of Applied Polymer Science*, 11:211–226, 1967.

[32] W.J. Jackson and J.R. Caldwell. Antiplasticization. III. Characteristics and properties of antiplasticizable polymers. *Journal of Applied Polymer Science*, 11:227–244, 1967.

[33] J.T.A. Kierkels, C.-L. Dona, T.A. Tervoort, and L.E. Govaert. Kinetics of re-embrittlement of (anti)plasticized glassy polymers after mechanical rejuvenation. *Journal of Polymer Science: Part B: Polymer Physics*, 46:134–147, 2008.

[34] C.J. Ellison, M.K. Mundra, and J.M. Torkelson. Impact of polystyrene molecular weight and modification to the repeat unit structure on the glass transition-nanoconfinement effect and the cooperativity lenght scale. *Macromolecules*, 38(5):1767–1778, 2005.

[35] P. Rittigstein and J.M. Torkelson. Polymer-nanoparticle interfacial interactions in polymer nanocomposites: confinement effects on glass transition temperature and suppresion of physical aging. *Journal of Polymer Science: Part B: Polymer Physics*, 44:2935–2943, 2006.

[36] P. Rittigstein, R.D. Priestley, L.J. Broadbelt, and J.M. Torkelson. Model polymer nanocomposites provide an understanding of confinement effects in real

nanocomposites. *Nature Materials*, 6:278–282, 2007.

[37] R.D. Priestley, P. Rittigstein, L.J. Broadbelt, K. Fukao, and J.M. Torkelson. Evidence fot the molecular-scale origin of the suppression of physical aging in confined polymer: fluorescence and dielectric spectroscopy studies of polymer-silica nanocomposites. *Journal of Physics: Condensed Matter*, 19:205120, 2007.

# Samenvatting

In de hedendaagse ontwerpomgeving zijn ontwerpers en ontwikkelaars voorzien van een aantal, veelal op de eindige elementen methode gebaseerde, simulatiepakketten die het werk vergemakkelijken en het ontwerpproces ondersteunen. Daaronder bevinden zich verschillende pakketten die inspuiten, nadrukken en koelen tijdens het spuitgietproces simuleren, alsook pakketten die de mechanische eigenschappen van het uiteindelijke product evalueren onder de gewenste mechanische omstandigheden. Blijkbaar worden er twee ontwerpgebieden onderscheiden, enerzijds die van het fabriceren van het product en anderzijds die van de mechanische prestatie in het uiteindelijke gebruik. Tussen die twee ontwerpwerelden bestaat weinig interactie. In het geval van polymeren is het echter zo dat de fabricage stap ook voor een groot deel de uiteindelijke mechanische eigenschappen bepaalt.

Voor polymere materialen geldt tevens dat met de juiste kennis van de thermodynamische toestand van het materiaal, zoals die bijvoorbeeld tot uitdrukking komt in de waarde van de vloeispanning, de mechanische eigenschappen van een product op korte duur accuraat voorspeld kunnen worden. Door de ontwikkeling van de thermodynamische toestand tijdens de levensduur van een product mee te nemen, een fenomeen dat ook wel progressieve veroudering wordt genoemd, middels de introductie van een effectieve tijd (een door verhoogde temperatuur versnelde tijd), worden ook de lange duur eigenschappen correct voorspeld. Deze aanpak kent vooralsnog één grote tekortkoming: de thermodynamische toestand van het materiaal moet initieel vastgesteld worden, middels een mechanische beproeving. Een dergelijke beproeving is in het geval van een gestandaardiseerd proefstuk met homogene eigenschappen een triviale exercitie, maar in het geval van een complex product met zeer heterogene eigenschappen is het dat zeker niet. Bovendien zal men in het geval van optimalisatie van het productontwerp, de uiteindelijke mechanische eigenschappen liefst a priori willen voorspellen middels simulaties in plaats van via een kostbare route van iteratieve proefontwerpen en proefproducten.

Dit proefschrift presenteert een methode om de thermodynamische toestand van een product, zoals die tot uitdrukking komt in de vloeispanning, te voorspellen op basis van de temperatuurgeschiedenis die het polymeer ervaart gedurende het fabricageproces. Allereerst wordt een methode gepresenteerd die gebaseerd is op de

ontwikkeling van de effectieve tijd, zoals die reeds eerder bepaald is. Uitstekende voorspellingen resulteren voor zowel de vloeispanning na verwerken als de ontwikkeling van eigenschappen gedurende de levensduur. Het kinetische karakter van de glasovergang wordt echter genegeerd bij deze methode. Daarom wordt een tweede methode voorgesteld, die gebaseerd is op structurele relaxatie, en toegepast op de ontwikkeling van de vloeispanning tijdens het afkoelen van het polymeer gedurende fabricage. Hiermee wordt het kinetische karakter van de glasovergang in rekening gebracht, alsmede de niet-evenwichtstoestand waarin het polymeer verkeerd in de verglaasde toestand. De aanpak geeft goede resultaten over de voorspelling van de vloeispanning direct na het fabricageproces, maar blijkt minder goed te werken bij de voorspelling van de ontwikkeling van eigenschappen gedurende de levensduur van het product. De methode gebaseerd op de ontwikkeling van de effectieve verdiend daarom de voorkeur en is gevalideerd met zowel standaard proefstukken als met meer complexe producten.

De voorspellingen van eigenschappen zijn gebaseerd op het optreden van ductiel falen en zijn toegepast op een materiaal dat hier normaal ook aan voldoet: polycarbonaat. Echter, door progressieve veroudering kan een verandering optreden naar bros faalgedrag. Deze verbrossing willen we natuurlijk ook voorspellen. Daartoe wordt een kritische hydrostatische spanning als drempelwaarde gentroduceerd: beneden deze waarde vinden we ductiel faalgedrag, erboven brosse breuk. Deze drempelwaarde blijkt, in tegenstelling tot de vloeispanning, afhankelijk van het moleculair gewicht van het polymeer.

De methoden voor de voorspelling van de vloeispanning, zoals die volgt uit de temperatuurgeschiedenis die het materiaal ervaart gedurende fabricage, gepresenteerd in dit proefschrift, faciliteren het voorspellen van de mechanische eigenschappen van producten van polymere glazen op zowel korte duur als op lange duur. Hiermee zijn de twee ontwerpwerelden verbonden en opent zich de mogelijkheid om productoptimalisatie op mechanische eigenschappen door te voeren in een volledige virtuele omgeving.

# Dankwoord

De afgelopen jaren heb ik met veel plezier mogen werken op vloeren 4 en -1 van W-hoog. In die tijd heb ik met velen mogen samenwerken: stafleden, ondersteunende staf en studenten. Ik wil die mensen hier allen bedanken. Bedanken niet alleen voor de samenwerking, maar in veel gevallen juist ook voor de gezelligheid, de lol. Deze woorden van dank zijn slechts woorden, vooropgesteld mag zijn dat de mensen die ik dank verschuldigd ben, dat weten, hetgeen dit dankwoord feitelijk overbodig maakt.

Aan de gezellige tijd op de TU als collega's komt door dit proefschrift een einde, maar met velen hoop ik dit voort te zetten in een gezellige tijd als vrienden (al dan niet onder het genot van een biertje).

Tot slot wil ik nog zeggen: Edwin, je had gelijk, in je tijd op de TU verandert er niets ...

De studenten die hebben bijgedragen aan dit werk zijn: Wouter Buysse, Johan van den Eynden, Tim van Erp, Erik Feron, Matthijs den Hartog, Ruud Hawinkels, Frits Hermes, Joep Holierhoek, Elgar Kleijne, Marcel Kouters, Niek de Kruijf, Peter Neerincx, Bart Maas, Wesley Ooms, Sebastian Purmann, Rene Rademakers, Martijn van Riel, Twan van Schijndel, Dirk Senden, Stefan Sturm, Eric Tellier, Thijs Thissen, Esther Weltevreden, Joris Wismans, Maarten van Zuilichem.

# Curriculum Vitae

Tom Engels was born on the fifth of December 1978 in Panningen, the Netherlands. After having taken a break from school for four years to work in a brickyard (Steenfabriek Engels, Panningen), he graduated from secondary school in 1999 (Luzac College, Eindhoven). He then enrolled as a student in the department of Mechanical Engineering at the Eindhoven University of Technology, where he received his Bachelor's degree (cum laude) in August 2002. Also he completed the Technical Management Certificate at the department of Technology Management of the Eindhoven University of Technology. He received his Master's degree (cum laude) in the beginning of 2005 on the thesis entitled 'Processing-induced properties in glassy polymers' and the work was performed in the Polymer Technology group chaired by prof.dr.ir. Han E.H. Meijer, under the supervision of dr.ir. Leon E. Govaert. During his time as a student he was a member of the Department Council for three years, of which one as vice-chairman.

After completion of his Master degree he took a position in the Polymer Technology group as a PhD student, the result of which is this thesis. During his PhD he successfully completed the postgraduate course Register Polymer Science of the National Dutch Research School PTN (Polymeer Technologie Nederland) and is given the title of Registered Polymer Scientist as of May 2006. The course consists of the following modules: A - Polymer Chemistry, B - Polymer Physics, C - Polymer Properties, D - Polymer Rheology, E - Polymer Processing and $\pi$ - Polymer Innovations.